RARE-EARTH-DOPED SINGLE-CRYSTAL YAG FIBERS GROWN BY THE LASER HEATED PEDESTAL GROWTH TECHNIQUE

by

CRAIG DANIEL NIE

A dissertation submitted to the

Graduate School – New Brunswick

Rutgers, The State University of New Jersey

In partial fulfillment of the requirements

For the degree of

Doctor of Philosophy

Graduate Program in Materials Science and Engineering

Written under the direction of

Professor James A. Harrington

And approved by

____

____

____

____

New Brunswick, New Jersey

January, 2017

ABSTRACT OF THE DISSERTATION

Rare-Earth-Doped Single-Crystal YAG Fibers grown by the

Laser Heated Pedestal Growth Technique

By CRAIG DANIEL NIE

Dissertation Director:

Professor James A. Harrington

The laser-heated pedestal growth (LHPG) technique is an unconventional method for growth of single-crystal (SC) fibers with the advantages of high pulling rates and crucible-free processing when compared to more conventional techniques such as the Czochralski technique. In this dissertation, the processing of rare-earth (RE^{3+}) doped yttrium aluminum garnet, $Y_3Al_5O_{12}$, (YAG) fibers using the LHPG technique was significantly improved upon as the result of the development of a new, more accurate method to align the CO_2 laser along with the minimization of waveguide irregularities.

Initially, the dominant loss mechanism in the fabricated SC fibers was bulk scattering, resulting from thermal stresses in the core due to inadequate alignment. Once these stresses were remedied by the implementation of new alignment techniques, absorption became the dominant loss mechanism with minimal scattering. For short fiber lengths, the absence of diameter control did not prove to be critical. However, when fibers exceeded 30 cm in length, the waveguide would couple low-order modes to high-order

modes that can become radiation modes at longer lengths. By implementing a diameter control feedback loop, these effects were minimized.

The fibers were characterized by studying the optical properties of an undoped and doped air-clad SC YAG fiber (typically 330 μm in diameter). The total attenuation and scattering loss was measured using visible and NIR lasers. The lowest losses were achieved with the growth of a 1 m long SC fiber - lower than any currently published. The total attenuation of the YAG fibers is now below 0.3 dB/m, at 1064 nm. This loss is primarily attributed to the bulk absorption of the raw material, with as little as 0.02 dB/m of this loss coming from scattering in RE doped YAG fibers. At non-absorbing wavelengths, the 0.5% Ho:YAG fibers have an equivalently low loss. This low loss is critical for applications of YAG fibers, specifically regarding lasing of 0.5% Ho:YAG. Lasing has been demonstrated with increasing slope efficiency as the quality of the crystal fiber was improved. At 72.3%, the fiber's slope efficiency with respect to incident pump power is approaching the slope efficiency for bulk Ho:YAG lasers.

Acknowledgements

To my wife, Taryn, and family. Without their love, support, and sacrifices I would not have been able to achieve this milestone. Thank you for challenging, inspiring, and believing in me.

To Professor James Harrington, for your patient guidance as I advanced my research interests. You facilitated an encouraging environment, which fostered my skills and provided opportunity. It has been an honor and a privilege to learn from you.

To all my colleagues in the Fiber Optics Group: Subhabrata Bera, Jeffrey Melzer, Carlos Bledt, Michael Soskind, and Wesley Kendall. Each played a valuable role in my research. A warm thanks, also, to rest of my colleagues in the MSE department for their time spent assisting with one idea or another, and to the Physics shop, especially William Schnider, for their quick assistance machining countless components used in this project

To my research collaborators at the University of Michigan and Clemson University. Dr. Rand, Elizabeth Cloos, Theresa Chick, and Long Cheng's excellent RiT work at Michigan was crucial, as was Dr. Johnson, Dr. Miller, and Yuan Li's focused efforts on the lasing of our SC fibers at Clemson.

A large thanks to my committee for their time and thoughtful input: Professor O'Carroll, Professor Mann, and Dr. Emge. A special thanks to Dr. Emge for performing single-crystal analysis.

I would also like to acknowledge both past and present MSE Graduate Directors, Professor Klein and Professor Mann, for their commitment to the students and open door policy. Thank you for the advice.

I am grateful to the High Energy Lasers Joint Technology Office (HEL-JTO) for funding my research.

Table of Contents

List of Tables

List of Illustrations

List of Abbreviations

CW: continuous-wave

EFG: edge-defined film-fed growth

ErAG: erbium aluminum garnet

FWHM: full with at half maximum

HR: high reflective

LHPG: laser heated pedestal growth

NA: numerical aperture

NIR: near infrared

OC: output coupler

P_{12}: Pockel's coefficient

RE: rare-earth

RiT: rod-in-tube

SBS: stimulated Brillouin scattering

SC: single-crystal

SM: single mode

SRS: stimulated Raman scattering

TEM_{00}: fundamental transverse electromagnetic mode

TIR: total internal reflection

YAG: yttrium aluminum garnet

Δn: change in refractive index

μ-PD: micro pulling-down

α_{ss}: attenuation from surface scattering

α_{bs}: attenuation from bulk scattering

α_s: attenuation from scattering

Chapter 1. Introduction

1.1 Motivation for Single-Crystal YAG Fibers

The field of optics was transformed by the application of the laser in 1960. It has led to numerous other fields and the discovery of endless technologies. One such branch, fiber optics, has led to the fiber laser and bulk crystal lasers, two notable and massive fields that have laid the ground work for the interest of single-crystal (SC) YAG fibers. Both fiber optics and the fiber laser have been primarily made of glass. These glass structures normally involve a double-clad structure in which the core glass has been doped with a variety of rare-earth (RE) ions, notably ytterbium. Glass has been proven to be an excellent host material for fiber lasers. These glass fiber lasers deliver a very high continuous-wave (CW) power with a single-mode (SM) output and broad gain bandwidths. 1.7 kW in output power of CW ytterbium-doped glass fiber lasers was achieved with a distorted SM.[1] However, their output powers, though high, are plateauing due to limitations in the glass host material. This limits the power scaling ability, primarily from laser induced damage to the small cores, nonlinear effects, and thermal loading. Thus, research is being done on potentially high energy fiber lasers based on crystalline materials rather than the conventional glass fiber structure. The basic premise of this work is the rather straightforward idea that crystalline materials such as YAG are known to deliver extremely high energies.

SC fibers have been grown since the early 1970s, with most of the work concentrating on passive (pure) SC sapphire fibers.[2] There has been some limited work on growing doped YAG SC fibers, some of which have been rather large in diameter (~1,000 μm) grown by edge-defined film-feed growth (EFG). SC YAG fibers grown from the LHPG technique can be grown with diameters as small as tens of microns, but typically are grown about 300 μm.[3] One of the greatest challenges since the inception of SC fibers has been to find a suitable cladding for the oxide crystal fibers. That is, to fabricate a true crystalline clad fiber with a lower refractive index, n, than the crystalline core. Presently there are only a few single clad SC fibers structures, most of which focus on using glass claddings that match the thermal expansion coefficient and have sufficient Δn. Digonnet's group showed this with $\Delta n=0.048$ but desired to lower it to 0.005.[4] The aspiration for an all crystalline clad is to reap the full potential of SC fiber lasers which surpass glass lasers. Among the advantages are greater efficiency and output for SC fiber lasers, greater damage threshold when pumped at high powers, significantly higher thermal conductivity, allowing the fiber to naturally dissipate the heat which can cause thermal lensing issues in glass fibers, and reduced nonlinear effects such as stimulated Brillouin scattering (SBS).[5] SC fibers have the potential to surpass the power output of glass fiber lasers, which have plateaued due to these limitations. With YAG's high SBS threshold, YAG fibers have the potential to deliver more than five times the peak power than conventional silica glass fiber.[5] YAG is an ideal host material for producing a fiber laser in the NIR because its transmittance range is beyond 4 μm, as demonstrated in Figure 1.1, where its multiphonon peak appears at

4.7 μm and its ability to dope with high RE concentrations. Thus, YAG has the ability to produce NIR lasers with ytterbium, erbium, holmium, and thulium dopants.

The critical limits of power scaling for fiber lasers include thermal limits, fiber non-linearities, end-facet damage, and the brightness of the diode pump laser. Dawson et al.[6] and Parthasarathy et al.[5] studied these limits in great depth and simulated plots that considered all these limits as a function of core diameter and fiber length. The thermal limits included the melting temperature, the rupture modulus, thermal conductivity, and thermal lensing.[7] Of all the limitations, SBS/SRS effects are the main mechanisms preventing higher output power for glass fiber lasers, as simulated in Figure 1.2. Both SBS and SRS are nonlinear effects observed in fiber optics. SBS scatters light from acoustic waves. Once its threshold is reached most of the light is reflected backward, limiting output power. SRS scatters light from vibrating molecules. In amorphous fibers, this scattered light can be red-shifted 100 nm in the NIR.[8]

These models examine the potential output power as a function of fiber diameter and fiber length. The figures are divided into three sections, and each represents the limiting property (SBS or SRS, thermal lensing, and pumping power) at different combinations of diameter and length. For instance, at larger diameters, thermal lensing was limiting the power increase; at smaller diameters and shorter lengths, pumping power was the limiting factor. Parthasarathy also points out that pumping limits could be improved with technological progress.

Unfortunately, YAG does not have a definitive measurement of the Brillouin gain coefficient and only a range has been offered, as seen in Table 1.1 with some other properties. But even with conservative estimates, the coefficient is similar to silica.

However, YAG still out performs silica in the models. Also, if the SBS gain coefficient is less than the conservative value of 10^{-12} m/W, then it is no longer SBS limited. SRS becomes more limiting than SBS and the theoretical output power can be increased from 6 kW per fiber to over 30 kW per fiber as seen with Figure 1.3 and Figure 1.4.[5, 6] This is a major increase from the 1.4 kW output for the ytterbium silica fiber. These calculations for SC YAG present a greater theoretical potential to deliver high power, in part, because of the major increase in thermal conductivity. Thermal conductivity does have a small dependence on dopant concentration and on crystal temperature, but it still remains low, settling to around 7 W/m*K. [9, 10]

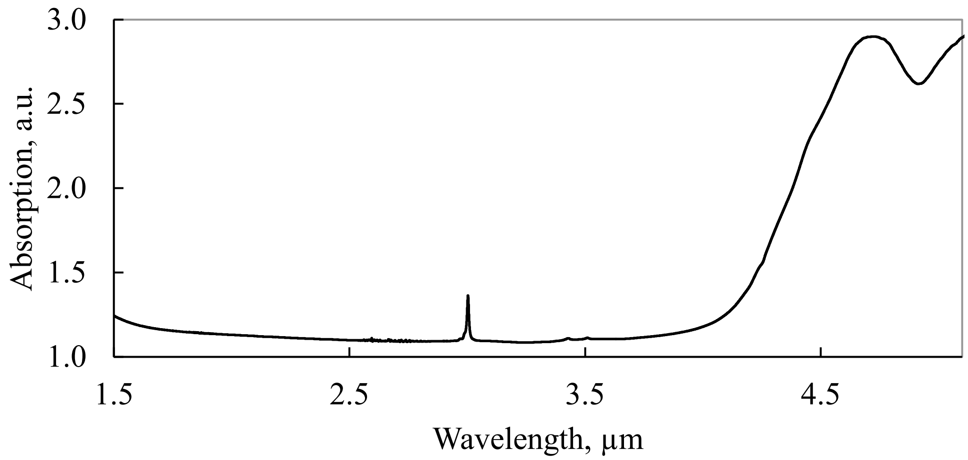

Figure 1.1 Absorption of YAG in the infrared with the multiphonon peak at 4.7 µm.

Table 1.1 Material properties of silica glass and SC YAG.[3, 6]

	T_g or T_m [°C]	Thermal Conductivity [W/m*K]	Hardness [kg/mm^2]	Refractive index @1.06 µm	Brillouin Gain Coefficient [m/W]
Silica Glass	~1000 (T_g)	~1 [6]	500	1.45	5×10^{-11} [6]
SC YAG	1950 (T_m)	~10 [10]	1350	1.81	2.5×10^{-11} [8] To 5×10^{-14}

The modeling by Dawson et al. shows the background loss of 0.2 dB/km for silica at 1.55 μm and 3 dB/m for SC YAG fibers. These high background losses in YAG will hinder the output power. He states that these losses will impact the laser efficiency and require strict limits on fiber length. [6] For this reason, a main objective of this dissertation was to engineer low-loss SC YAG fibers, namely, below this 3 dB/m range.

If the optical efficiency increases from 0.5 to 0.8, the Yb:YAG multimode fiber's theoretical maximum output increases by 30% from 6 kW to 8 kW.[11] This optical efficiency is not unlikely, as work has been published demonstrating efficiencies around 78%[12] and 67%[13] in Yb:YAG and Ho:YAG, respectively. Both Parthasarathy and Dawson agree that improving background loss in the laser host material will result in improvements in output power. Dawson specified that, with an improved background loss in YAG to 1-2 dB/m, more than a 20% increase in output power was possible. The promising aspect of this improvement in loss is within the scope of this dissertation, namely that the background losses have been improved to below 0.3 dB/m for SC YAG fibers - drastically increasing the theoretical output. However, even with these improvements, it should still be recognized that the fiber background loss will increase with smaller diameters. This fact was not addressed in either of the above works, nor will it be in this dissertation.

With respect to the improvement of SC fibers, a parallel to telecommunication fibers can be made. In the 1960's glass fibers were considered to have too high of signal loss for the application of communications. Attenuation was on the order of 1 dB/m, but use in communications over long distances would require losses less than 20 dB/km. It only took 4 years for a reduction from 1,000 dB/km to 20 dB/km when Corning used the chemical vapor deposition. This was accomplished by focusing on eliminating impurities, using extremely pure fused silica, and engineering a core/clad architecture that could produce a SM output. In 1986, glass fibers were improved to the level of having an attenuation of about 0.2 dB/km by moving to longer wavelengths, such as 1.55 µm. This experimental loss level is nearly at the theoretical intrinsic minimum for silica.[14-16]

Although this dissertation has little to do with glass optical fibers, the parallel of the drastic improvement in telecommunication silica glass fiber (losses reduced from ~1 dB/m to <0.2 dB/km), through material processing and engineering, simply illustrates the same concept can be applied to SC fibers, only for the different application of the fiber laser. Previous researchers have reduced, losses for SC YAG fibers to the 2-20 dB/m range. This work uses the similar ideology glass processing engineers used in the 1960s-70's to improve SC YAG fibers. This work has successfully grown low-loss SC YAG fibers consistently to 0.5 dB/m and as low as 0.2 dB/m at 1.064 µm. This feat was accomplished primarily by focusing on engineering a more uniform waveguide geometry, providing a more uniform CO_2 radiation to the molten zone to improve the bulk crystal, and by using high-quality SC starting material.

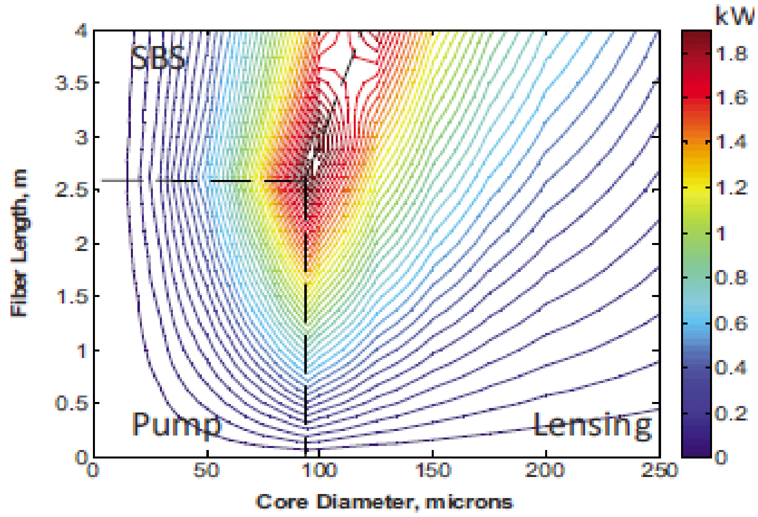

Figure 1.2 Predicted performance of multimode Yb doped silica fiber in continuous operation. The maximum power is limited to 1.6 kW per fiber with thermal lensing limiting power at greater diameters and SBS at longer fiber lengths. [Reprinted with permission][11]

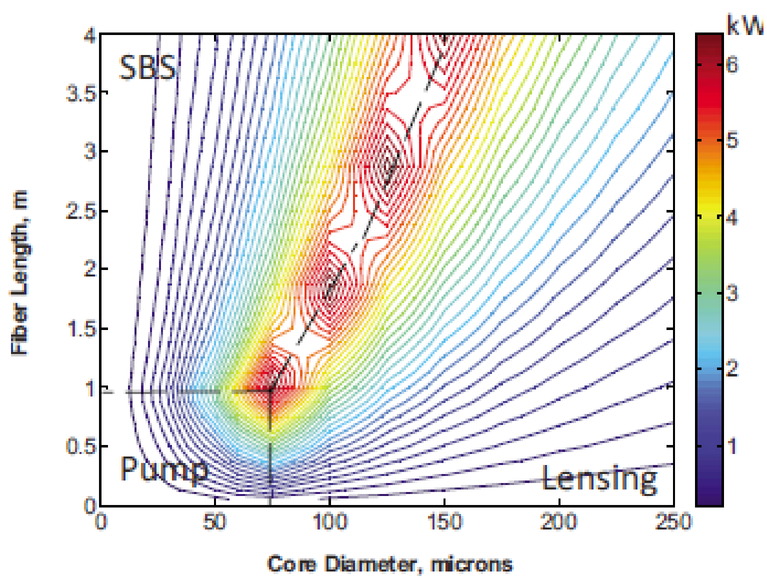

Figure 1.3 Predicted performance of multimode Yb:YAG fiber with SBS gain >10 ^{12} m/W in continuous operation. The maximum power for this conservative case was three times greater than for Yb:silica fiber. [Reprinted with permission][11]

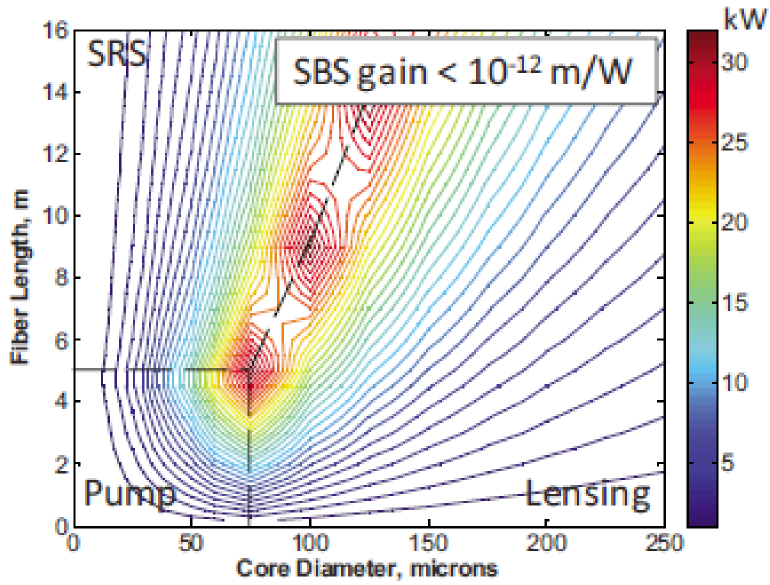

Figure 1.4 Predicted performance of multimode Yb:YAG fiber with SBS gain <10 ^{12} m/W in continuous operation. With this less conservative SBS value, SRS takes its place as limiting, but now the peak power is approximately 30 kW. Both cases have the potential for significantly greater output power. [Reprinted with permission][11]

1.2 Crystal Growth Methods from a Melt

SC fibers have been grown by several methods, including Edge-Defined Film Fed Growth (EFG)[17], μ-Pulling-Down (μ-PD)[18], and the Laser Heated Pedestal Growth (LHPG) method[19, 20]. The most common method used today is LHPG. This method was first patented by Haggerty[20] at MIT and then further refined by a number of researchers including those at Stanford University[21], Bell Labs[22], Rutgers University[23, 24], University of South Florida[25], Shasta Crystals, Inc.[3], and others[26]. In the LHPG technique, a CO_2 laser beam is focused onto the tip of an oxide crystal source rod, creating a small molten self-contained zone. A seed fiber is dipped into the molten region and slowly pulled upward, forming the single-crystal fiber. The source rod, is simultaneously fed upward to replenish the supply of molten material. A schematic diagram of our setup is shown in Figure 2.1.

Crystals can be grown at various velocities. This is largely due to the varying size of the crystals grown and the difference in the thermal gradients between these methods. The crystal growing method determines the order of magnitude of the velocity allowed to grow quality crystals. Czochralski growth is performed at a velocity on the order of 1 mm/hr (17 μm/min) for a 1.5 cm diameter crystal.[27] This compares to μ-PD which uses a slightly faster range from 2 mm/hr[28] to 1 mm/min[29] for YAG crystals ranging in diameter from 400 μm to 1,000 μm. Both methods are drastically slower than crystal growth using LHPG, largely due to the high thermal gradients observed in LHPG. Velocities are commonly on the order of a few mm/min. While Czochralski growth is slow, taking weeks to grow a boule, it does have the advantage of producing a large quantity of material. YAG boules of

100 mm in diameter and 350 mm in length have been grown. From this bulk material however, only laser rods are possible after core drilling and polishing. These rods can be as small as 1 mm, but are not flexible. They also have a much lower surface-to-volume ratio that can have deleterious thermal effects at high operating powers, as compared to thinner fibers.

EFG and μ-PD crystal growth utilizes a crucible and a die that melts starting material as powders, and capillary forces moves material either up or down through the die. A seed can be dipped into the melt and drawn out. Benefits of this system are that different shapes can be pulled (e.g., tubes, rods, and ribbons) and the crystal orientation can be controlled using a seed with the desired orientation. However, the need for smaller diameters and flexibility leads EFG and μ-PD to primarily grow mini-rods, about 600-1000 μm diameters. These two growth techniques do have the advantage of growing longer length crystals (up to 1 m) than Czochralski method.[18] The diameter variation for this technique has been reported to not exceed ±2-3%.[30] This is higher compared to LHPG ranging from ±0.5-1%, for smaller scale fibers. These mini-rods were produced for amplifiers[31] and laser results,[32, 33] but do not offer the higher surface-to-volume ratio of a fiber. For the purpose of this dissertation the term fiber will be used when the guide can be flexible. At 350 μm an air-clad SC YAG fiber is flexible to a bending radius less than 10 cm before failure. The LHPG technique has the ability to grow fibers 25 μm in diameter (but is not limited to 25 μm) with a bending radius of 4 mm.[34, 35] This process is more complicated than for glass drawing, because it requires multiple growths to get this size. Glass can be drawn down to micron size diameters from large preforms because the viscosity of the glass melt is much greater than oxide melts.[30] The focus at Rutgers has been on growing fiber diameters of 330 μm from a single growth.

The LHPG method will be discussed in much greater detail in Chapter 2. It is included here so that a direct comparison can be made to the other methods. It has the advantage of growing much smaller fibers, though multiple growths are needed for diameters less than 200 μm. The starting material can be either ceramic or SC rods. Ceramic offers the benefit of being cheaper and the ability to customize the dopant concentration without long lead times, however it does pose issues of purity, density, and straightness. Ceramic source material was attempted with unfavorable results. Other groups such as Shasta Crystals use all ceramic materials to grow their fibers.[36] With SC rods you are ensured to have a straight uniform diameter starting material, both of which can impact the quality of the fiber's diameter control and length. The SC starting material has been core drilled from a SC boule. The facts that it is optically transparent initially and that the source geometry is straight and uniform are its main attractions in contrast to μ-PD and EFG which are grown from a crucible and pulled through a die, leaving a much greater chance of additional contamination.

In summary, these four methods have some advantages, and all produce high-quality crystals that can be doped with RE ions. However, in practice, only LHPG offers the ability to create smaller diameter fibers at longer lengths without diminishing the crystal quality.

1.3 Loss Values of YAG and Cladding Attempts in Literature

This chapter analyzes research from multiple research groups who have studied YAG. Many have focused on the lasing properties of RE doped SC YAG in both mini-rod and fiber form and with that have reported both percent power transmitted and percent power guided. A higher percentage of power would be transmitted than would be guided through. The percent guided is more comparable to current loss measurements, thus, the percent guided is plotted in dB/m in Figure 1.5, unless only transmission was reported. Each publication number corresponds to Table 1.2; which indicates the wavelength measured at, the length and diameter of the sample, if the sample was clad, and RE doped YAG material it was. Diameter and length are the two key differences when comparing these data points to one another and later to mine. The longest sample is 15 cm long and most are less than 6 cm compared with 50-100 cm. Diameters vary widely from 10 µm to 1,000 µm, and loss will increase at smaller fiber diameters. In the figure the total attenuation varies from 2- 95 dB/m, with an averaging range between 4-15 dB/m, with each publication having little repeatability.

In order for step index change claddings to work, small diameter SC YAG fiber cores must be fabricated to achieve a SM output. Publications 1, 2, and 8 from Table 1.2 focus on cladding the SC YAG with high index oxide based glasses with a coefficient of thermal expansion matching YAG. One issue is matching the coefficient of thermal expansion with the index of refraction results because they vary differently as a function of temperature, and the crystal will heat up when pumped at high powers. Specifically, Digonnet et al.[4] worked with a comparable diameter range and reported large diameter variation on the order of 5- 10 percent rms and attributed these variations to their high propagation loss. They speculated that the residual fiber diameter variations were coupling to higher order modes becoming radiation modes. A year later, they produced a 40 μm fiber with 0.5 percent rms diameter variations and a high index glass that has the advantage of tuning the refractive index with either the cooling rate or composition.[4] They reported four different claddings with a refractive index change in the range of 0.05. They concluded that lowest loss clad fiber was 3 times lower than unclad fiber with similar diameter variations and reduced mode coupling. Finally, they believed a change in index closer to 0.005 would reduce surface scattering.[4]

Shaw et al.[35] also used a glass cladding. They demonstrated a 35 μm core of 10% ytterbium doped YAG with a double glass cladding 230 μm. The optical loss of this fiber was comparable to Digonnet's fiber of similar diameter, at 15 dB/m.[35] They differed from Digonnet by achieving a smaller index change, 0.001-0.002.

The only currently published SC cladding was developed by Onyx Optics Inc.[12, 37] seen in Table 1.2 as publication 9. They patented an adhesive free bonding technique that can clad a small diameter crystal core (40 μm) with undoped YAG for a small index change on the order of 0.002. Then, applying the process again, can add a second cladding of spinel with an index change of 0.113. They estimated the propagation loss to be 5.6 dB/m for a 300 μm core with scattering dominating the loss in the outer ceramic spinel cladding. The issue with this process is the limitation on cladding fibers of reasonable length and the question of whether the clad fiber can remain flexible. Regardless of these details, they produced a laser output power with a slope efficiency of 78% with a single clad crystal fiber waveguide.[12]

Publications 2, 4, 5, and 6 from Table 1.2 were fibers grown from μ-PD technique. They were included to compare their losses with the LHPG, and because there are very limited publications on the SC YAG fiber losses grown from the LHPG. The main difference is the large diameter with short lengths, limiting the coupled light's interaction with the surface. Yet, their losses are still equal or greater than SC YAG grown from LHPG either clad or unclad, implying an issue with bulk scattering or perhaps additional absorption from contamination.

One research group not included in the figure or table was Shasta Crystals. They do not publish their fibers total attenuation, but do report on their scattering losses measured by a scattering sphere. Yb:YAG grown at 3 mm/min with diameter control was reported to be as low as 0.14 dB/m at 532 nm. This value increased to 0.25 dB/m when grown at 5 mm/min. The length of these samples were still fairly short (less than 12 cm), with diameters around 120 μm.[3] This scattering loss was an improvement from 1.5 dB/m a year earlier.[36] To decrease the amount of bulk scattering, they were the first group to implement a YAG sol gel layer as a cladding. This has the limitation of only a thin layer can be applied on the order of a few microns.

Compiling these different publications, losses seem to vary dependent on the group and method. Digonnet first writes they believe their dominant loss to be both bulk and scattering loss.[38] The next year, however, they believe their losses are primarily surface scattering when they added a glass cladding.[4] A majority of the small diameter fibers make a statement attributing their losses to surface scattering from one cause or another. Only the μ-PD samples have neither a cladding interface on which surface scattering could occur or many surface interactions because of the large diameter. Yet, for all of these, the purity of their starting materials could be affecting the magnitude of their absorption. Considering the range of these data points, consistently growing quality fibers at 1 dB/m would be in itself a successful objective.

Table 1.2 Additional details of the measurement conditions from Figure 1.5. If both transmission and percent guided were given, only loss for percentage of guided light was plotted. The superscript in the Pub. # column is the reference for each publication.

Pub. #	Wavelength	Length	Diameter	Cladding	Material
0[38]	1064/1032	<12 mm	78-230 µm	No	Nd:YAG
1[4]	1150	<30 mm	37-125 µm	Yes	Nd:YAG
2[30]	1062	60 mm	1,000 µm	No	Nd:YAG
3[35]	-	150 mm	35 µm	Yes	Yb:YAG
4[32]	1064	50 mm	1,000 µm	No	Nd:YAG, Yb:YAG
5[33]	1064	50 mm	1,000 µm	No	Nd:YAG
6[32]	633	40-60 mm	500-1,000 µm	No	RE:YAG
7[39]	1064	40 mm	400 µm	No	Er:YAG
8[40]	1064	50 mm	10-17 µm	Yes	Cr:YAG
9[12]	633	100 mm	300 µm	Yes	Yb:YAG

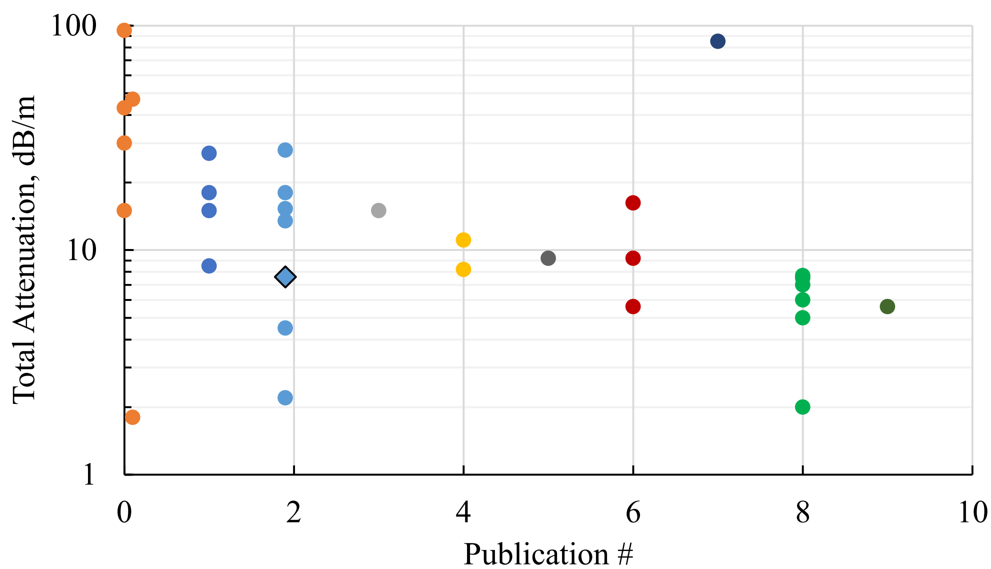

Figure 1.5 Compiled total attenuation measurements of ten publications. The blue diamond in publication 2 represents the average of the 16 samples measured in this one publication.

1.4 Intrinsic Loss and Experimental Absorption in Bulk YAG

The theoretical intrinsic loss in bulk YAG are a combination of UV absorption, scattering, and IR absorption. Firstly, UV absorption, discovered by F. Urbach in 1953 and now referred to as the Urbach tail, is the result of exponentially increasing absorption in the UV as the wavelength decreases.[41] This sharp increase is the result that the absorption depends on the electronic bandgap energies. The Urbach tail extinction coefficients are available in Palik[42], however, due to its sufficiently sharp absorption at short wavelengths (~200 nm, 50,000 cm^{-1}) it does not contribute significantly to the overall intrinsic absorption seen in Figure 1.6. Secondly, scattering can be either Rayleigh (elastic) or Brillouin (inelastic). In theory, for perfect single crystals there is no Rayleigh scattering - only Brillouin scattering. Finally, the IR absorption, or multiphonon absorption, results from the coupling of photons to lattice vibrations creating phonons.[43] These multiphonon extinction coefficients in Palik[42] demonstrate at increasing IR wavelengths the material becomes opaque, followed by a short period that is more transparent before it transitions back to being opaque. This effect results in a multiphonon hump at 4.7 μm.

The main contributing factor for the intrinsic loss in YAG is the scattering losses and these scattering losses are lower than silica. Using the Equation 1.1 from Pinnow et al.[44] this intrinsic scattering can be calculated by

$$\alpha_s = \frac{8\pi^3}{3}\frac{1}{\lambda^4}\left(n^8 P_{12}^2\right)\left(k_B T \beta_T\right) \qquad \text{Equation 1.1}$$

The equation has a strong λ^{-4} and n^8 dependence, with $P^2{}_{12}$ is the Pockel's coefficient, k_B is the Boltzmann's constant, T is the absolute temperature, and β_T is the isothermal compressibility. The Pockel's coefficient, P_{12} is 0.0091.[45, 46] The isothermal compressibility is 5.4 x 10^{-12} Pa^{-1}.[47] With the scattering and multiphonon edge, the characteristic V-curve can be constructed to determine the minimum attenuation coefficient at each wavelength. Figure 1.6 shows the theoretical minimum loss is 8 x 10^{-9} dB/m at 1.7 µm. This was determined by extrapolating the multiphonon data from the full range of data 4.2-6.8 µm. However, if the range 4.2-4.6 µm is used when extrapolating, then the theoretical minimum loss is slightly lower at 4.6 x 10^{-9} dB/m and shifts to 1.98 µm. In either case, the theoretical loss of YAG is less than silica. It is unlikely, however, that these losses will ever be experimentally reached, in part due to the concept of an atomically perfect SC (that this calculation assumes), is not allowed thermodynamically. Point defect imperfections are inherently present in a SC fiber grown from a melt, especially, when ppm contamination is present in the raw materials.

More details on the contamination will be given in Chapter 2, but Figure 1.6 demonstrates the experimental absorption loss at different wavelengths. Data from figure 2 of Innocenzi's research was extrapolated and converted to wavenumber and dB/m to be represented here in Figure 1.6.[48] It, combined with work from Mann et al.[49], demonstrates a second characteristic V-curve with a minimum loss of 0.04 dB/m at 3.0 µm. Mann's bulk absorption coefficient data point was the average of three YAG rods measured at 1062 nm. These experimental absorption losses are more practical with the current purity levels. Fiber losses are approaching this bulk absorption limit.

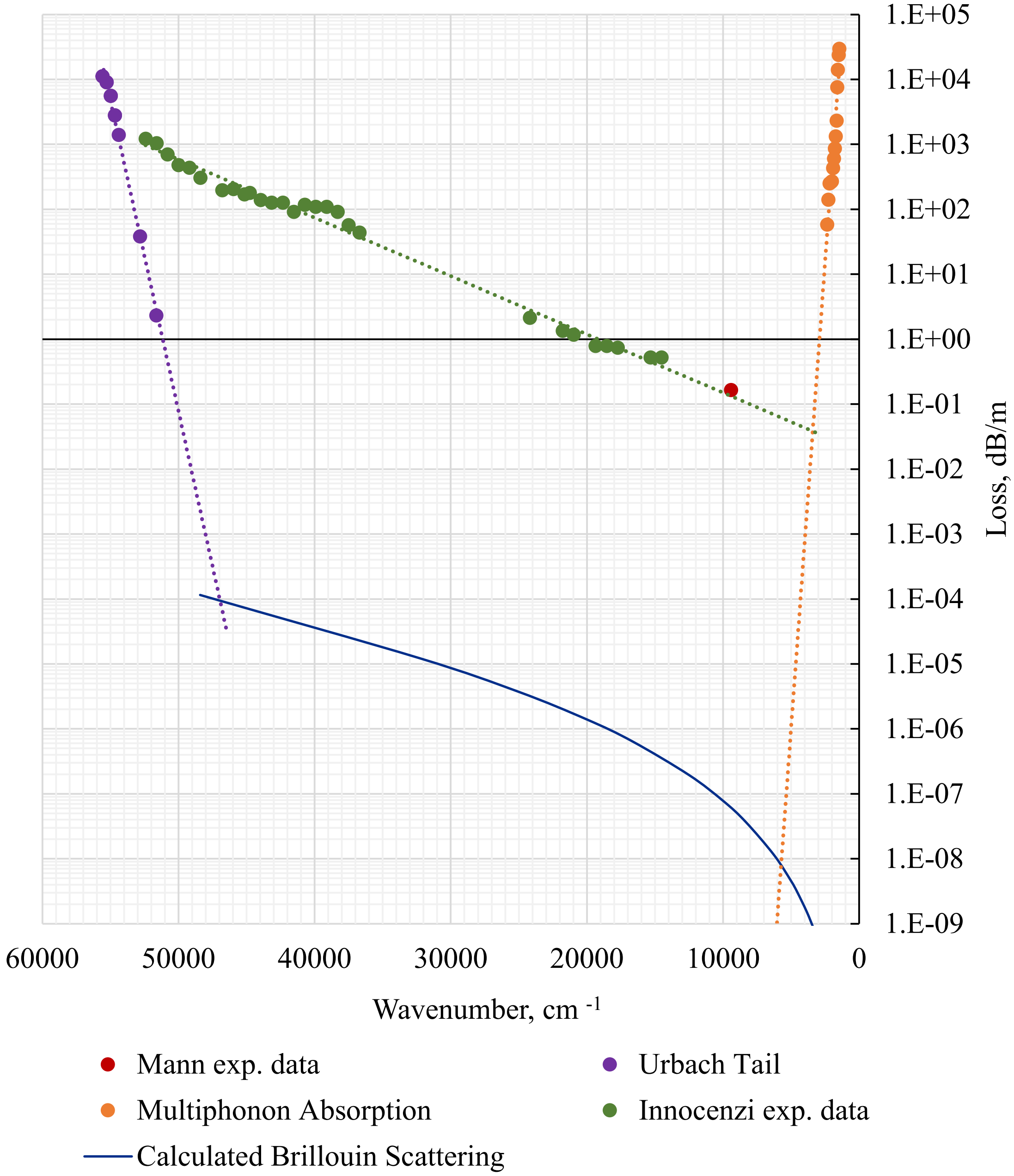

Figure 1.6 Theoretical loss of SC YAG with experimental absorption data by Innocenzi et al. [48] and Mann et al.[49]. Innocenzi's data from his figure 2 was extrapolated and converted to get these data presented here. Theoretical minimum of YAG is at 5,900 cm^{-1} (1.7 µm) with a loss of $8*10^{-9}$ dB/m.

Chapter 2. Laser-Heated Pedestal Growth

2.1 Description of LHPG Apparatus

2.1.1 Modifications to Other LHPG Systems

The LHPG technique has had numerous modifications over the last few decades. Many of them revolve around the concept of lowering the thermal gradient of the heat zone, such as changing the reflaxicon, Gaussian reflector, afterheaters, improved reflaxicon, and modifying the focal spot.

The reflaxicon optic was a major improvement, designed by Fejer et al.[50], and truly made the LHPG what it is today. This optic transformed the LHPG from four CO_2 laser beams focusing on the source to using one Gaussian CO_2 laser beam that is converted into a collimated ring and focused onto the pedestal.[51] The original design left three shadowed areas on the molten zone. So Nubling et al.[23] designed a ZnSe window that would replace one of the two optics in the reflaxicon and remove the shadows.

The above modifications have been focused on optics and delivering the CO_2 radiation to the pedestal, but there were many other modifications that resulted in improved SC fiber. One very important improvement was the ability to control fiber diameter, first achieved by using an interferometer.[52] There are two other means of controlling the fiber diameter.

First, was using a laser micrometer[23] and second a CCD camera image feedback loop[53]. All three have different advantages and disadvantages. The laser micrometer has a resolution of 0.1 μm even though a large separation distance is needed between the source and detector. Another issue is that the laser micrometer has a fixed scan speed, which can limit the response time of the motors to once per second. The interferometer provides a faster response time, but is easily affected by the fiber geometry, especially if the geometry is changing during the growth. It also has been reported that a resolution of 0.02% is possible for transparent fibers.[52] The CCD imaging offers slightly poorer control at about 2%. Other important design differences that vary between different research groups are the fiber and source translation drives. At Rutgers a belt drive system and a V-groove is used to translate the source and fiber vertically, while other groups use a coiling wheel similar to glass fabrication.[36]

2.1.2 LHPG Overview of YAG Crystal Fibers

While other methods use a crucible to contain the melt from which the seed fiber is pulled, LHPG holds the molten zone in place by surface tension. Thus, eliminating the need for a crucible and die, whose surfaces can pose an additionally source of contamination during the solidification process. The crucible and die are made of platinum and iridium.[32] In Czochralski growth, contamination of highly pure (99.999%) raw powders (Y_2O_3 and Al_2O_3) still result in a total of 10-11 ppm seen in Table 2.1.[48, 54] These impurity levels will be found in LHPG fibers because of the purity of the starting materials in the source rod.[2]

To melt the source rod and create the molten zone, LHPG uses ~10 W of an amplitude-stabilized 30-W CO_2 laser that is transmitted through two ZnSe axicons. This set of axicons convert the Gaussian beam into a collimated ring, which is focused with uniform 360° heat from a parabolic mirror on to the tip of the source rod. This focused CO_2 radiation allows for crystals with a high melting point to be grown. YAG melts congruently at 1940°C, meaning that the composition of the liquid is the same as the composition of the solid. Once the seed fiber is inserted into the molten tip of the source rod, the source and the seed fiber are continually translating vertically at a fiber-to-source velocity ratio of ~10:1. This ratio satisfies the mass transfer from the larger diameter 1 mm source to a ~330 μm diameter fiber seen in Equation 2.1,

$$\frac{d_s}{d_f} = \sqrt{\frac{v_f}{v_s}} \qquad \text{Equation 2.1}$$

where d_s and d_f are the diameters, and v_s and v_f are the velocities of the source and fiber, respectively. The growth rates are slow compared with glass and typically vary from 1 mm/min to about 3 mm/min. You will recall however, that is approximately 60 times faster than Czochralski growth. This increase in crystal growth is possible because of the very high thermal gradients caused from the focus of the CO_2, on the order of 10^3- 10^4 °C/cm.[55] If the growth rate is too great, however, thermal stress will result in cracking at the core. The growth velocity can be a minor indicator of the alignment of the optical system. When the alignment is poor, we experienced maximum growth rates of 1 mm/min before visible cracking occurred. With proper alignment, 4-5 mm/min can be used before cracking occurs, but at these velocities our diameter control degrades. There has been work done on sapphire where the growth rates were as high as 20 mm/min using a pressured helium atmosphere ideally at 15 torr.[56] Unlike other atmospheres, helium gas is not entrapped in the fiber at high growth rates and the exchange gas properties of helium also provide better thermal conditions for growth.[57] Figure 2.1 shows a schematic of the LHPG apparatus with the main components: CO_2 laser, transmissive axicon pair, turning mirror, parabolic mirror, source belt drive, and fiber belt drive.

While growing, a sapphire guide tube is placed on the end of the fiber translator to minimize side-to-side motion of fiber. A laser micrometer sends the diameter at the molten-solid interface to a LabView feedback loop. The feedback appropriately adjusts the fiber motor's velocity in response to the diameter. With this system, we can grow fibers with diameter fluctuations less than 1%, compared with 5% with it turned off. This feedback, as well as the stabilized laser, reduce instability in the molten zone and produce better diameter control.

In his dissertation, Fejer[58] studied the molten zone and showed it is a function of laser power, diameter reduction, and the material being grown. These findings show that the low viscosity of the molten YAG region limits the source-to-fiber diameter reduction to 3:1 to maintain optimal stability.[58, 59] This is reflected in Figure 2.2 where the contact angle at the freezing interface is ~8°±2° for a steady-state growing condition of YAG fibers.[26, 60, 61] Therefore, this limit from the surface tension, requires multiple re-growths of the same fiber to achieve smaller diameter fibers, and the fiber length is only dependent upon the length of the initial source rod available. Fejer's thermodynamic models of the molten zone also found the ideal length for stable growth of the molten zone to be approximately equal to the diameter of the source. This is determined by using different laser power, increasing power will lengthen the molten zone.

The viscosity of a glass follows an Arrhenius dependence on temperature, decreasing gradually as it is heated, allowing it to be pulled into a smooth fiber. SC YAG on the other hand has a non-Arrhenius dependence with a much lower viscosity with a definite phase transition from solid to liquid at the melting point.[62, 63] Since the molten region is held in place simply by surface tension, any air currents, vibrations, laser power fluctuations, etc. will have an effect on the stability of the low viscous molten zone. These disruptions lead to scattering during growth, but can be mostly isolated using a box enclosure to prevent air currents and floating the optical table to dampen vibrations. The laser power fluctuation can be more challenging.

Fejer predicted, and also observed here, that a major contribution to diameter fluctuation during growth is an unstable laser. In Nubling's LHPG design, the laser micrometer was fixed and could not easily be adjusted for different laser powers. This can result in diameter fluctuation as a simple result of the micrometer reading 50 µm above or below the freezing interface if the power changes a few percent. From Figure 2.2, demonstrates the concept of the molten zone length vertically and how it would lengthen with increasing power. This will affect the diameter control response because the laser micrometer will now be reading a diameter in the molten zone that is larger than the true diameter of the fiber.

In Figure 2.1, a schematic of the CO_2 laser has a power meter measuring the power transmitted through a 99.7% reflective mirror from the rear of the laser. This power can be used to stabilize the output power of the laser through a closed feedback loop and keep it from drifting over time. Figure 2.3 shows that the laser requires about an hour to warm-up to reach a stable power. Once warmed-up the power stability is less than 0.5%. Numerous long length fibers have been grown with these stability levels, however, even with laser control on, the laser will occasionally line hop. This produces a sudden increase in power affecting the length of the molten zone and thus the diameter control. Even in the unfortunate scenario where this happens in the middle of growing a fiber, the diameter response will change, but reasonably low losses were still achieved. This was in part due to modifying the laser micrometer to allow for the height to be adjusted during growth without affecting the molten zone, fixing the diameter response.

The laser micrometer, Model 162-100, has remained unchanged and is in fact the same unit installed in 1992. It has the ability to achieve a diameter resolution of 0.1 μm and the measurements are fed through a serial port to a feedback loop to control fiber diameter during growth. This loop is limited to one averaged sample per second. This will result in issues when growing at speeds over 4 mm/min, in part because at this velocity there are 67 μm between averaged readings. This causes the control loop response to the diameter change to be slow. With 2 mm/min as the standard growth speed, the diameter will be controlled to less than 1 %, but frequently will be below 0.5%. Even with this velocity limit when using diameter control, this method has proven to be as good as or better than other diameter measuring methods like camera imaging techniques and interferometry.[52] This is achieved because both can allow for higher feedback loop rates. Figure 2.4 demonstrates the improvements the diameter control loop makes on the fiber diameter variations. The standard deviation with diameter control on is 0.89 and a range of ±3µm, while without diameter control it is 7.71 and has a range of ±25 µm.

Figure 2.5 and Figure 2.6 represent the frequency of the fiber diameter and velocity in a histogram for a 1 meter fiber. Figure 2.5 demonstrates a near Gaussian distribution of the 30,000 diameters sorted into 0.1 µm bin sizes. 99% of the diameters are within 1% of the average diameter 335.0 µm. During growth, this fiber had one dip below 310 µm, presumably due to the source slipping in the belt drive. Figure 2.6 represents the velocity change needed to control the fiber diameter. The velocity is programed to only fluctuate a percentage from the set velocity. For this figure, it was set to 20%, allowing the velocity to vary between 1.6-2.4 mm/min. This parameter is in place to prevent a situation that could result in a portion of the fiber being grown at drastically faster velocities that could induce defects. The obvious result of this is an increase in occurrences at the velocity limits in Figure 2.6. Both figures skew slightly to the right due to a slight miscalculation in the fiber-source ratio.

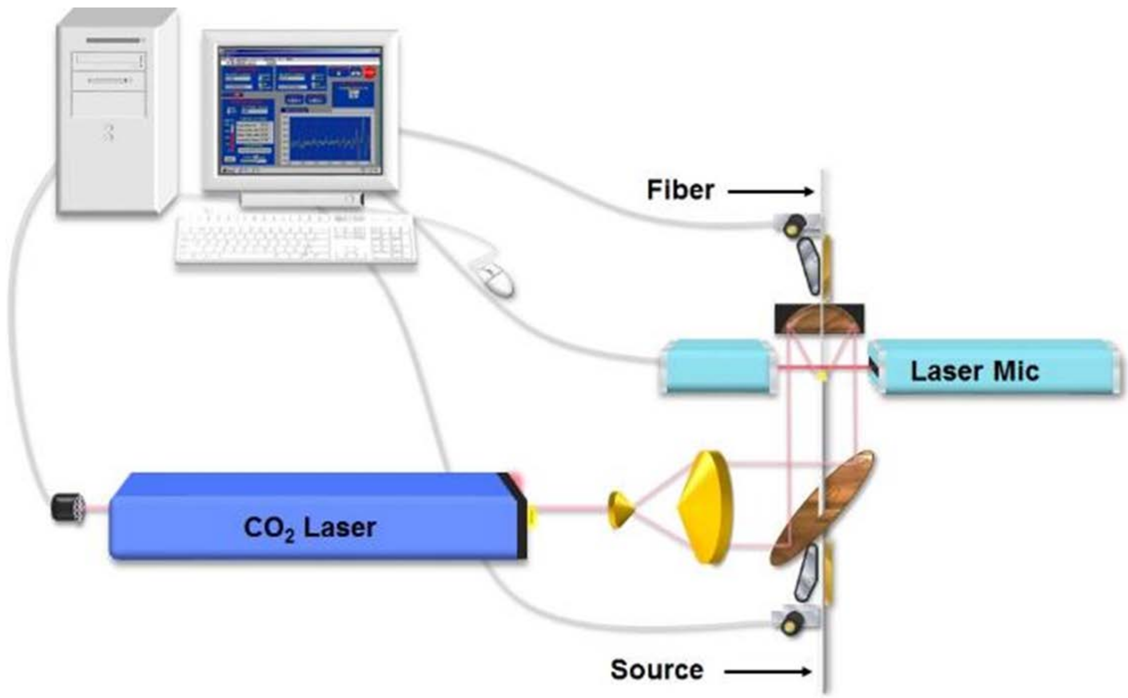

Figure 2.1 LHPG depiction with modified transmissive axicons and CO_2 laser.

Table 2.1 Contamination in Czochralski grown YAG boule, impurity elements are present in the raw powders (Y_2O_3 and Al_2O_3). Data from Innocenzi et al. measured by Northern Analytical Laboratory using spark source mass spectrography.[48] The < are present at the detection limits and where possible interference from clusters of the same weight may have occurred.

Element	**YAG I, ppm**	**YAG II, ppm**
Cl	3	3
Mg	2	2
Si	2	2
S	2	1
Ca	0.5	0.7
Na	0.3	0.4
B	0.2	0.2
F	0.2	0.1
K	0.2	0.2
Ba	<0.09	<0.09
V	<0.07	<0.07
Fe	0.07	0.2
Ce	<0.07	<0.07
Ga	0.05	0.05
Zr	<0.04	<0.04
Dy	0.04	<0.03
P	0.03	0.03
Cr	0.03	0.05
Cu	0.02	0.01
Zn	0.02	<0.01
Ho	0.02	0.01
Mn	0.01	0.007
Ni	0.01	0.01
Tb	<0.01	<0.01
Co	<0.007	<0.007
Total ppm	**10.3**	**11.0**

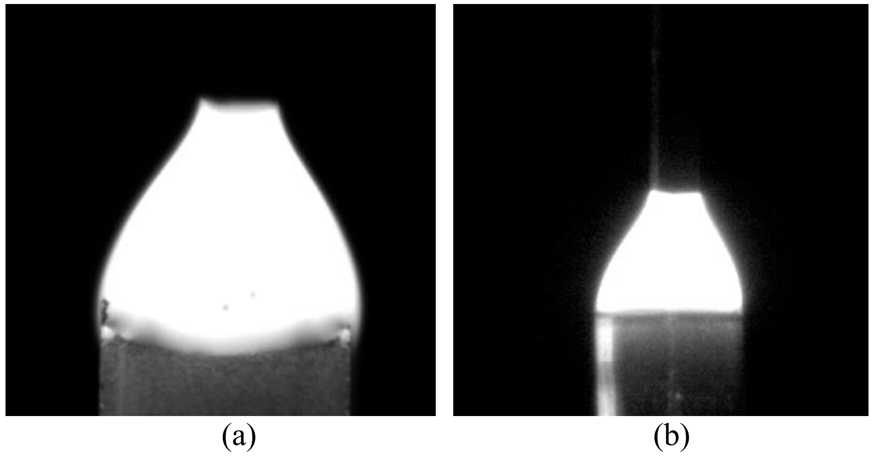

Figure 2.2 (a) Molten zone of a square 1x1 mm YAG source bar into a 300 μm fiber. The square corners of the source can be seen sticking slightly out of the melt. (b) A round 300 μm YAG fiber 'source' grown into 100 μm fiber. From these images it is clear that with increasing laser power that the length of the molten zone will also increase.

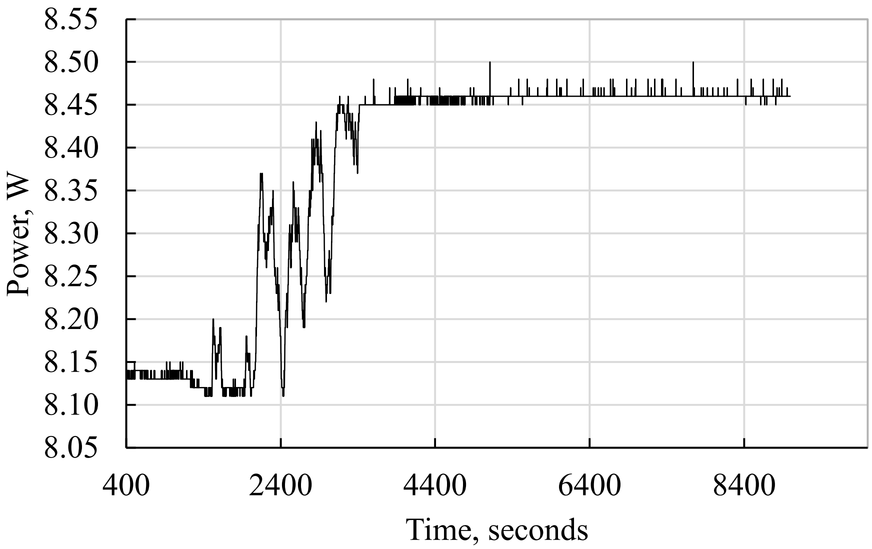

Figure 2.3 CO_2 laser warm up period of one hour before it stabilizes. Once stable, the laser fluctuation is typically less than 0.5% throughout the entire growth.

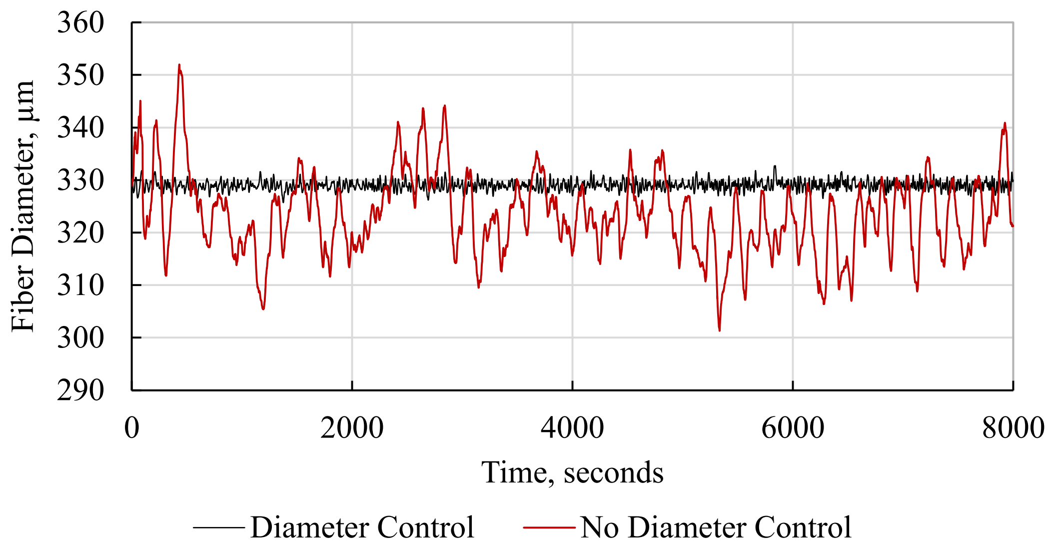

Figure 2.4 Fiber diameter fluctuations over time. The standard deviation with diameter control on is 0.89 and a range of ±3 µm. The standard deviation without diameter control is 7.71 µm and has a range of ±25 µm.

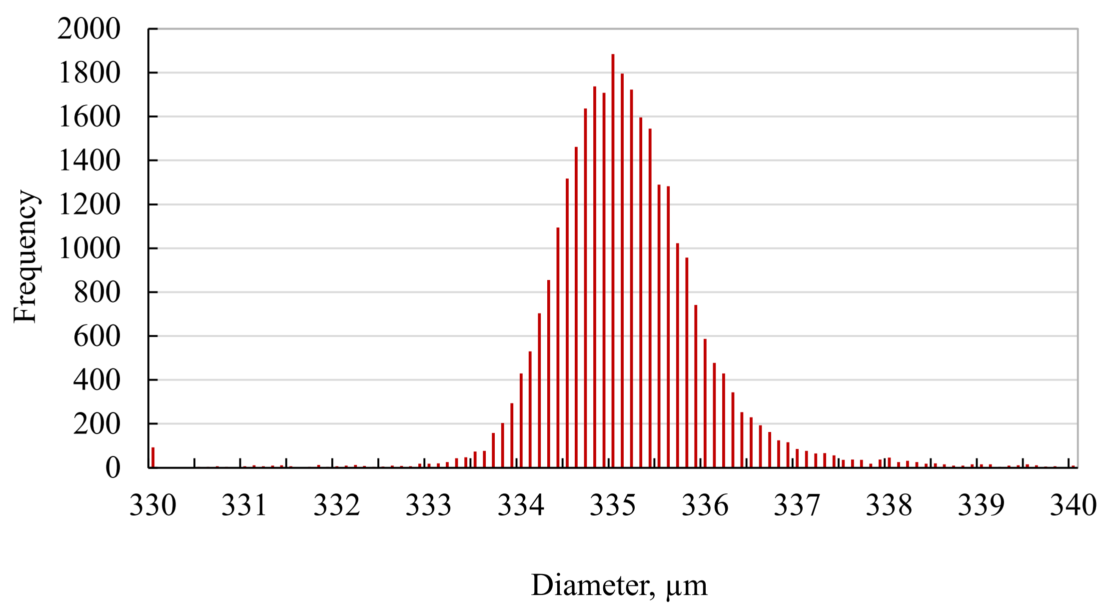

Figure 2.5 A histogram of a SC YAG fiber with ideal diameter control plotted with 0.1 µm bin sizes. The standard deviation of the diameter control was 1.23 µm for the 1 meter YAG.

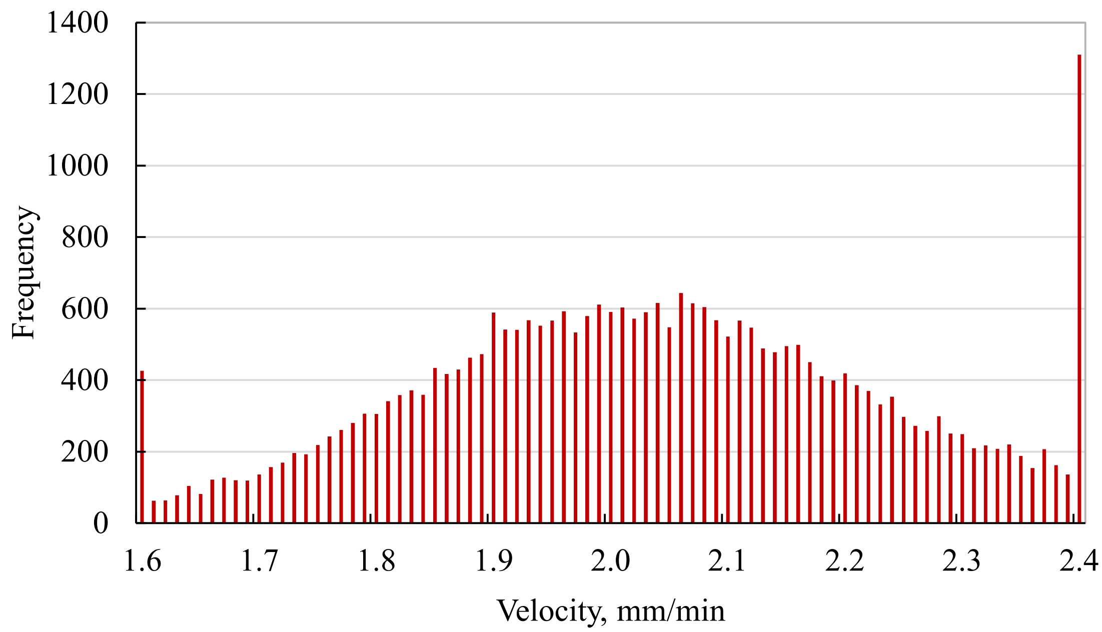

Figure 2.6 A histogram of a SC YAG fiber with ideal diameter control plotted with 0.01 mm/min bin size. Each end has a spike in frequency because the diameter control limits the velocity of the motors, in this case 20% of the velocity.

2.2 Optical Systems

Figure 2.7 illustrates the reflaxicon optical system originally designed by Haggerty.[51] Nubling et al.[23] designed a very similar system, but he made a concave axicon instead of the convex axicon illustrated here. He designed the concave axicon by diamond turning the shape into a ZnSe window and gold coating it. This design improved upon Haggerty's because this left the ring of radiation unimpeded by the convex axicon holder, improving the uniformity of the heat to 360°. Unfortunately, the optic had degraded over the two decades as seen in Figure 2.10. With higher than expected fiber losses being realized, it was decided to replace it with transmissive axicons.

A pair of transmissive axions fabricated out of ZnSe can be used to create the ring of CO_2 light, demonstrated in Figure 2.8. The first axicon will result in a diverging ring diameter, but with a second axicon matching the apex angle of the first, will collimate the light. The distance, *L*, from the second axicon determines the diameter, *d*, of the collimated ring, seen in Equation 2.2

$$d = 2L\tan\left[\left(n-1\right)a\right] \qquad \text{Equation 2.2}$$

where n is the refractive index of ZnSe and α is the angle. These axicons have a matching α angle of 10° and are spaced 12 cm apart for a ring size of 42 mm. This axicon pair resulted in a uniform ring of light seen in Figure 2.9, as well as when the two axicons are misaligned by 1 mm from one another. This cardioid shaped will appear in the axis of misalignment and will worsen over longer path lengths. Therefore, a red HeNe alignment laser was used to minimize this affect over a longer path length than the LHPG needs for growth. However, further tuning was needed once focused on the pedestal. The turning mirror and the parabolic mirror remained from Nubling's design. The turning mirror was a 4x5.66 in. ellipse. The parabolic mirror had a 1 in. focal length.

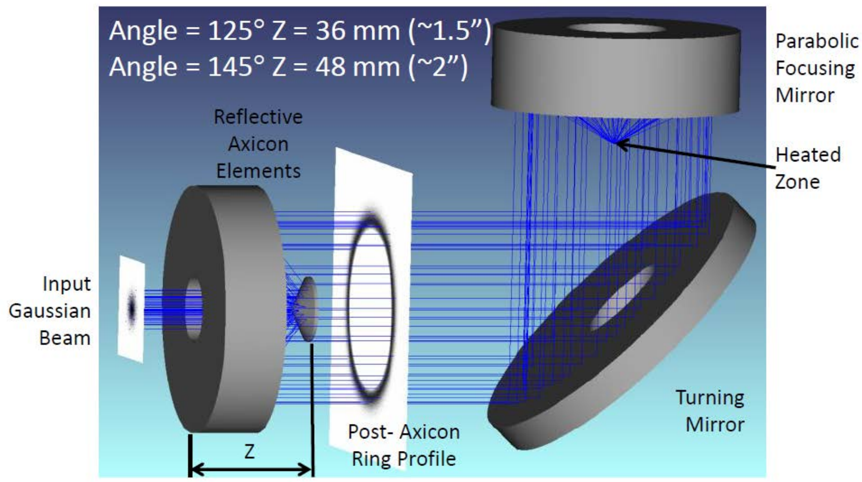

Figure 2.7 Modeling of the original reflaxicon optical components.

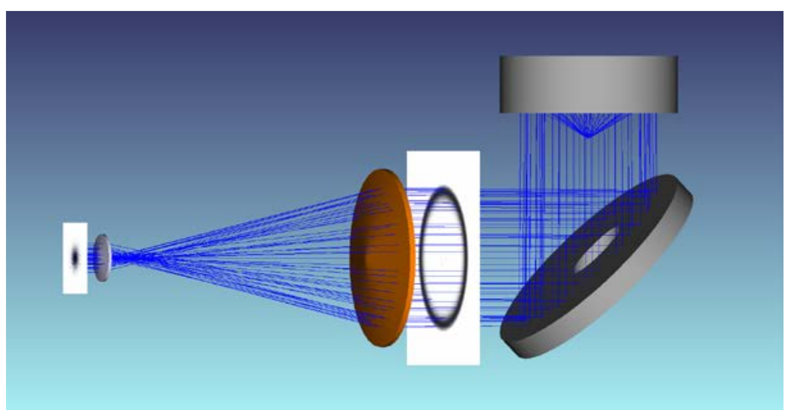

Figure 2.8 Modeling of the transmissive axicons with the same turning mirror and parabolic mirror. The tranmissive axicons have matching conical angles.

Figure 2.9 Modeling of a Gaussian input beam after the two transmissive axicons were properly aligned and misaligned by 1 mm.

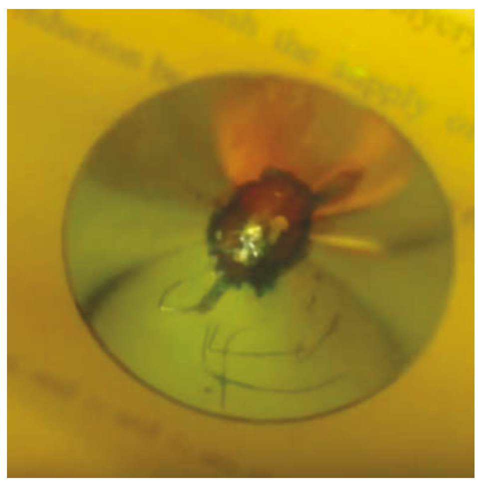

Figure 2.10 Axicon diamond turned into ZnSe window with the existing damage, originally designed by Rick Nubling.[23]

2.3 Modifications to LHPG

Figure 2.11 indicates the improvement in SC YAG fiber attenuation measured at 1064 nm. Fiber lengths vary from 15 to 40 cm, except for the two fibers with low loss at 0.3 dB/m. These fibers were 62 cm and 104 cm and are nearly at the bulk loss of the raw material. These improvements came about after modifications to the optics, procedures, and other LHPG components, all while using the same source material.

Two factors that can affect the quality of the crystal: temperature fluctuations that cause undercooling and thermal stresses at the solidus/liquidus interface. Both can be minimized with improved optical alignment of the LHPG system. The main issue was alignment of an invisible CO_2 beam. The obvious solution of implementing a red alignment laser is only a partial answer. Even with the two beams co-aligned such that both are collimated and have uniform intensity, further alignment is needed to have a perfectly aligned system. Figure 2.12 is an optical image of the molten zone viewed from above with the source bar above the focus, resulting in the dark spot in the center. The asymmetrical image would represent alignment that is close, possibly from only using an alignment laser, but it is clearly not ideal, especially when compared to the symmetrical image. The LHPG technique will grow fibers when the alignment is asymmetrical, but the quality of the crystals suffers as a result. The asymmetry results in different thermal gradients within the fiber as it is grown. This was evident in the measured loss values in Chapter 4. This asymmetrical misalignment was not initially observed because the CO_2 ring remained collimated and uniformly distributed over much longer path lengths than the LHPG system required. This new imaging angle demonstrated that there could be microns of misalignment between the two axicons and the collimation and intensity would remain unchanged over long path lengths (3 m), but at the focus the symmetry was changed.

This imaging technique was critical in the ability to improve the alignment, and it was possible because the camera imaging system was replaced and upgraded. Initially, there was a long-distance microscope, but this only provided an image from one axis. Therefore, a flip mirror was set up that allowed me to image the molten zone from two axes offset by 90°. This still only allowed me to view one direction at a time and during the alignment process. It was critical to be able to see the molten zone interfaces, both the bottom and top, from both angles to know if the source was truly centered and if the CO_2 was uniformly radiating the source.

The solution to the two axis problem was to buy two cameras allowing for both angles to be view simultaneously. With the digital camera, the gain and exposure time can be changed revealing the molten zone in different ways. For example, these settings can be increased to see if there is any scattering occurring in the newly grown fiber or decreased to get crisp molten zone lines. The smaller, more compact size and much shorter (9 cm) focal length allowed for the camera to temporarily be mounted above the molten zone, to view the alignment of the radiation as it approaches the focus. These new cameras allowed Figure 2.12 to be imaged and the final tuning of the alignment to be performed.

Besides the important alignment process and improving it, the second most important modification made to the LHPG system was the laser micrometer mounting. It was previously in a permanent position and the parabolic mirror had to be moved microns in the vertical axis. This did not allow for adjustments to the laser micrometer's reading position to be made during growth. To remedy this, the laser micrometer was removed from its fixture and placed on two vertical translators. Because it is a noncontact measurement, the position could then be adjusted during growth.

There were numerous other small changes, from replacing XY translation stages, the source motor was raised up to allow for longer length fibers to be grown, and replacing the reflaxicon optical system with the transmissive axicons. But the final improvement came most recently in part because of the increased magnification from the new digital cameras. At this time, fiber losses had improved to around 1 dB/m, and while growing a fiber, shifting from side-to-side in the molten zone became more easily evident over long periods. It was decided that shifting could be a partial cause of the remaining loss, evidence of these irregularities can be seen in Figure 2.13. The irregularity is not a diameter control issue, in fact, the diameter remains controlled, but instead the fiber shifts and the crystal starts to grow with a slight microbend that then straightens out again. They are small shifts, especially when compared with the diameter of the fiber, but if these microbends were to continue it could account for a significant percentage of the remaining fiber loss.

Previously, a 300 μm fiber would be grown in a 400 μm inner diameter guide tube, but this would allow for up to 100 μm extra space for the fiber to shift from side-to-side. The extra space was initially the procedure in part, because at the time the fiber growth would terminate when growing in a tight fitting guide tube. This was due to a slight misalignment in the LHPG system that resulted in fibers curving and either jamming or breaking in the guide tube. Thus, the larger guide tube allowed me to grow crystal fibers, but the new alignment procedure allowed me to improve the cylindrical geometry to further improve the fiber losses. With the amended protocol was in place, much straighter fibers were being grown allowing for a much tighter fit between the fiber and the guide tube, resulting in approximately 20 μm space for the fiber to shift.

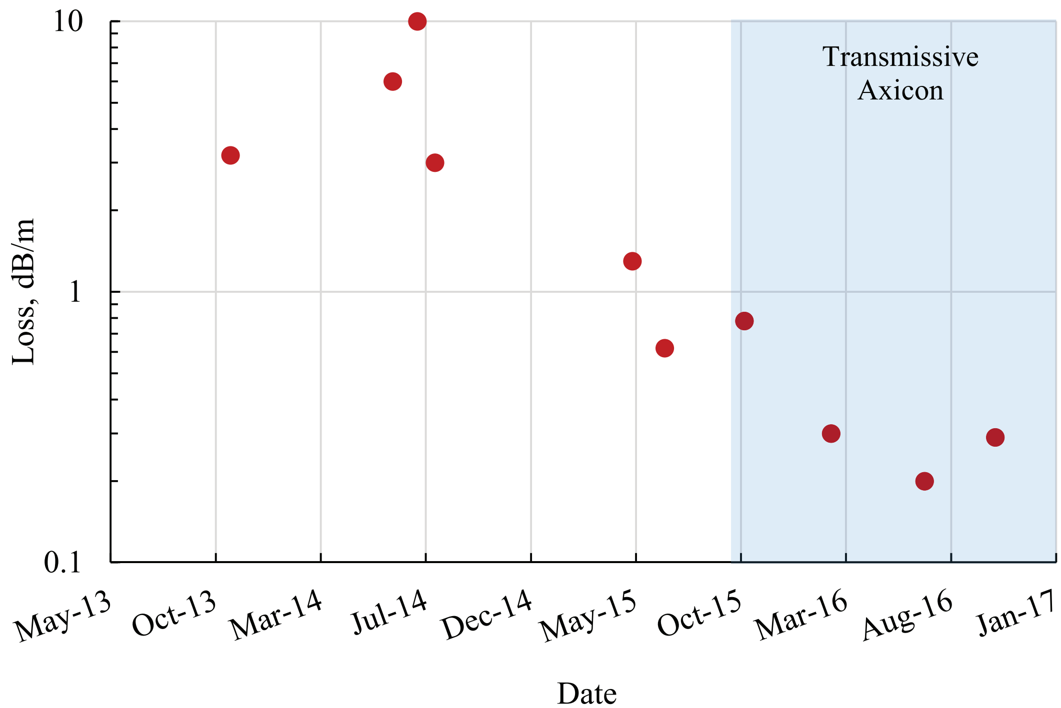

Figure 2.11 The improvement of SC YAG fibers measured at 1064 nm. Fiber lengths vary from 15 to 40 cm, except for the two fibers with low loss at 0.3 dB/m. These two fibers were 62 cm and 104 cm and are nearly at the bulk absorption loss of the raw material, but these losses are still much greater than the intrinsic loss.

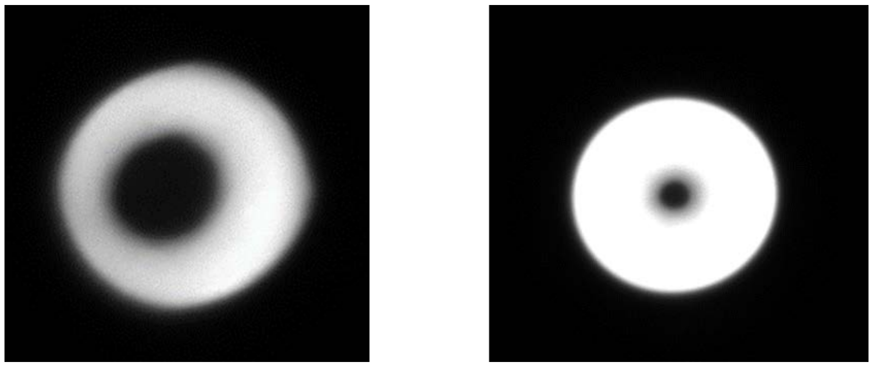

(a) (b)

Figure 2.12 Camera image of the molten zone, 1 mm diameter, taken from above with (a) slightly asymmetric alignment and (b) very well aligned, resulting in symmetric heating. These assessments were only possible using the new camera imaging system.

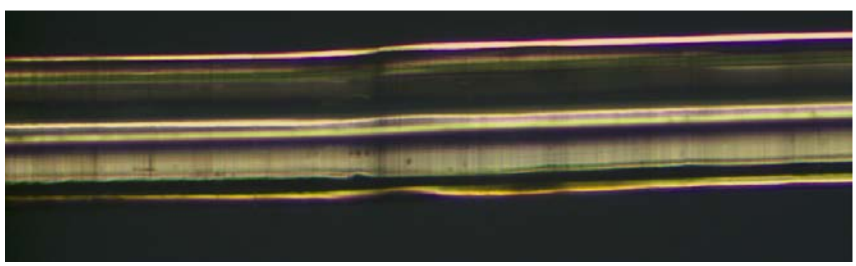

Figure 2.13 Microscope image, lit from below. The irregular fiber geometry in the center, with constant diameter was caused from a fiber translation issue in the belt. It can be minimized by using a tighter fitting guide tube to prevent side-to-side translation during growth.

2.4 Defects in YAG crystals

Geometric fiber irregularities will naturally occur in cylindrical fiber shape. One such irregularity are microbends and Section 2.3 discusses how they can be minimized with a tighter fitting guide tube. Another type of irregularity, seen in Figure 2.14, occur where obvious facets and an apparent diameter change can be seen. However, upon closer observation, the diameter remains unchanged and only the top edge is transmitting light differently from below. The cause of this cylindrical lensing affect or its effect on loss is not certain, but effort was made to create as uniform of a fiber as possible. Especially, once a fixed seed orientation was used to provide a standard cross sectional shape, then fibers could be inspected at full length and see that minimal irregularities occurred. This is discussed further in Chapter 4.1.

When growing other crystals from the melt, a balance between the number of vacancies and interstitials can be achieved by controlling the growth rate of the crystal. For example, in silicon grown by Czochralski technique at high pulling rates, vacancies increase and can form octahedral voids on the order of 100 nm.[64]

Dislocations have not been studied in LHPG grown YAG, but have been studied in Czochralski grown YAG, as well as other crystals at various diameters. The number of dislocations has been observed to decrease with decreasing diameter, but dislocation loops are still present.[65] At very small diameters, they even observed a complete absence of dislocations, attributing this affect to the reduction of thermal stress generated during cooling at smaller diameters. During the tapering down process of Czochralski growth silicon, x-ray topography has been used to demonstrate the dislocations that were removed at smaller diameters.[66, 67] For YAG boules, chemical etching has revealed an estimated 10^4 dislocations per cm, with even fewer in the center of the boule.[68, 69] Also, as stated, there should be even fewer dislocation at the 200-400 μm diameter range per unit area.

The contamination in the raw powders result in approximately 10 ppm when using 99.999% pure materials. This is believed to be the reason for the significantly higher absorption loss than theory predicts. In silica glass fibers, 1 ppm of Fe^{+2} can result in an estimated absorption coefficient of 0.02 dB/km.[70] The data from Innocenzi and Mann are isolated from Figure 1.6 and plotted in Figure 2.15 with absorption loss as a function of wavelength. Recall the characteristic V-curve with a minimum loss of 0.04 dB/m at 3.0 μm, therefore it would be expected for the absorption loss to be approximately 0.1 dB/m at 2 μm. These absorption loss values are the goal for the SC fibers, with minimal scattering from irregularities, cracking, or index inhomogeneity. Figure 2.16 demonstrates a very high-loss SC YAG fiber grown before any of the modifications were made. It exhibits interior cracking and facets isolated to one side; both are products of poor alignment. Figure 2.17 represents what the entire fiber length should ideally look like.

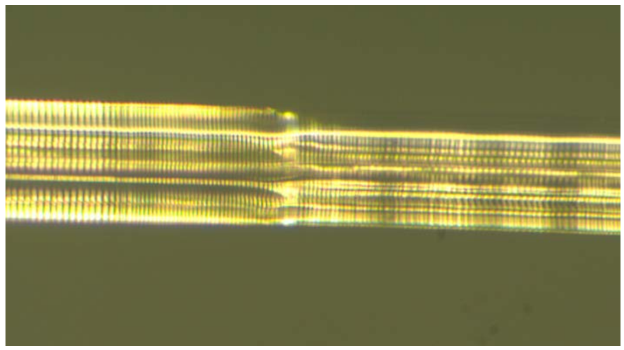

Figure 2.14 A bright-field microscope image lit from below of a 0.5% Ho:YAG fiber 250 μm diameter with obvious facets and an apparent diameter change. However, upon closer observation the diameter remains unchanged, only the top edge is not transmitting light, presumably due to a change in fiber cross-section during growth.

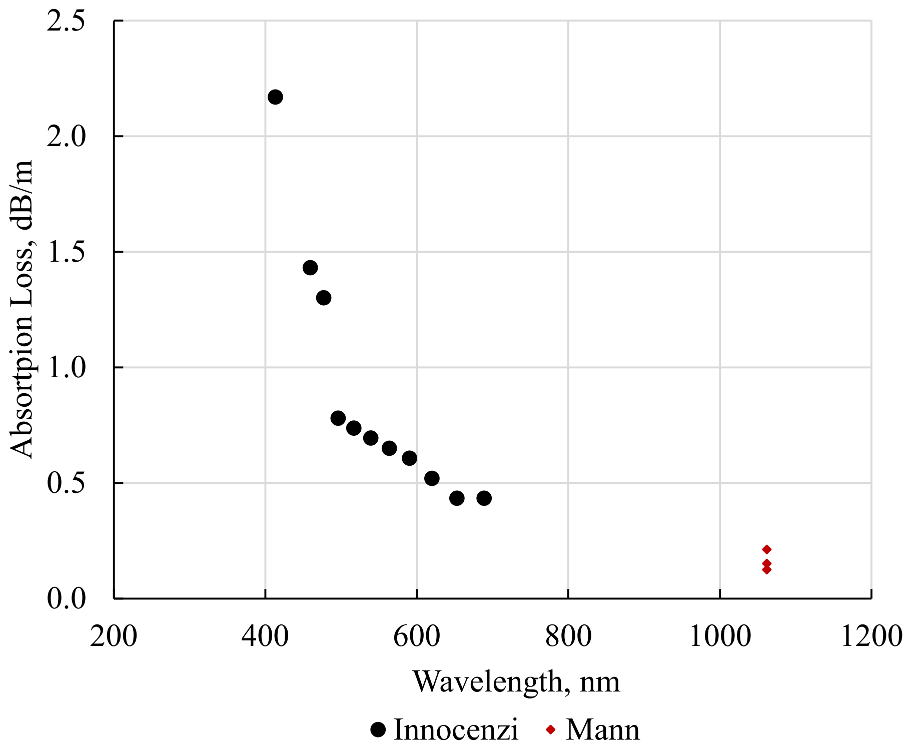

Figure 2.15 Absorption data from Innocenzi and Mann demonstrating the minimum loss at various wavelengths. Contamination in the starting materials seem to be the current absorption limit, but not the intrinsic limit.

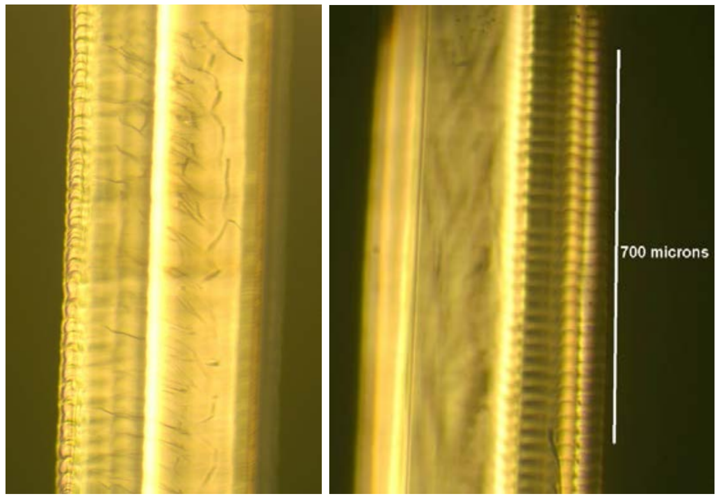

(a) (b)

Figure 2.16 (a)(b) Microscope images of a SC YAG fibers first grown by the LHPG. Obvious internal cracking was visible during growth without a microscope. (b) The average facet spacing was approximately 23 μm.

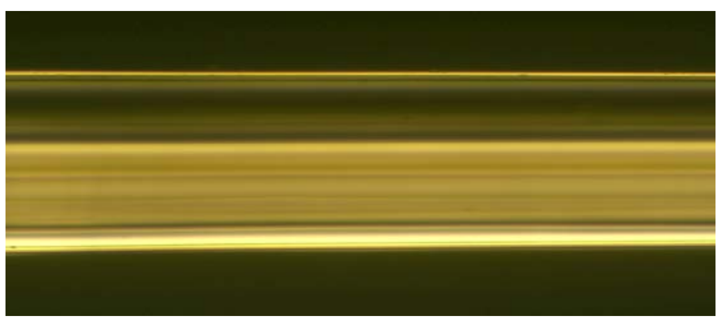

Figure 2.17 Ideally uniform SC YAG fiber with 330 μm diameter lit from below. Irregularities will result in the light transmitting through to be less uniform.

2.5 Graded Index Profile/modeling

The RiT method has been used in pulling viscous glasses for the purpose of developing a graded index or a step index fiber. Here, the glass only needs to reach its glass transition temperature so either profile is possible, depending on the designed RiT.[71] For the first time, adapting RiT has been attempted for the LHPG technique. The main issue results from the melt of YAG being a very low viscosity, especially compared to glass. This, plus the fact that crystals are grown at slow speeds compared to fast glass pulling, leads to diffusion being controlled by the duration in the melt. Therefore, by using a 50% erbium doped YAG core and YAG tube, it is our desire to develop a graded index of refraction by having the erbium be radially distributed, with higher concentrations in the center. Thus, the growing rate must overcome the rate of diffusion for the fiber not to diffuse to equilibrium.

A SC YAG source rod, approximately 1.1 mm in diameter, was initially cut into one centimeter long sections. These sections were then mechanically drilled with an inner diameter of approximately 550 μm, at which point a 50% erbium doped YAG fiber was inserted inside the tube, with the expectation of more erbium remaining in the core. The essential question presented by this experiment became, "What effect will distributing the erbium ions have on the index?" A study done by Onyx Optics used interferometry to measure the change in refractive index of RE doped YAG and undoped YAG.[72] They determined the Δn for 1% RE doped YAG, and then, by extrapolating a linear increase, demonstrated the Δn with greater RE concentration for neodymium, holmium, and erbium in Figure 2.18. This extrapolation was also confirmed by a research group that replaced all the yttrium ions to form ErAG the index increased by 0.022.[73] However, it is more realistic to expect a Δn in the range of 0.001-0.0025 for this diffusion process. This range is possible with only a 5-10% radial change in erbium concentration. This range in index change is in agreement with other groups that suggest a suitable cladding material would be undoped YAG with a Δn ≈ 0.0013 in addition to using a secondary glass outer cladding.[74] It is also pointed out that this low Δn will potentially yield an ultra-low NA that should lead to a single transverse mode.[75]

Three types of index profiles were calculated as possibilities for the graded index fiber seen in Figure 2.19. The calculations were performed for a circular cross section, diameter 370 µm for q = 1, 2, and 100. The latter would indicate a profile very near a step index with no graded index. These calculations follow from Equation 2.3, where n_1 is the index of the core, *a* is the radius, Δ is $(n_1-n_2)/n_1$, and *q* is the modeling profile parameter. The parameter q has been addressed for two values, q=1 a linear index change, and q=2 a parabolic index change will occur. Both of these are possible diffusion configurations.

$$n^2(x) = n_1^2\left(1-2\Delta\left|\frac{x}{a}\right|^q\right) \qquad \text{Equation 2.3}$$

These index profiles should be indicated by the Er^{3+} ions diffusing outward into the pure YAG during the LHPG process. Therefore, time in the molten zone has the largest impact on diffusion, with temperature held constant. The two most controllable factors that affect the duration molten when using constant temperature, are changing the diameter of the grown fiber and/or changing the growth velocity. Both of these are limited, because the larger diameter grown, the less length produced from the preform, and at too fast of growth velocities the fiber quality begins to degrade. Multiple tubes can be stacked on top of one another, but a continuous growth between them is not currently possible because of surface tension pulling the tubes apart as it approaches the end.

With these graded index profiles, the question of what coupling conditions are needed for light to be refracted rather than reflected became apparent. Figure 2.20 indicates that for a fiber diameter of 370 μm and an index change of 0.001, that an angle <3.4° must be coupled into the fiber. The amplitude, on y-axis, refers to the radial distance the light will propagate from the center of the fiber before the light is fully refracted back to the center of the fiber, much like a sinusoidal function. If the change in index is increased to 0.003 then an angle <5.7° must be coupled into the fiber seen in Figure 2.21. In either case at larger launch angles the light will be refracted out of the fiber. The maximum angle in both of these cases is independent of which modeled index profile is used because both intersect when the radius of the fiber is reached. The linear parameter is slightly more ideal because it remains at a lower amplitude for the same coupling angle. As Figure 2.20 and Figure 2.21 indicate, with smaller launch angles the refracting light has smaller amplitudes, therefore, confining the light to narrower core. The calculations were made from Equation 2.4 and 2.5 for the linear parameter. For the Figure 2.20 and Figure 2.21, only the peak amplitude was of interest, which occurs at ¼ z_p, where z_p is the period, a is the radius, and the propagation constant, $\overline{\beta} = n_1 \cos\theta$, θ is the angle inside the fiber. These equations assume a circular cross section, a meridional ray path, and no small random variations of the refractive index along the fiber axis. Equation 2.6 was used to calculate the amplitude for the parabolic parameter. Here, the equation is simplified for the peak amplitude because when z= ¼ z_p, the sine function equals 1.

$$x(z) = -z^2 \frac{n_1^2 \Delta}{2a\bar{\beta}^2} + z \frac{(n_1^2 - \bar{\beta}^2)^{1/2}}{\bar{\beta}}$$
$$x > 0; \quad 0 < z < \frac{1}{2} z_p$$ Equation 2.4

$$x(z) = \left(z - \frac{1}{2} z_p \right)^2 \frac{n_1^2 \Delta}{2a\bar{\beta}^2} - \left(z - \frac{1}{2} z_p \right) \frac{(n_1^2 - \bar{\beta}^2)}{\bar{\beta}}$$
$$x < 0; \quad \frac{1}{2} < z < z_p$$ Equation 2.5

$$x(z) = \frac{a \sin \theta_1}{\sqrt{2\Delta}} \sin\left(z \frac{n_1 \sqrt{2\Delta}}{a\bar{\beta}} \right)$$ Equation 2.6

Utilizing the RiT method, a radial distribution of erbium in SC fibers is expected if grown before diffusion equilibrium occurs, with an expectation that more erbium would remain in the core of the fiber. In order to achieve this, the growing rate would need to be sufficiently fast to overcome diffusion equilibrium. It is expected that erbium will diffuse sufficiently to be present at the periphery.

There is currently no published value for the diffusion of erbium in YAG, but there is literature on the self-diffusion of yttrium in YAG. Because of its size, it has the smallest ion diffusivity in a YAG crystal when compared to oxygen and alumina. Erbium has a very similar ionic radius and can be 100% substituted into the yttrium site to form SC ErAG. It is therefore expected for the diffusion coefficient of erbium to be very similar to yttrium in YAG, 5.59 x 10^{-9} m^2/s.[76] At this time, this graded index design would remain air-clad, therefore at a radius of 185 μm the index would drop to 1. It is possible for a secondary glass clad to also be applied, similar to glass fiber applications.

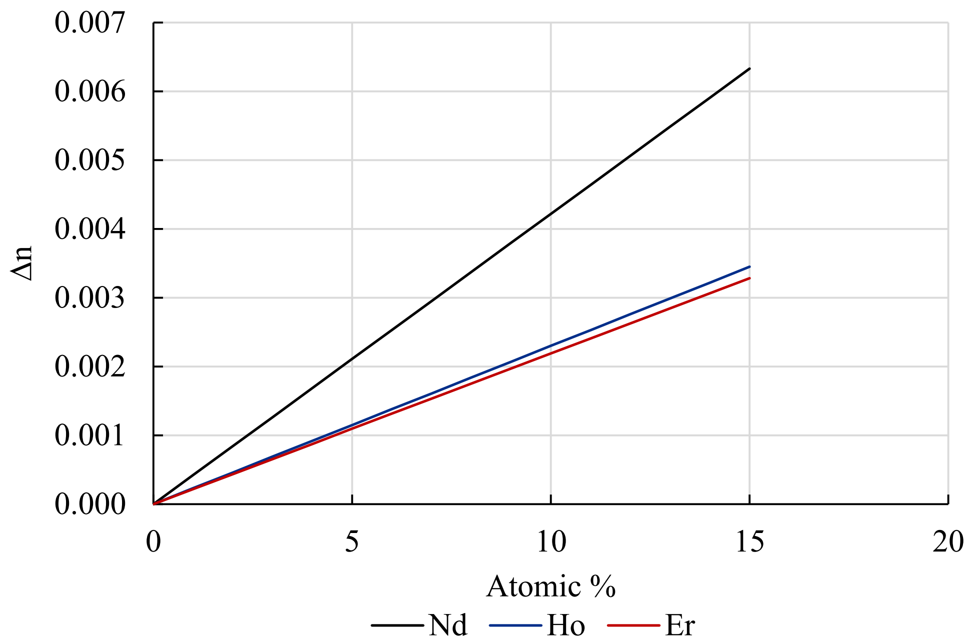

Figure 2.18 The change in erbium concentration and the change in refractive index.[72]

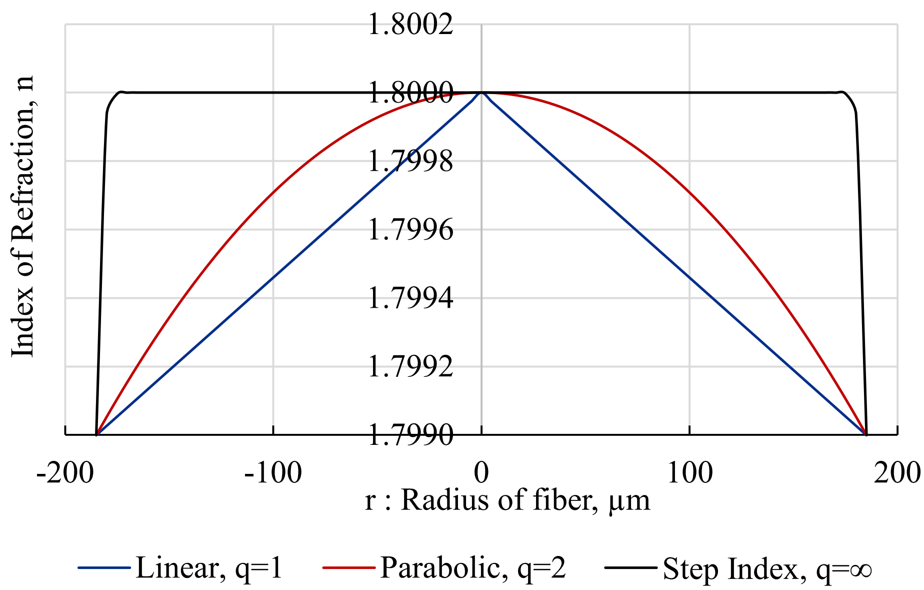

Figure 2.19 Index profiles calculated with an index change of 0.001 at 2 μm.

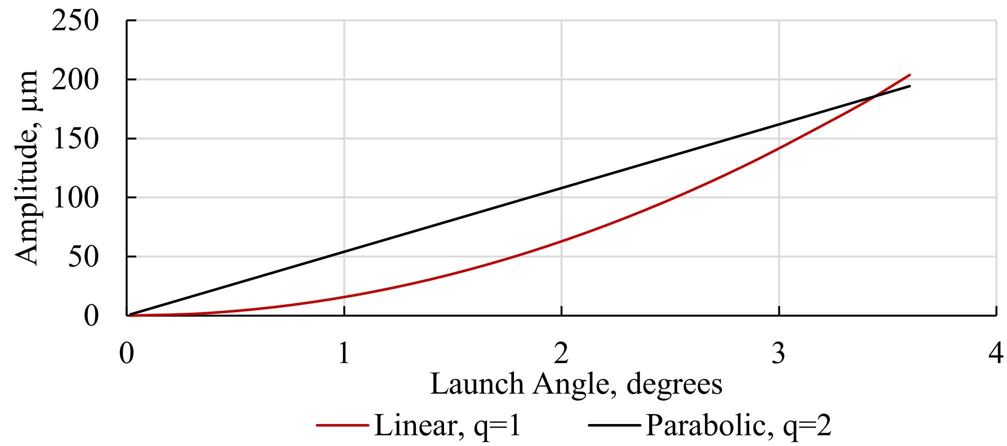

Figure 2.20 Theoretical calculations of two types of index profiles for a conservative Δn=0.001. The model shows that for a 370 μm fiber the highest order modes will have an amplitude of 185 μm when the coupling angle into the fiber is 3.4 degree.

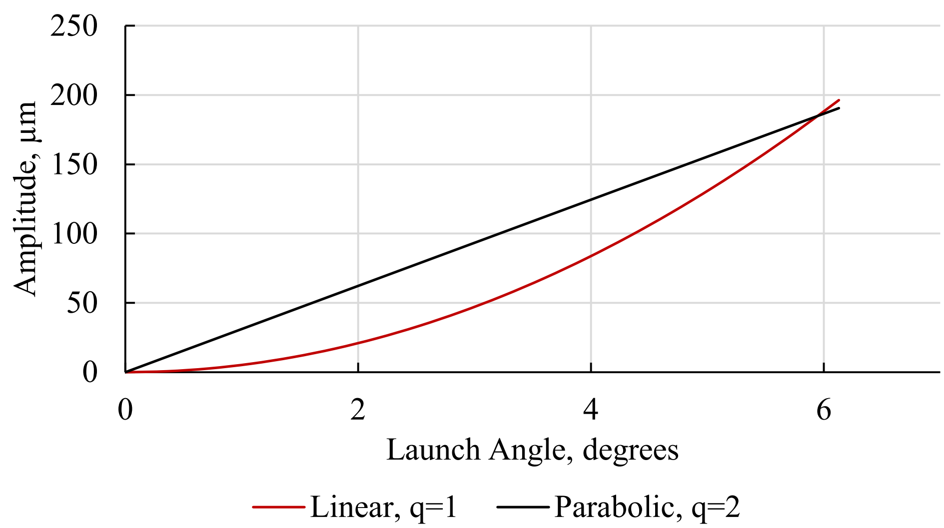

Figure 2.21 Theoretical calculations of two types of index profiles for a conservative Δn=0.003. The model shows that for a 370 μm fiber the highest order modes will have an amplitude of 185 μm when the coupling angle into the fiber is 6 degree.

Chapter 3. Experimental Procedures

3.1 Lasers and Profiles

Four lasers were used for the characterization of these SC YAG fiber. The characterization included total attenuation measurements, scattering measurements, and occasionally beam profiles of the light transmitted through the fiber. Below in Figure 3.1 through Figure 3.8 the laser profiles are shown in both 2D and 3D. An Ophir Spiricon profiler, model SP503U with half inch image format was used. It has a spectral response from 190 – 1100 nm with an accuracy of beam width of ±2%.The laser wavelengths are 532 nm, 635 nm, 808 nm, and 1,064 nm. All four are laser diodes from OptoEngin LLC. The advertised specifications of the 532nm and 1064 nm lasers are to have a TEM_{00} mode, but the profiler indicates that the 1064 nm is slightly skewed. The 808 nm laser is supposed to be near TEM_{00} and the 635 nm is supposed to have a beam spot that is 'round' as defined by manufacturer. Figure 3.3 shows the intensity of the 635 nm laser is 'round' because how multimodal it is.

Table 3.1 indicates its high degree of divergence. For these reasons the 635 nm laser is not used for all laser measurements because of inconsistent results.

Table 3.1 also indicates the output power and beam diameter of each laser. Figure 3.9 indicates how the SM laser is converted to the multimode profile when coupled through a short, 20 cm, 330 μm SC YAG fiber.

Table 3.1 Diode lasers from Opto Engine LLC.[77]

	Output power	**Mode**	**Divergence**	**Beam Diameter**
532 nm	~50 mW	TEM_{00}	<1.5 mrad	8 mm
635 nm	~50 mW	Round	<8.0 mrad	30 mm
808 nm	~100 mW	Near TEM_{00}	<1.0 mrad	10 mm
1064 nm	~210 mW	TEM_{00}	<1.5 mrad	15 mm

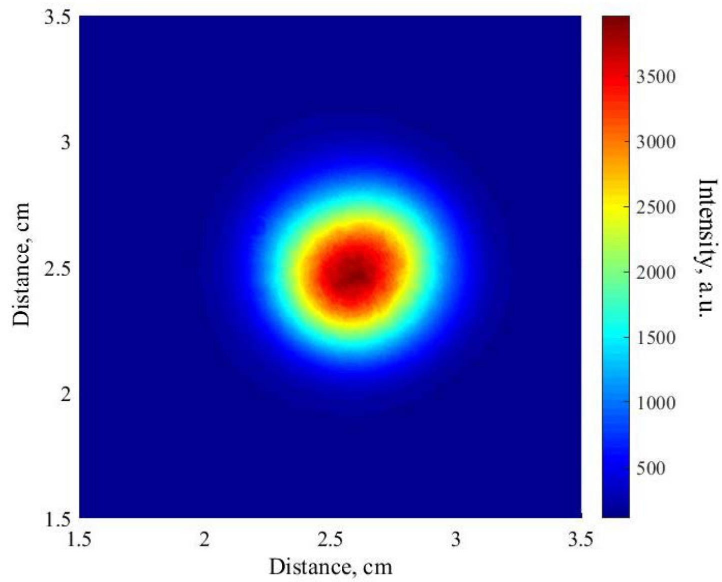

Figure 3.1 Mode profile of the 532 nm laser at full power.

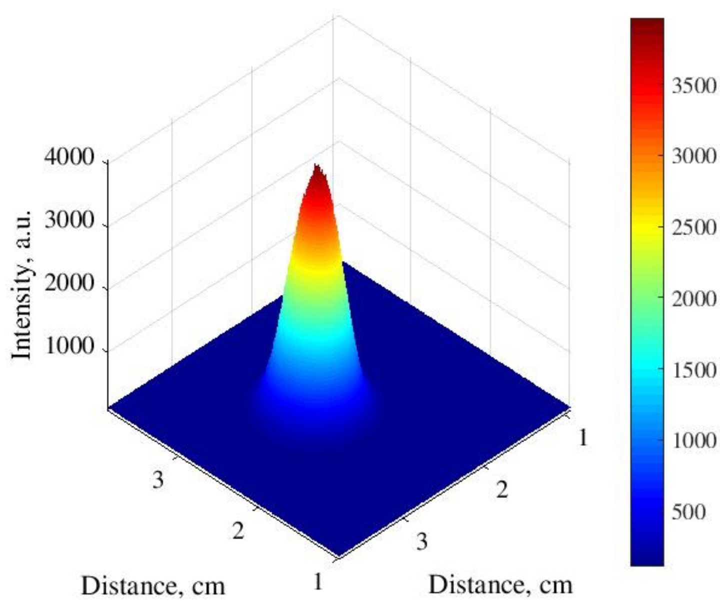

Figure 3.2 3-D mode profile of the 532 nm laser at full power.

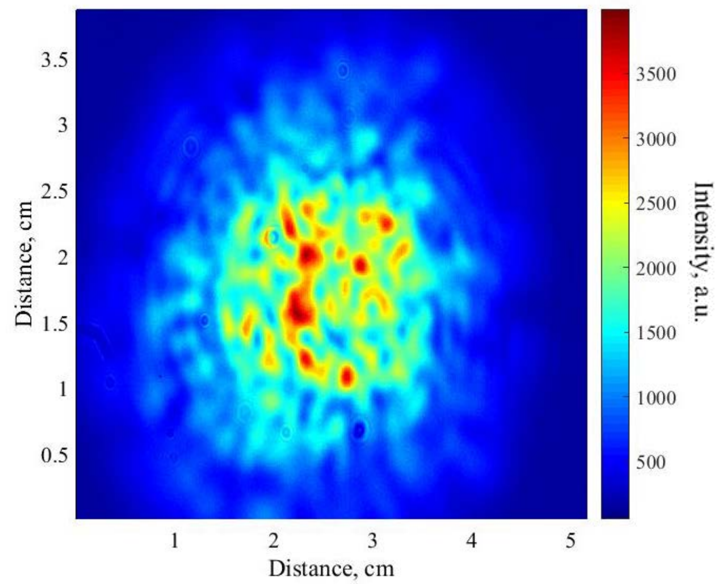

Figure 3.3 Mode profile of the 635 nm laser at full power.

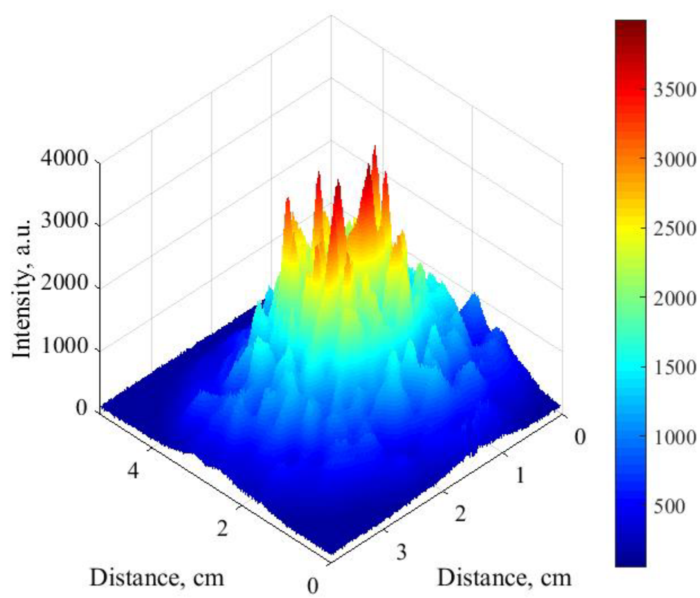

Figure 3.4 3-D mode profile of the 635 nm laser at full power.

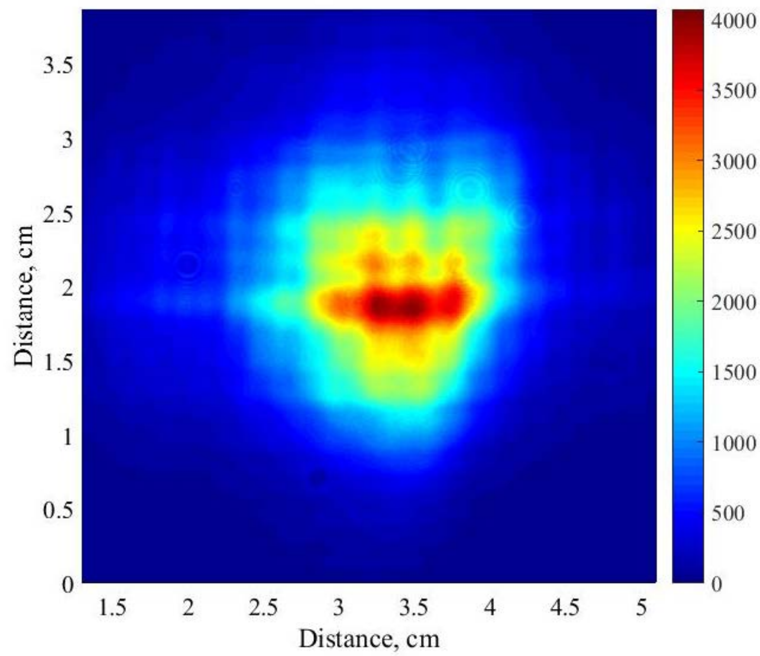

Figure 3.5 Mode profile of the 808 nm laser at full power.

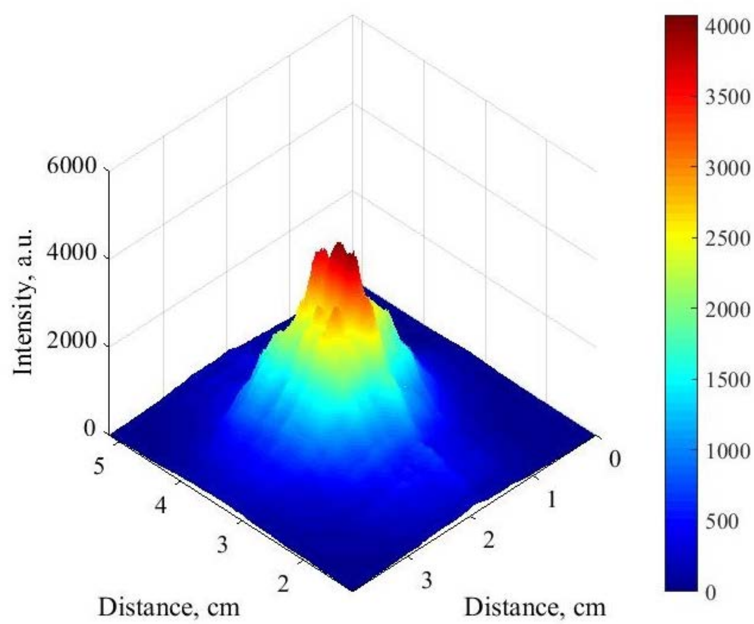

Figure 3.6 3-D mode profile of the 808 nm laser at full power.

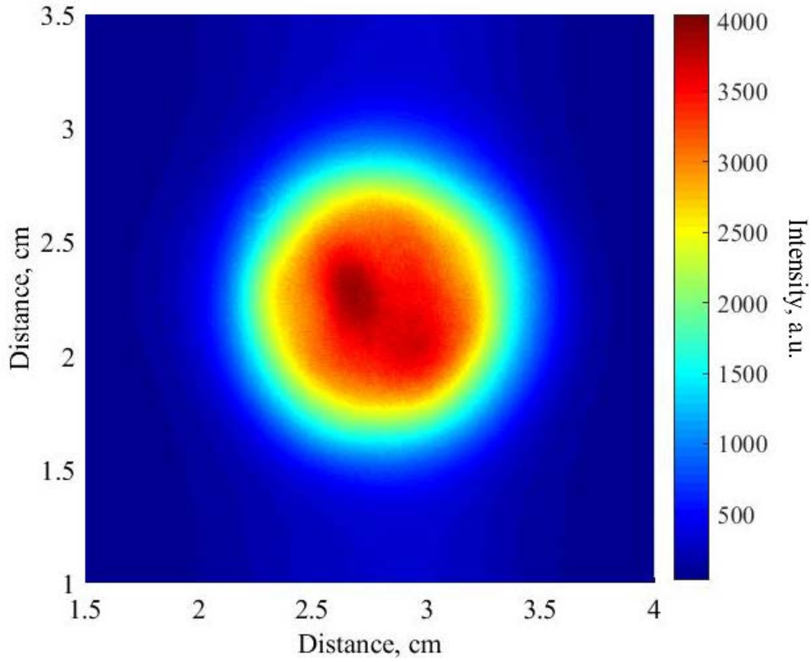

Figure 3.7 Mode profile of the 1064 nm laser at full power.

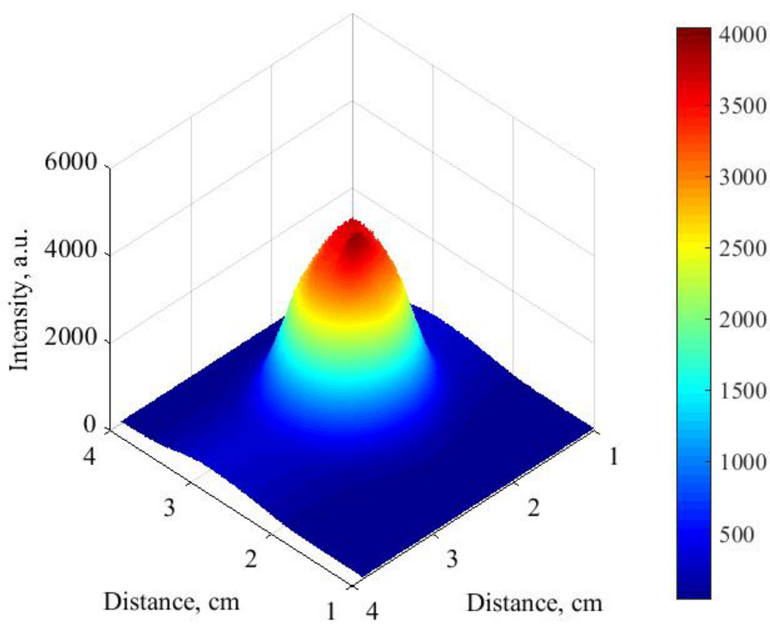

Figure 3.8 3-D mode profile of the 1064 nm laser at full power.

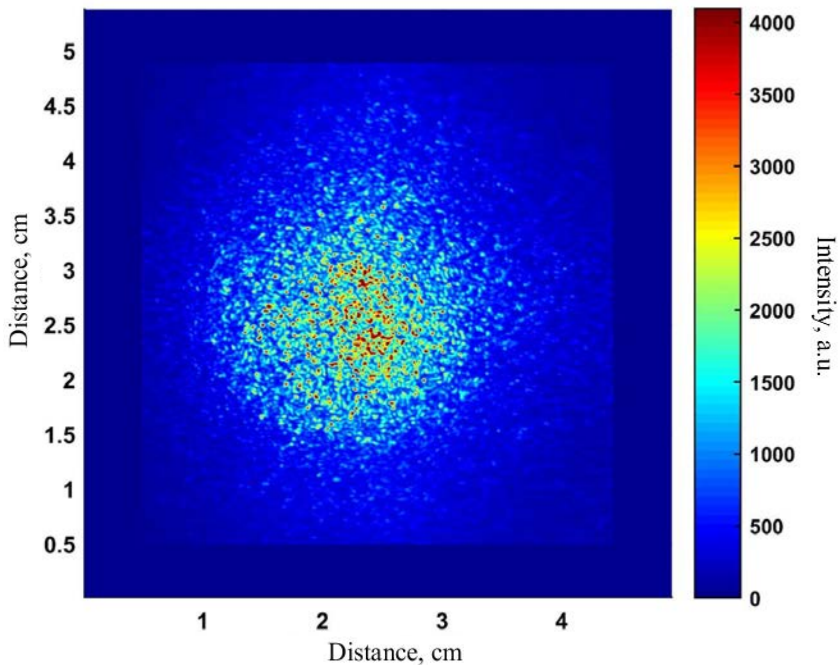

Figure 3.9 Multimodal profile of a Nd:YAG laser, 1064 nm, propagating through a SC YAG fiber 20 cm long.

3.2 Total Attenuation Measurements

The theoretical NA of a traditional step index fiber is given by the equation NA= $(n_{core}^2 - n_{clad}^2)^{0.5}$ where n_{core} and n_{clad} are the refractive indices of the core and cladding, respectively. However, for the current air clad YAG fibers the theoretical NA > 1 with a refractive index 1.82 at 1 µm. This means that in theory all rays of light incident on the front input face will be transmitted into the YAG fiber. The V number conventionally used for step index fibers is a dimensionless parameter and is defined in Equation 3.1.

$$V = \frac{2\pi}{\lambda} aNA = \frac{2\pi}{\lambda} a\sqrt{n_{core}^2 - n_{cladding}^2} \qquad \text{Equation 3.1}$$

where *a* is the radius. For an unclad SC YAG fiber 330 µm diameter, at a wavelength of 1.064 µm the V number is approximately 900. By using the multimode approximation of $M \approx V^2/2$, an estimated calculation of the number of modes is 0.4 million modes. Figure 3.9 demonstrates these SC YAG fibers experimentally profiled to be very multimodal. This makes analysis of attenuation more difficult, because the total attenuation is the average loss of all the modes. It does not differentiate between low and high-order modes, but higher order modes will inherently be more likely to refract out of the fiber.

The total attenuation, α_T, are a sum of the scattering, α_s, and absorption, α_a, losses seen in Equation 3.2.

$$\alpha_T = \alpha_s + \alpha_a \qquad \text{Equation 3.2}$$

Scattering loss can be broken into bulk scattering, α_{bs} and surface scattering, α_{ss}, seen in Equation 3.3. Determining which type is the dominant scattering mechanism has proven difficult, but in the end fiber irregularities were causing light to couple out of the fiber. Light propagating in a fiber optic cable is governed by the following and thus affects the attenuation: the wavelength of light, angle of incidence, indices of refraction of the core and cladding, length, bending radius, size of the core, design of the core and cladding, fiber variations, as well as a few others.[78] These factors are relevant and studied for SC YAG fibers as well.

$$\alpha_s = \alpha_{ss} + \alpha_{bs} \qquad \text{Equation 3.3}$$

The total attenuation of light transmitted through the SC YAG fiber was determined by using a combination of four different laser wavelengths. Measurements were taken in both the NIR and the visible spectrum, however the current main wavelength range of importance is in the NIR. Fibers measured ranged in length from 10-120 cm. The fibers of longer length will be more accurate, but upon the start of this project the length of fibers grown were much shorter about 20-30 cm. Since then modifications have been made to allow a maximum length of about 65 cm to be grown without posting the source bar. The limit of fiber length is only due to the length of the source bar.

The laser profiles can be seen in the figures above. They are all nearly SM, with the red laser being less consistent. The power was unstable and the mode was not only inconsistent but highly divergent. For these reasons the measured attenuation was unreliable and the red laser was not used for measurements. Each laser is aligned on an optical table and a borosilicate lens is used to couple the light into the fibers. The lens has a focus length of 9 cm. The high index of YAG and the absence of a material cladding allow for all angles of light to be accepted into the fiber, with a small critical angle. This allows all angles greater than ~33° to propagate, resulting in a highly multimode fiber.

Two different methods of obtained the total attenuation were used. First, is the well-known cut-back technique and second is the insertion loss. The insertion loss, theoretically corrects for the Fresnel reflections when coupling the light into and out of the fiber. The cut-back method is difficult to use due to the short lengths of fiber. Also because YAG cannot be properly cleaved the fiber must be removed from the set-up and repolished to perform a cut-back. During this period the lasers can have small shifts in power affecting the measurements. Therefore, after measurements using both methods on the same fiber were confirmed to be consistent, the theoretical insertion method was selected. Figure 3.10 shows the refractive index as a function of wavelength for undoped YAG. This data is needed to calculate the reflection of each fiber face at the respective wavelengths used in the insertion loss. The equation 1 used to measure total attenuation for the traditional cut-back method. In this equation the transmitted power P_{out} is defined through the full length

$$\alpha = \frac{-10}{L_L - L_S} \log\left(\frac{P_{out}}{P_{in}}\right) \qquad \text{Equation 3.4}$$

of fiber L_L, and the transmitted power P_{in} is defined through the short length of fiber L_S. If the lengths are in meters, then the units will be in dB/m.

The alternative option correcting for Fresnel reflection uses the equation

$$\alpha = \frac{-10}{L} \log\left(\frac{P_{out}}{P_{in}}\right) \qquad \text{Equation 3.5}$$

Now P_{in} is the power of the laser after the lens, times (1-R) to account for the front reflection, and T_{out} is the power measured through the full length of fiber L and divided by (1-R) so that the power is just before the end reflection. The Fresnel reflections are easily accounted for at normal incidence where n is the index of refraction at the wavelength of the laser

$$R = \left(\frac{n-1}{n+1} \right)^2 \qquad \text{Equation 3.6}$$

where R is the per surface reflectance at normal incidence seen in Table 3.2. With this calculation the log can be taken of the ratio between the power just inside the fiber and the power right before the light exits the fiber. Once again if the length is in meters, then the units will be in dB/m. Table 3.3 displays the relationship between percent transmitted power per meter of fiber with the log scale of dB/m. The progress from 3 dB/m to 0.2 dB/m results is 45% more power transmitted per meter.

For all of our loss measurements we are forced to assume the modes have reached a steady state condition because of the limited lengths of the SC YAG fibers. Traditionally for attenuation measurements tens of meters of fiber are required for a steady-state condition, where the coupling of light energy to the various modes reach an equilibrium. The cut-back insures the elimination of the high-order coupling modes in the early lengths of the fiber. Also due to different scattering mechanisms modes that are launched into the fiber may be coupled to high-order modes while propagating through longer fiber lengths. These higher order modes are more likely to refract out of the fiber increasing scattering loss. This is evident in Figure 4.16 and Figure 4.17. The power is launched in with low-order modes and after the light propagates 42 cm it has spread to high-order modes. This can be attributed to bulk scattering in the core, to the surface roughness of the fiber, or irregularities in the fiber geometry. Rayleigh scattering and Rayleigh-Gans scattering are two possible bulk scattering mechanisms. Rayleigh-Gans has been the observed cause in other IR crystalline fibers, with bulk defects large in the transverse dimension, but small in optical path difference compared to the wavelength of light.[23, 79] Strong forward scattering can be another indication that the mechanism is Rayleigh-Gans. Whereas, Rayleigh scattering occurs at all angles. This forward scattering could result in loss being dependent on the length of the fiber. This length dependence has been measured and is believed to be because as the light is scattered to higher order modes it is more likely the light will scatter out of the fiber, no longer confined to the unclad core. This can occur due to irregularities in fiber geometry, diameter variations, or bulk scattering defects. An example of irregular fiber geometry was seen in Figure 2.10.

Table 3.2 Refractive index and reflectance of YAG at each laser wavelength for each surface.

Wavelength	n	R	1-R
532 nm	1.8381	0.0872	0.9128
635 nm	1.8293	0.0859	0.9141
808 nm	1.8212	0.0847	0.9153
1064 nm	1.8147	0.0838	0.9162

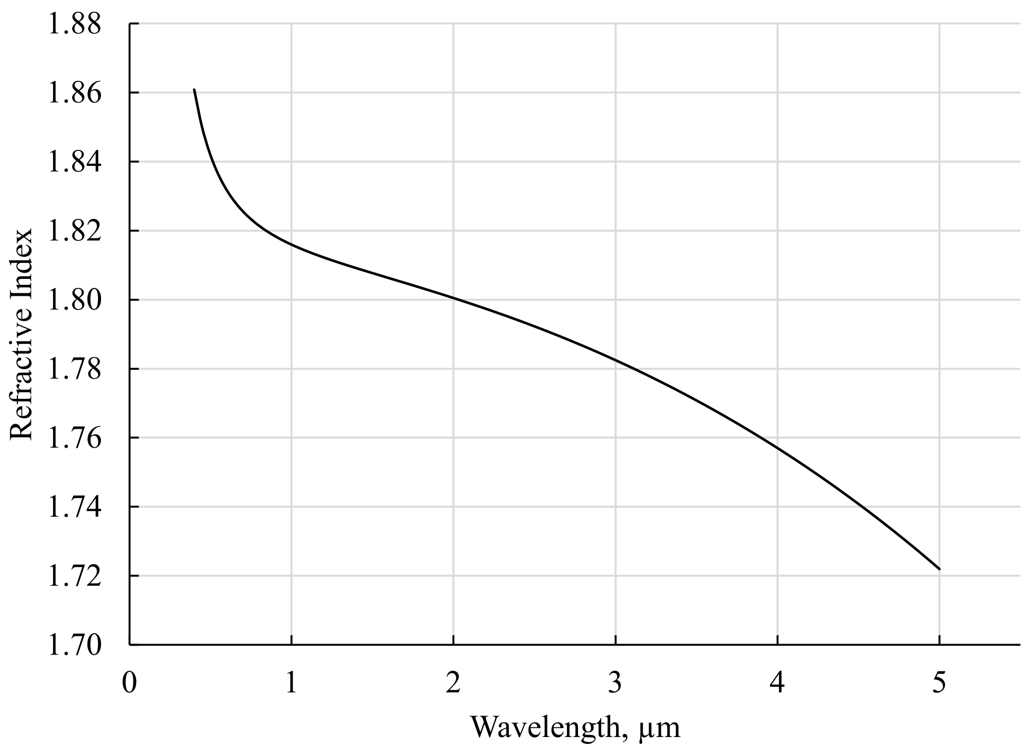

Figure 3.10 Refractive index of undoped YAG as a function of wavelength.[80]

Table 3.3 The relationship between percent power transmitted per meter of fiber to the log scale of dB/m.

dB/m	**% Transmitted /m**
10 dB/m	10%
7 dB/m	20%
5.2 dB/m	30%
4 dB/m	40%
3 dB/m	50%
2.2 dB/m	60%
1.5 dB/m	70%
1 dB/m	80%
0.5 dB/m	90%
0.2 dB/m	95%
0.1 dB/m	97.70%
0.04 dB/m	99%

3.3 Integrating Sphere

The previous section demonstrated the means of determining the total losses, α_T. An integrating sphere was used in order to quantify the degree of scattering, α_s, and locating regions of greater scattering in order to improve the fiber processing in those areas or for the entire fiber. A 2 inch diameter scattering sphere was used to take measurements along the fiber at 1 cm increments. Each measurement was an average of the 5.08 cm length covered by the sphere, graphically a 1 mm hot spot will have the width of 5 cm. Scattering measurements were performed using the same lasers used to measure the total attenuation. A fiber needs to be greater than 30 cm to get meaningful data, because the fiber mount does not allow for the first measurement to be taken until about 12 cm. The fiber will also increase in scattering over the last 10 to 15 cm as a result of back reflection. This 8% of power is more readily scattered out of the fiber and collected by the silicon photoconductive detector. The detector has a wavelength range from 350 nm to 1100 nm and the Thorlabs sphere IS200 has a reflectance of ~99% over a wavelength range of 350 - 1500 nm.

The loss due to scattering is calculated using Equation 3.7,

$$dI_s = -I(x)\alpha_s dx = [-I_o \exp(-\alpha_T x)]\alpha_s dx \qquad \text{Equation 3.7}$$

where dI_S is the intensity of light captured in the sphere with diameter dx = 5.08 cm and $I(x)$ is the intensity of the light at position x along the fiber.[81] The data taken using a green 532 nm laser consistently yields a higher scattering loss compared to the data taken with an Nd:YAG laser operating at 1.06 μm. This wavelength dependence is expected, as scattering varies as $1/\lambda^n$ where *n* depends on the type of scattering. In general, scattering losses increase with decreasing wavelength. The most common bulk scattering mechanisms in fibers being Rayleigh, n = 4 or Rayleigh-Gans scattering, n = 2. This however does not take into account the surface scattering of the unclad fiber. It is difficult to separate these types of losses from one another.

3.4 Sample Prep

After the fibers are grown and before they can be characterized, the fiber samples need to be polished. YAG is a very hard material at 8.5 on the Mohs scale, only slighlty lower than sapphire. For this reason sapphire lapping paper can be used, but it is not aggressive enough at the larger particle size to remove material to get to a flat starting surface, and YAG does not have a cleaveage plane. Thereore, diamond lapping paper with 30, 6, 3, and 1 μm particle size were used in decending size. Smaller 0.5 μm diamond lapping paper was also used, but no noticeable difference in attenuation or scattering losses were observed. A small handheld microscope was used to inspect the fiber cross-section at each polish stage. Unfortunately with no cleaving plane, a flat consistent surface did not exisit, seen in Figure 3.11 using phase shift interferometry. These constructive and destructive interference fringes indicate the degree of flattness of the sample's end. The image shows a cleaved fiber with a saddle like shape and very steep differences in flattness. The surface would have different curvature each time and would leave a small chip on the edge at the point the diamond edge scored the fiber. Figure 3.12 shows the interference fringes with center to edge flattness of about 1.5 μm. This degree of flatness was consistently possible when using a lapping wheel. This figure represents the fiber polish and flatness for the fibers measured using a 1 μm final polish.

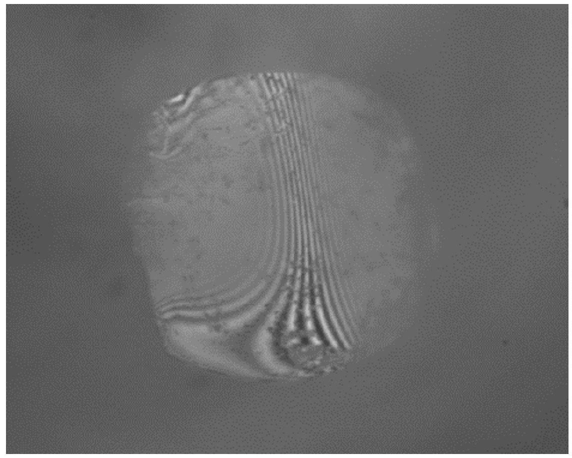

Figure 3.11 Phase shift interferometry used to image a diamond cleaved cross section of a SC YAG fiber. The interference fringes indicate a saddle-like surface. Image taken by Dr. McCahon.

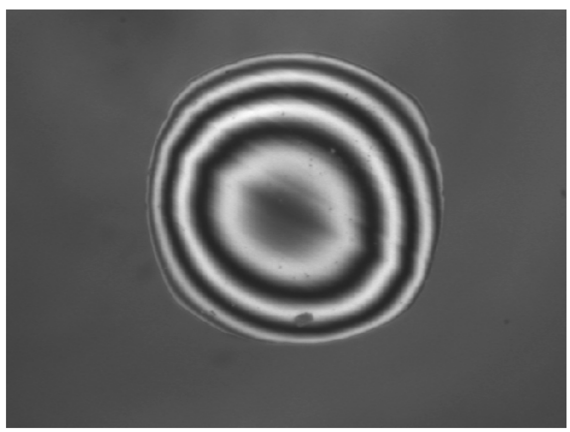

Figure 3.12 Phase shift interferometry used to image a 1 μm polished SC YAG fiber. The interference fringes indicate a center to edge flatness of about 1.5 μm. Image taken by Dr. McCahon.

Chapter 4. Single-Crystal YAG Results

4.1 Orientation, Facets, and Crystallography

Ribbed facets on the lateral surface are intrinsic to YAG growth, and there was the initial hypothesis that these facets would correlate with higher losses. Thus, methods to suppress the facets were investigated. It was found that they could be suppressed in two ways: using certain seed orientations (15° from [100] to [110] direction)[82] or with uniform thermal symmetry.

A series of experiments were conducted evaluating orientation, facets, and their effect on loss (using a standard 40 cm fiber length). Surprisingly, there was no discernable difference in attenuation between a fiber that was randomly or specifically oriented, or between a facet-free fiber and a faceted fiber. Thus, it was concluded that neither of these caused the attenuation to improve below 0.4 dB/m. Since this seed orientation still led to occasional facets, excellent thermal symmetry was deemed the more critical component. Figure 4.1 is evidence supporting this. At the seeding interface, the top seed was a randomly oriented crystal fiber with visible facets. The fact that the newly grown fiber did not exhibit any facets, verified that while the certain seed orientation (15° from [100] to [110] direction) was not necessary to grow a facet-free fiber, thermal alignment was influential.

Figure 4.3 demonstrates a possible reason why facets might not have affected the attenuation. This AFM image shows the facet height to be approximately 40 nm on a fiber diameter of 330 µm. At that height, the wavelength of light transmitted through the fiber is over 25 times larger than the defect at 1064 nm and should have negligible impact on total internal reflection (TIR). Comparatively, Figure 4.4 shows an AFM image of an oriented, visibly facet-free YAG fiber, with a low rms of 2.1 nm (an rms <1 nm is smooth on the atomic scale).[83]

Despite the facets having no great effect on loss, a significant effort was made to produce facet-free fibers because the possibility remained that they could have a small, albeit currently unmeasured, impact. Additionally, as shown in Figure 4.2, a standard seed was put in place in order to grow consistently oriented fibers moving forward. This rounded square orientation provides a template, and allows us to determine if the crystal axis is wandering to a new orientation during growth. Having such a simple, efficient indicator is important because – while the majority of fibers maintain the orientation [100] throughout the full fiber length – some fibers do not and a complete analysis on every fiber cannot be performed. According to Ishibashi et al.[82] at this [100] crystal direction the fiber should have facets, leading us to believe it is the result of thermal asymmetry at the freezing interface that arises from poor alignment.

Maintaining orientation throughout the fiber length was confirmed by a combination of single-crystal x-ray diffraction, using a Bruker SMART APEX diffractometer, and cross-section microscope analysis. Using the former, both the top and bottom of the crystal fiber were analyzed, and instead of the expected crystal orientation of 15° from the [100] to the [110] direction, both fiber ends had a growth direction of [100]. With the latter, an entire fiber is translated under a backlit microscope, allowing one to observe the continuously uniform cross-section throughout. In addition to this positive crystal orientation characterization, its crystallinity was verified to be a well-ordered SC with no indications of amorphous disorder or twinning. The diffraction analysis determined the single phase, cubic crystal to have the correct space group Ia-3d, with the lattice parameter of 12.0070(8) Å using a wavelength of 0.7173 Å. The stoichiometry was confirmed to be YAG, $Y_3Al_5O_{12}$, with one unit cell comprised of eight formula units.

Figure 4.1 Bright-field microscope image lit from below. The top faceted portion is followed by the seeding interface, which is facet-free. This led to the conclusion that the facets are primarily impacted by the thermal alignment.

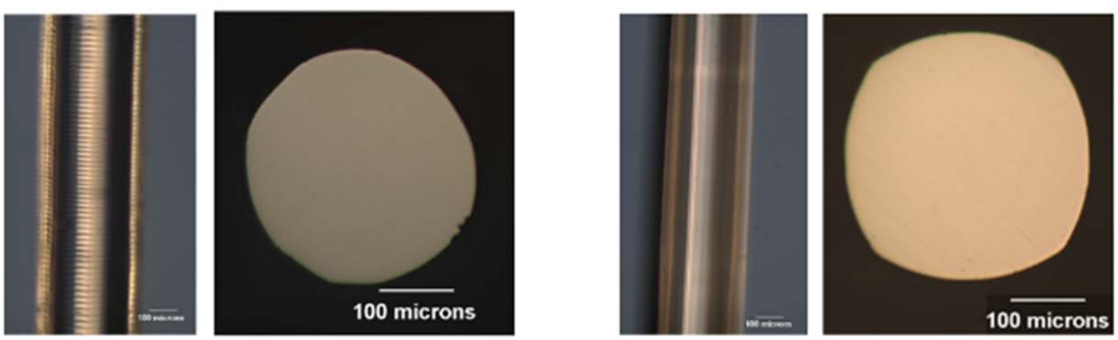

(a) (b)

Figure 4.2 (a) Randomly oriented crystal with facets and an off circular cross section. This cross-section would change with different random seed oriented crystals. (b) When oriented with [100] growth direction, the crystal was facet-free with a consistently rounded square cross-section.

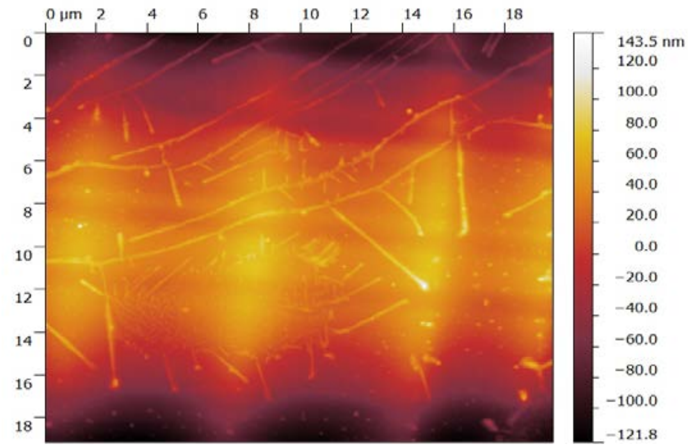

(a)

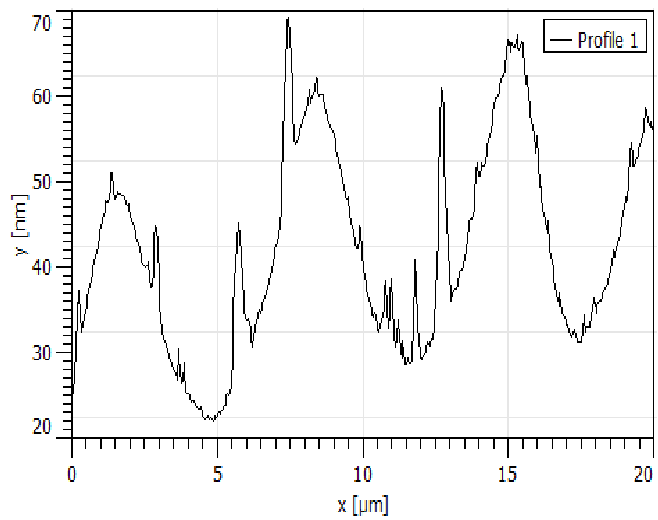

(b)

Figure 4.3 (a) AFM image of a SC YAG fiber's surface with periodic facets. (b) Amplitude profile of the facets, peak to valley approximately 40 nm. The sharp lines are presumed to be contamination. This AFM image was performed at Clemson University.

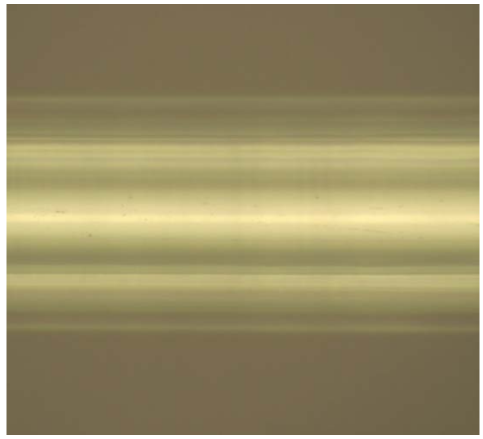

(a)

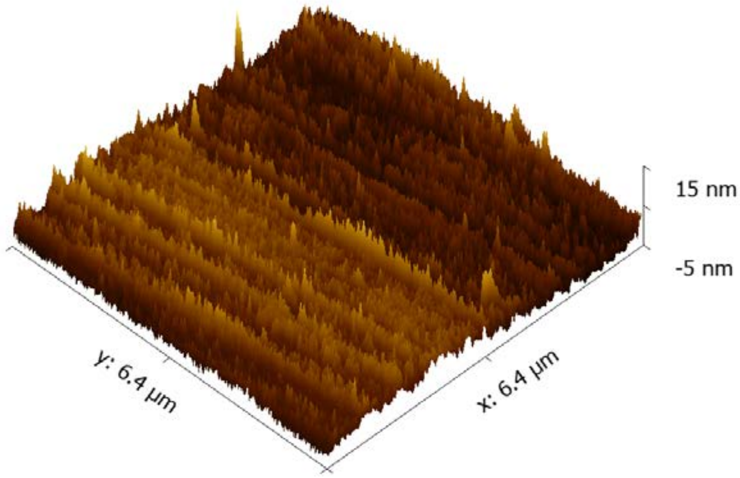

(b)

Figure 4.4 (a) Optical image of a 330 μm SC YAG fiber, without visible facets. (b) AFM image of this SC YAG fiber with an rms of 2.1 nm.

4.2 High-Loss YAG Fiber

Recognizing the quality of an SC YAG fiber - and how to improve that quality – is fundamental. Historically, the quality of SC YAG has ranged widely. Yet, a majority of the loss values that have been recorded were for YAG rods, approximately 1 mm in diameter, and only a few centimeters in length, not for fibers. While such previous work certainly demonstrates the challenges in growing low-loss YAG fibers, Figure 2.11 shows the improvement of SC YAG fibers grown at Rutgers University. So, as disappointing as this high-loss SC YAG fiber was, it does offer insight into how the scattering mechanisms have changed.

Initially, the SC YAG fibers' loss at longer lengths (approximately 40 cm) was rather high, and the poor alignment of the optical system was the primary cause. However, implementing different techniques to align the invisible CO_2 beam improved the thermal distribution of the molten zone. Consequently, this reduced strain on the crystal lattice's core, evidenced by the fact that high-loss fibers displayed interior cracks at a growing velocity of 1 mm/min while current growths at an increased velocity of 4 mm/min reveal no visible cracking. Images of this cracking was seen earlier.

The 38 cm long high-loss SC YAG fiber discussed here was unclad, with a 300 µm diameter and a standard deviation of 1.4 µm. All fiber loss measurements were on unclad SC YAG fibers roughly 330 µm in diameter of varying lengths, using the insertion method described earlier. Figure 4.5, comparing total loss and minimum scattering loss at 532, 808, and 1064 nm wavelengths, shows that minimum scattering accounts for approximately one-third of total loss, with increasing loss at shorter wavelengths. This increasing trend holds true for all undoped YAG fibers, only in doped YAG fibers will the absorption of the RE ions alter this outcome. The total loss is very high, 1064 nm above 10 dB/m, which means a meter long fiber would transmit only 10% of the initially coupled light.

The scattering data as a function of fiber position has a very different shape in Figure 4.6 than the low-loss fiber seen later in Figure 4.8. Here the scattering data increases right after the initial fiber position, whereas for the low-loss fiber, loss remains flat for a length before increasing at the end. The immediate increase in scattering loss is recognized to be the result of bulk scattering in the fiber, and is converting the scattered light to higher order modes. These higher order modes continue to propagate in the fiber, but eventually no longer satisfies TIR and scatter out. This result has also been observed in high-loss similar diameter sapphire fibers grown by the LHPG; while the low-loss sapphire fiber had consistent scattering loss.[23]

A second reason for this ever-increasing scattering loss is bulk scattering and not surface scattering as evidenced by comparing the standard deviations of fiber diameters. The standard deviation of the diameter during growth was 1.4 µm. This is slightly higher than the average standard deviation of about 0.7 µm, but fibers have been grown to similar lengths, with standard deviations greater than 3 µm, and a low-loss fiber below 1 dB/m was achieved at all wavelengths. The larger diameter guide tubes used on this fiber were also used for some initially low-loss fibers before the transition to smaller diameter guide tubes. Therefore, with the surface quality on the same order of variation, it has been concluded that this improvement must be primarily due to defects in the bulk of the fiber and not surface scattering. These bulk defects, for example interior cracking, were a result of the fiber being under high thermal stress due to the asymmetric alignment.

The scattering in Figure 4.6 increases above 20 dB/m at the back end of the fiber. This is not the result of the fiber becoming poorer in quality, but the light as it propagates is scattered to higher order modes and proceeds to radiate out of the fiber. When the fiber is flipped end for end a similar result will occur with the lowest loss at position 15 cm and a high loss at 30 cm. A second issue is that even though the scattering value at a point is higher than the total loss, this is possible because the total loss is assuming a homogeneous loss throughout the entire fiber. This means the low scattering measured at the front averages with the high scattering at the back to approximately the measured attenuation.

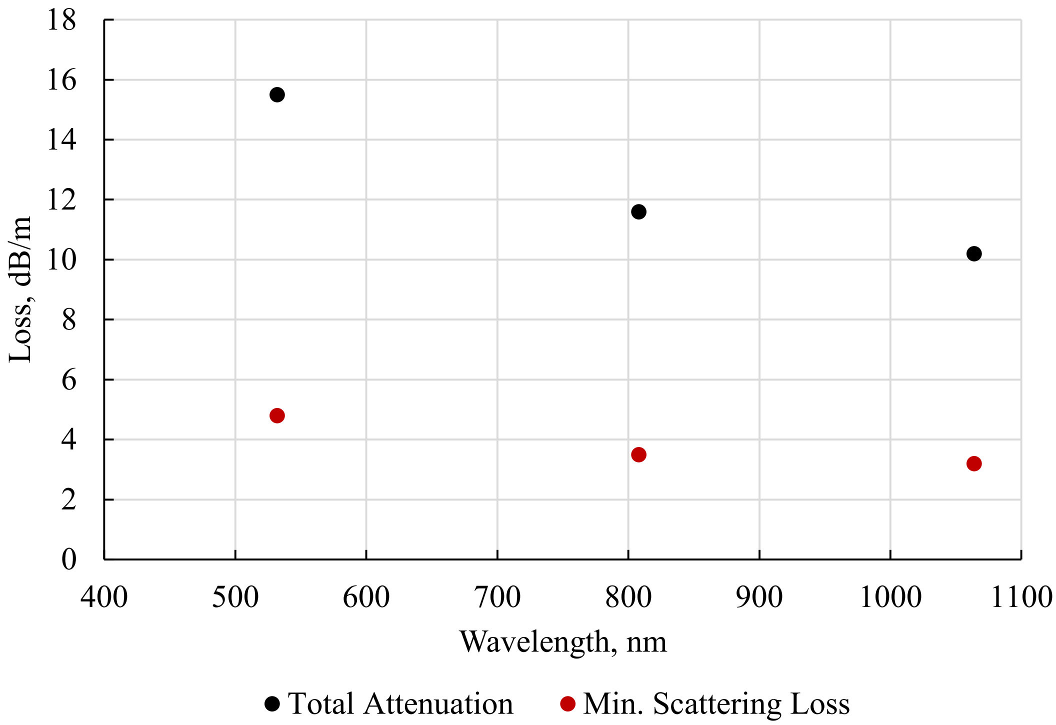

Figure 4.5 Total loss and minimum scattering loss measured for a very high-loss YAG fiber at three wavelengths. Both total and minimum scattering increase at shorter wavelengths.

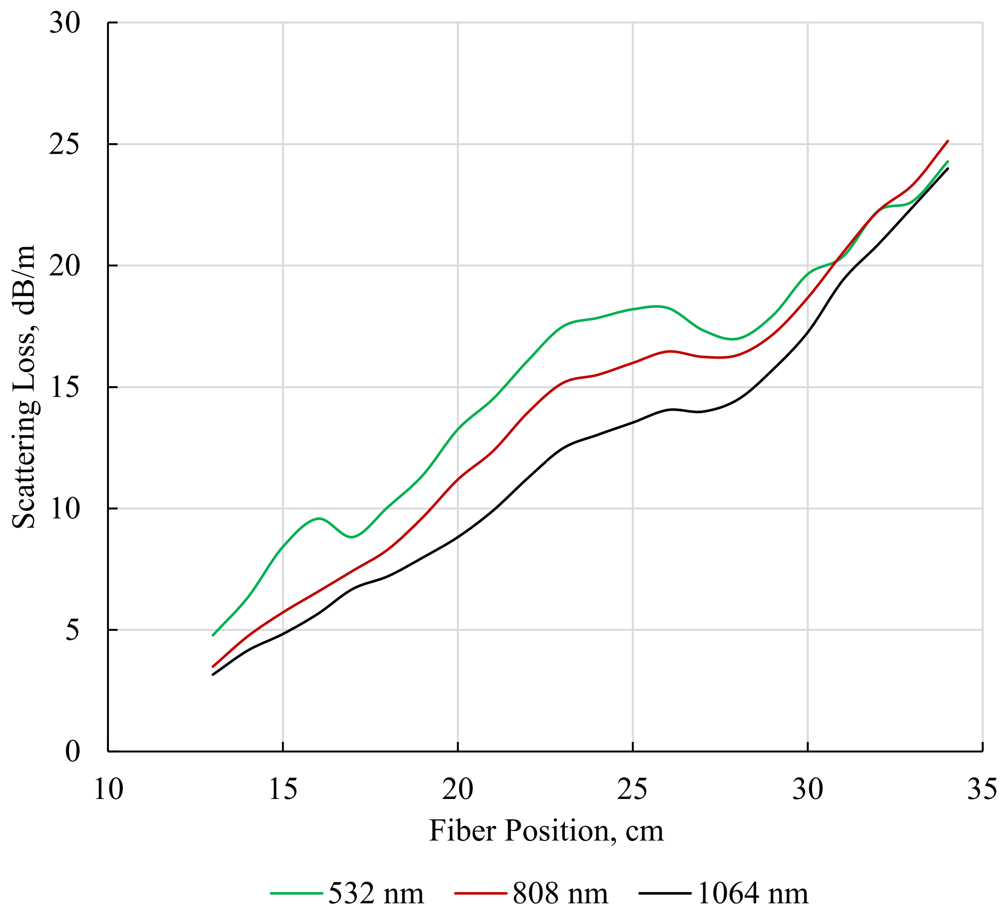

Figure 4.6 Scattering loss as a function of fiber position for a high-loss SC YAG fiber. The scattering loss is greater for the shorter wavelength.

4.3 Low-Loss YAG fiber

Beyond the purity of the SC source material (from a Chinese vendor), which has remained constant, there are a number of other factors which can influence fiber loss. Our reduced losses have primarily resulted from engineering a better fiber waveguide, including refining alignment methods to focus CO_2 radiation on the source.

These improved alignment techniques led to a drastic reduction in bulk scattering, both measured and visually observed, which in turn yielded fibers with significantly less loss. The fact that the diameter control displayed similar standard deviations both before and after the alignment improvements, further points toward bulk scattering as the principal cause of loss in the initial improvements. This SC YAG fiber's total loss is drastically better than the previous high-loss fiber of a similar length (40 cm and 38 cm, respectively). The total loss here is 0.3 dB/m at 1064 nm, compared with the previous 10 dB/m, resulting in an increased power transmission of 10% to 94% through a meter length.[24]

This fiber was grown under standard conditions, at 2 mm/min with diameter control turned on. The total loss can be seen in Figure 4.7, measured at two different fiber lengths. First, it was measured at its full length of 52 cm. After removing the section of the fiber following the seeding interface, it was then 40 cm. The fiber was repolished using the same 1 μm diamond lapping paper and remeasured. The figure clearly shows an improvement from the 52 cm to the 40 cm measurement. The standard deviation of the diameter control for the 52 cm length was 1.89 μm and 0.89 μm for the 40 cm length, a difference attributed to instability caused by a laser fluctuation during the initial stage of growth.

The scattering loss can be seen in Figure 4.8. The scattering as a function of fiber position indicates a few issues. Beside an increase at the output end, there are three key features at positions 28 cm, 40 cm, and 44 cm that may be seen more easily in the 532 nm curve. For example, the increase at the 44 cm point is due to a pulling-induced, microbend defect. The minimum scattering loss at each wavelength is also plotted in Figure 4.7. At 1064 nm it is quite low, 0.1 dB/m, but does start increasing after 35 cm at all wavelengths. However, an increase in the last 10 cm is expected because of the Fresnel reflection, ~8% of light scattered back into the fiber, with this light radiating out of the fiber. The minimum scattering loss results in a quarter to a third of the total loss, depending if compared to the 52 or 40 cm length. This has been the typical range of the minimum scattering loss of the total attenuation.

After achieving considerably lower losses by improving the quality of SC bulk scattering, more emphasis could also be placed on improving surface quality. With the assistance of the new digital camera system's magnification, the fiber's lateral shifts during growth became more evident and pertinent. These shifts resulted in surface defects known as microbends. To minimize shifting, a guide tube with a tighter inner diameter was used.

This SC YAG fiber's diameter was approximately 330 μm, grown inside a 350 μm guide tube. This left only 20 μm for the fiber to shift laterally within the tube, compared to the 100 μm space in previous guide tubes, and thus sustain microbends of lower magnitude. After removing the 12 cm section the attenuation improved by about 0.2 dB/m at all wavelengths, likely due to a combination of factors: the improved standard deviation of the fiber diameter and the elimination of microbends, but most notably the shorter length. Although improving surface quality is inherently worthwhile, the results that follow demonstrate the magnitude of loss correlates with fiber length rather than the removal of surface defects. Unfortunately, it is currently difficult to quantify the microbends effect on loss when the loss is length dependent.

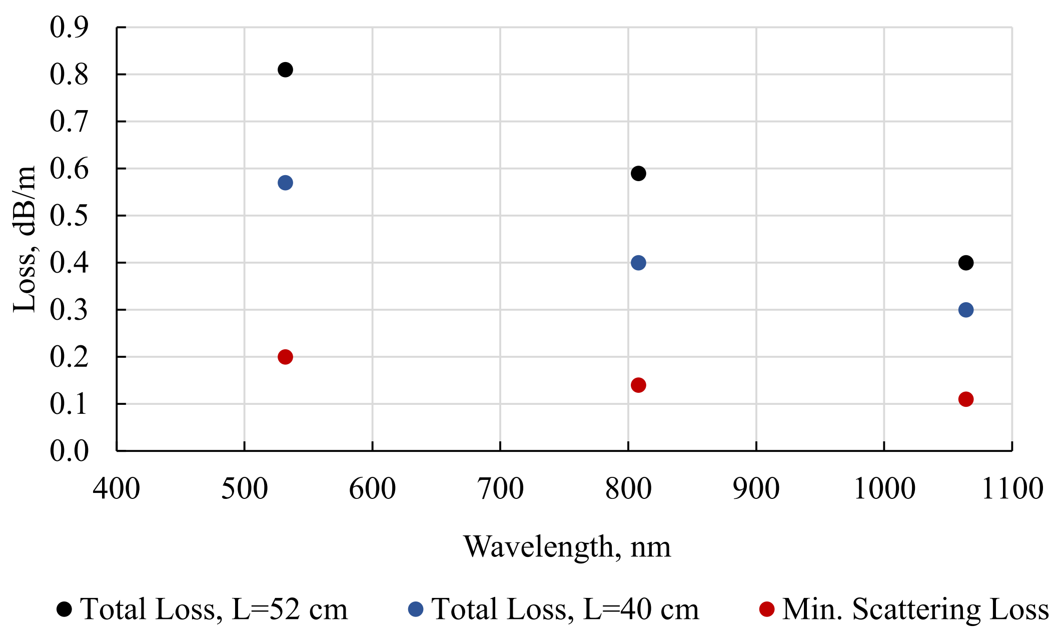

Figure 4.7 The total loss of one SC YAG fiber at three wavelengths and two fiber lengths. After removing the 12 cm section, the fiber improved by more than 0.1 dB/m at all wavelengths. This was initially done to remove a defect in the growing process and determine its loss, however it has since been demonstrated that the improvement was at least partially because the fiber was shortened. The minimum scattering is also plotted to compare to the total loss.[24]

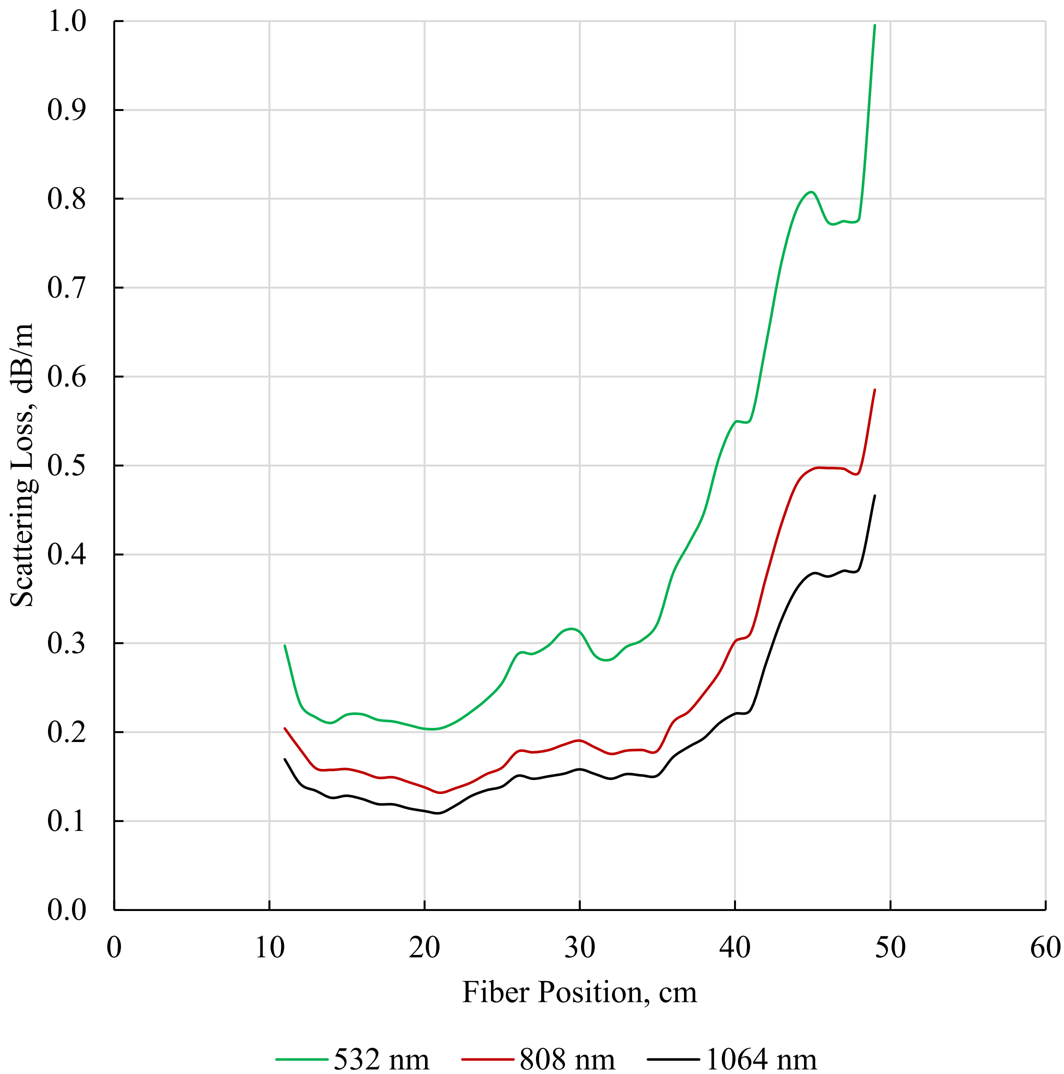

Figure 4.8 Scattering loss as a function of fiber position at three wavelengths. The sudden increase at the end is due to ~8% of the power being back reflected and scattering out.

4.4 YAG fiber without Diameter Control

To better understand the importance of the diameter control system, a 62 cm long YAG fiber was grown without the diameter control feedback loop at a velocity of 2 mm/min. This resulted in roughly ten times greater standard deviation than the diameter controlled fiber (0.74 μm compared with 7.6 μm), and a min/max range of approximately 25 μm. This natural diameter variation can have dire consequences for fibers of longer length.

The comparison with and without diameter control is shown in Figure 4.9 and this effect on scattering loss and total attenuation will be demonstrated in the next two sections. Here, the diameter controlled SC YAG fiber demonstrates fluctuations as small as 0.5%, on an unclad core. Considering that glass diameter fluctuations are within 0.1%[78] and have a cladded structure, SC YAG fibers will naturally have more surface scattering than their glass fiber counterparts.

The minimum scattering measured on fibers with no diameter control is only slightly higher than diameter controlled fibers, but the rate at which scattering increases for the former is far steeper. This is because the fiber without diameter control will couple modes to higher order modes that are less than the critical angle and refract out of the fiber (see Figure 4.12 and Figure 4.14). These results indicate that at shorter lengths, less than 30 cm, the propagating light remains guided within the fiber. However, after 30 cm the scattering loss increases very rapidly, particularly without diameter control. This is demonstrated in Figure 4.11, where the total losses at 1064 nm follow the same trend as the scattering losses. Figure 4.10 demonstrates for the fiber without diameter control, the total attenuation improved with shorter fiber lengths, by measuring the insertion loss through the full fiber length at three wavelength: 532, 808, and 1064 nm. It is immediately clear that the loss is still rather high when compared to diameter controlled fibers measured at the same lengths and wavelengths.

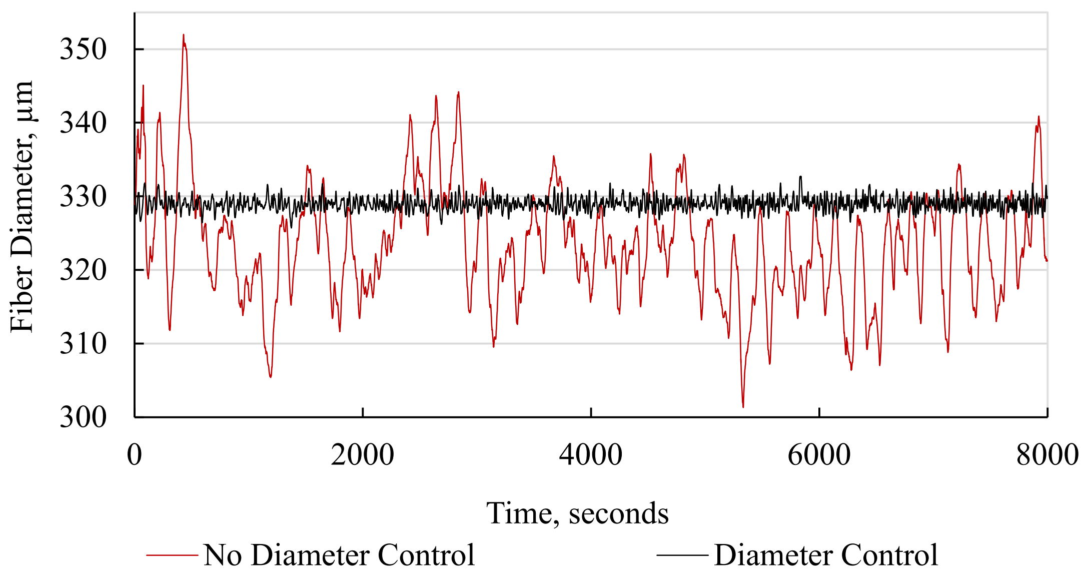

Figure 4.9 Fiber diameter measured during growth for two fibers, one with a diameter control feedback loop and a second fiber grown without diameter control.

It is important to recall the widely held assumption that loss is homogenous when measuring total attenuation of a fiber. This experiment disproves this assumption, for both diameter controlled and uncontrolled fibers.

First, consider the SC YAG fiber without diameter control shown in Figure 4.10, where total loss is a function of length and wavelength. Three different lengths of fiber are measured at three wavelengths. An increased loss at shorter wavelengths is seen in all three lengths. However, at the two shorter lengths (21 cm and 31 cm) the loss is quite low throughout all three wavelengths, comparable to a 40 cm long fiber with diameter control.

Figure 4.11 demonstrates the total loss of the fiber without diameter control, measured with the 1064 nm laser at various lengths. The fiber was initially polished and measured at 62 cm. Then, 10 cm was removed off the back end and the resulting 52 cm fiber was repolished and remeasured. This was repeated at 42, 31, and 21 cm lengths, always maintaining the same fiber direction towards the laser. From 42 cm to 52 cm, the measurement at 1064 nm nearly doubled from 0.8 dB/m to 1.7 dB/m. So, while the loss is obviously less at shorter lengths, this figure continues to demonstrate that fibers without diameter control exhibit sharper loss increases more quickly than those with diameter control (compare to Figure 4.15).

The scattering loss data further confirms this trend of increasing loss at longer lengths, as shown in Figure 4.12, just as the total attenuation measurement did. As previously noted, scattering loss will increase at the back end of the fiber due to reflection – around 50 cm in this case. Here, though, scattering begins to sharply increase as far back as 33 cm, an early spike that cannot be attributed to reflection. To confirm that the fiber was not simply of lower quality at the 40-62 cm position, a 10 cm section (52-62 cm) from the first cutoff was polished and measured as an isolated sample. It was confirmed to have a loss less than 1 dB/m, therefore suggesting that high-order modes were no longer guided by TIR and were scattering out of the fiber. It remains unverified if the main mechanism is bulk scattering or surface scattering. Either case could result in the guided light being converted to higher order modes that then radiate out of the fiber. However, this study of diameter control indicates that the converted high-order modes are eventually scattering out of the fiber as a result of diameter variations. These fibers are all unclad, so there would likely be a significant amount of light coupling to different modes from a fiber's surface, as the diameter varies during growth.

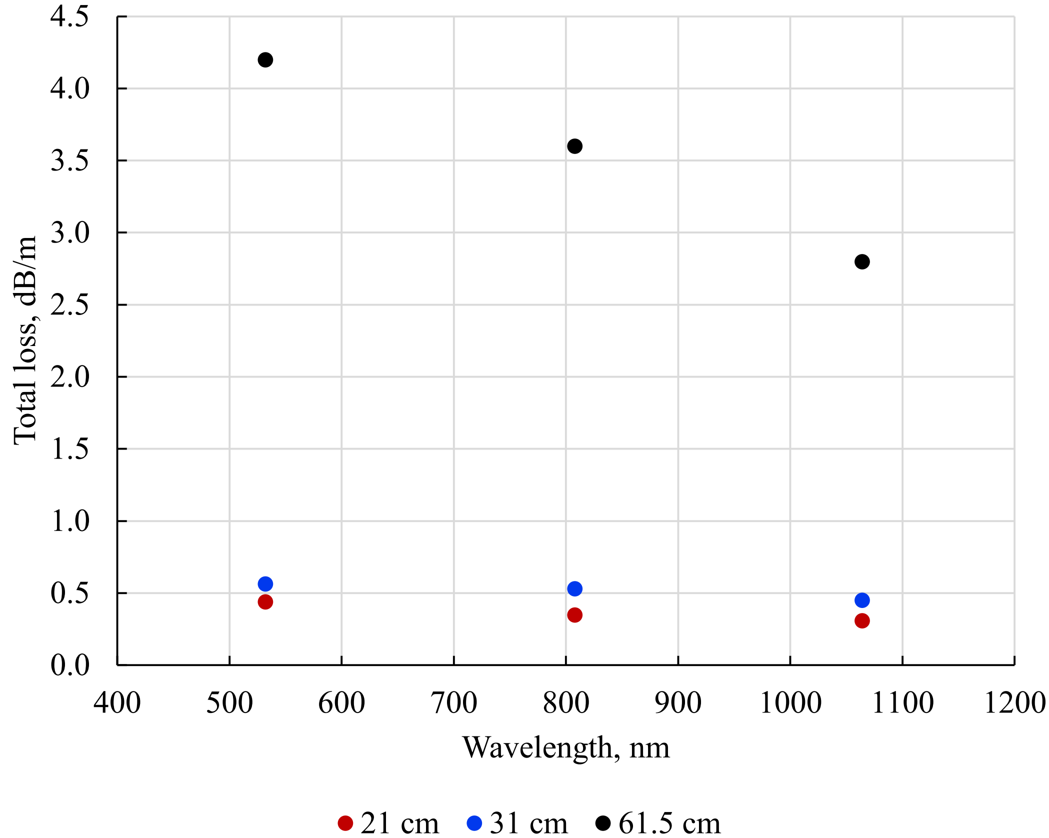

Figure 4.10 The total loss as a function of wavelength and length for one SC YAG fiber grown without the diameter control feedback loop measured at three lengths 21, 31, and 61.5 cm.

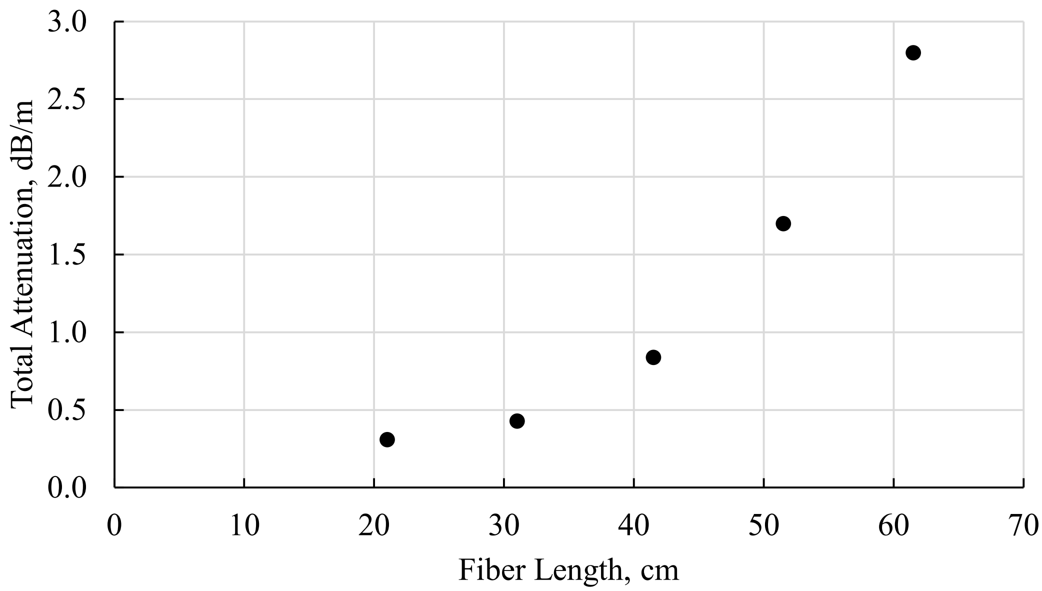

Figure 4.11 The total attenuation of one SC YAG fiber grown without the diameter control feedback loop, measured at different lengths. The attenuation decreases drastically as the fiber is shortened, when measured at 1064 nm.

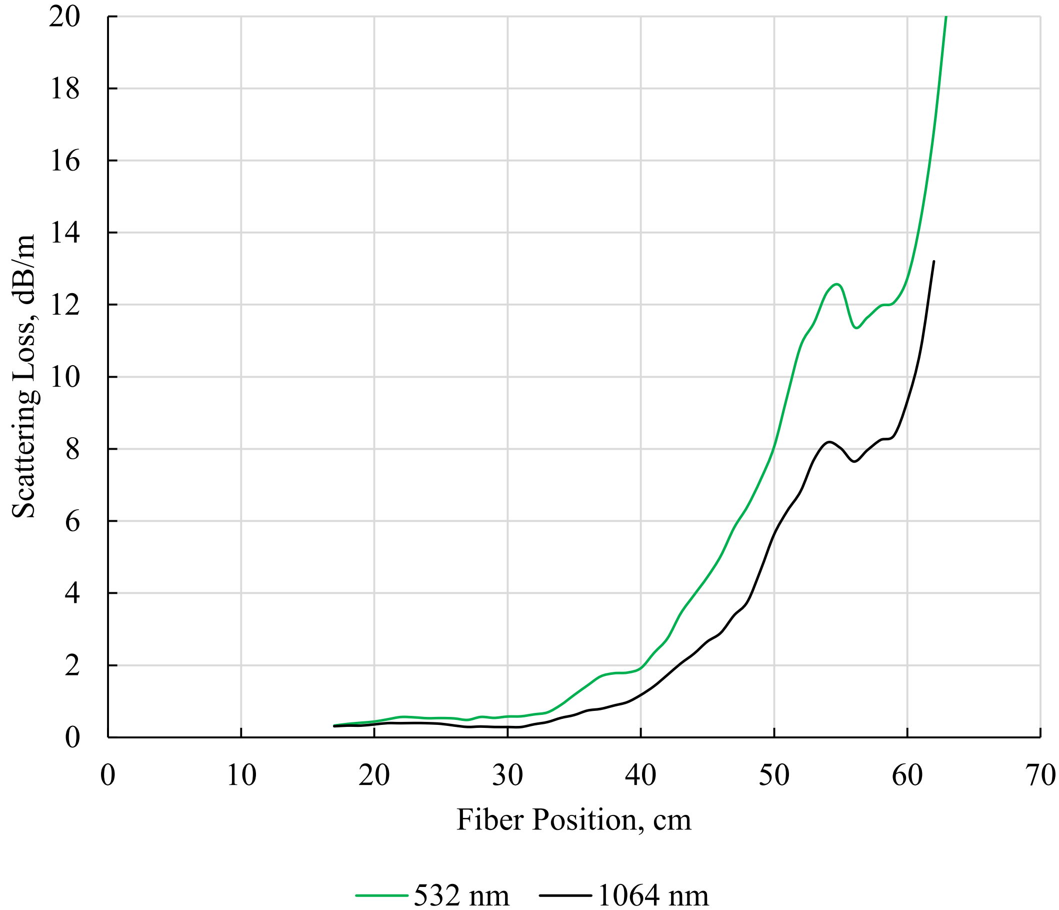

Figure 4.12 The scattering loss of the SC YAG fiber without the diameter control feedback loop as a function of fiber position at two wavelengths 532 nm and 1064 nm. Back reflections do not account for the sudden increase at 30 cm and is a result of modes being coupled to radiation modes.

4.5 YAG Fiber with Diameter Control

Next, a high-loss, no diameter control YAG fiber will be compared to a low-loss diameter controlled fiber that was also measured at multiple lengths. This combined data will indicate the impact of surface scattering loss over bulk scattering loss given the assumption that the quality of the bulk crystal is consistent between these two fibers. This is mostly a valid assumption because the same parameters were used to grow each and were grown using the same optical alignment.

This SC YAG fiber was 52 cm in length, 330 μm in diameter, and was grown at 2 mm/min with a diameter standard deviation of 0.74 μm. The total attenuation, scattering, and transmitted power mode profiles are presented. Figure 4.13 shows the total attenuation at 52, 40, 30, and 10 cm for three laser sources: 532, 808, 1064 nm again using the insertion loss method and an 9 cm focal length lens. The total attenuation clearly improves after removing the first 12 cm to below 0.2 dB/m at 1064 nm. This fiber is 10 cm shorter than the fiber without control, but the trend of increasing attenuation remains quite evident in Figure 4.13 as the fiber is cut back. These different lengths all show a similar increasing trend in attenuation at shorter wavelengths. The scattering data in Figure 4.14 shows an increase in scattering loss after 40 cm at both wavelengths compared to an increase at 33 cm for the uncontrolled fiber. The minimum scattering values for both controlled and uncontrolled fibers are also very similar. The difference is how they scatter after the turning point mentioned. The uncontrolled fiber increases much more drastically than the diameter controlled fiber, especially at shorter wavelengths. This is also true for the total attenuation of both fibers seen in Figure 4.15 measured at 1064 nm. The increase in attenuation for the uncontrolled fiber at longer fiber lengths is much greater than it is for the low-loss fiber, however both are still increasing. This presents the issue that attenuation is length dependent.

It is also reasonable to assume for the high-loss fiber in Figure 4.5 that if the fiber was cut shorter, the total loss would decrease similarly as seen here in Figure 4.13 and previously in Figure 4.11. The scattering plot in Figure 4.5 indicates that with the ever increasing scattering loss, it could be improved by even a greater magnitude if cut to shorter fiber lengths. For this reason, losses are compared to similar length fibers measured by the insertion method.

While performing the multiple measurements on this low-loss YAG fiber, fiber output mode profiles were taken. These profiles were taken at the same distance from the fiber face at all fiber lengths. The exposure of each image was maximized to include the full intensity range. Figure 4.16 are the multimode profile with light propagating through a 10 cm segment of the fiber. This light was coupled with the same 9 cm focal length lens used for all previous fibers measured at both wavelengths. These profiles become informative when comparing them to light propagating through 52 cm of fiber seen in Figure 4.17. Seen here at both 532 and 1064 nm wavelengths, the lower order modes have been converted to higher order modes over the 42 cm length. Some of these higher order modes will continue to propagate until TIR is no longer satisfied at incident angles less than the critical angle. When this occurs modes will become radiation modes, resulting in increasing loss at longer fiber lengths. This is in agreement with the scattering loss at further fiber positions and the total attenuation measurements.

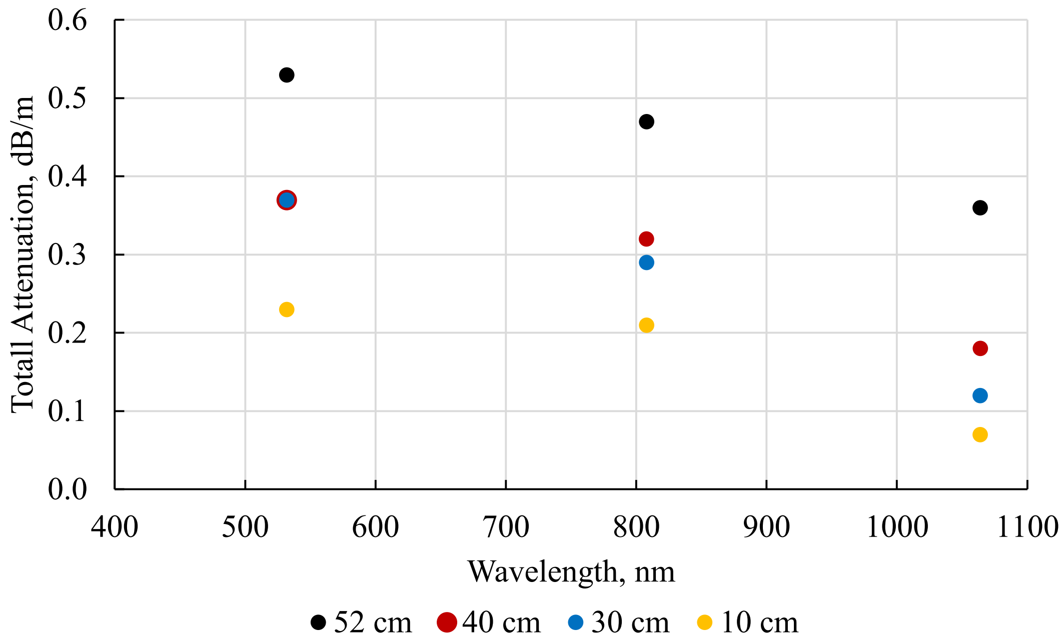

Figure 4.13 SC YAG fiber with the diameter controlled feedback loop, measured at different wavelengths and fiber lengths.

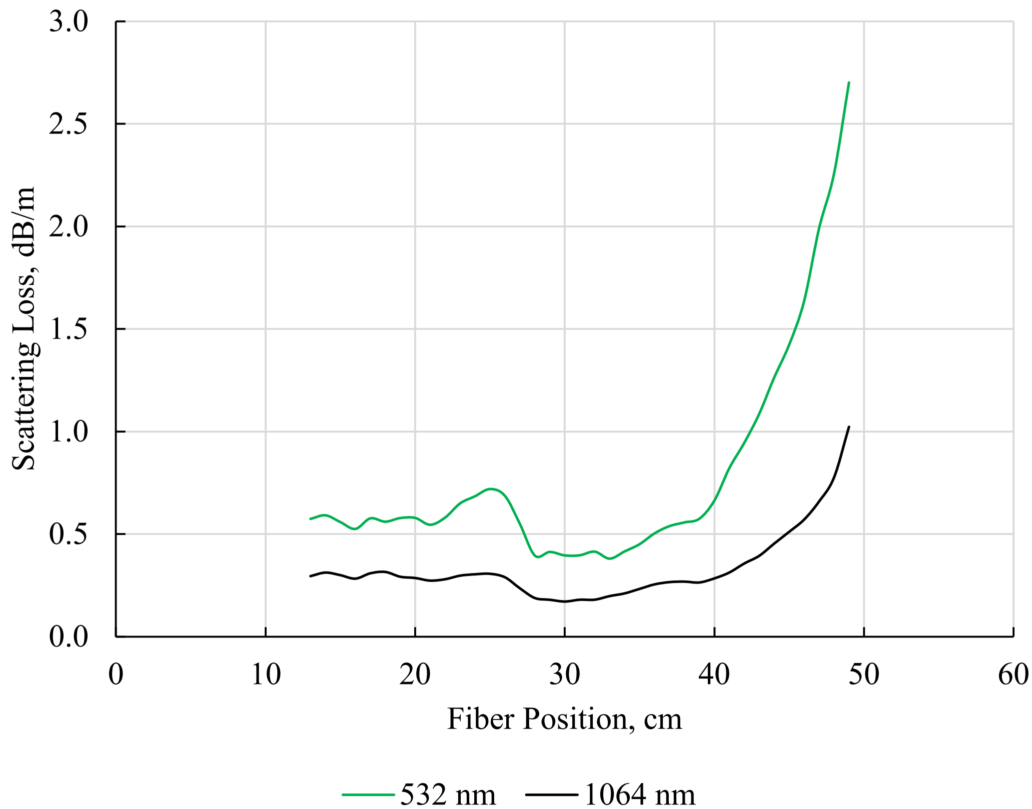

Figure 4.14 A 52 cm SC YAG fiber with the diameter control feedback loop on, showing the scattering loss along the fiber at two wavelengths. The increase over the last 10 cm is primarily due to back reflections.

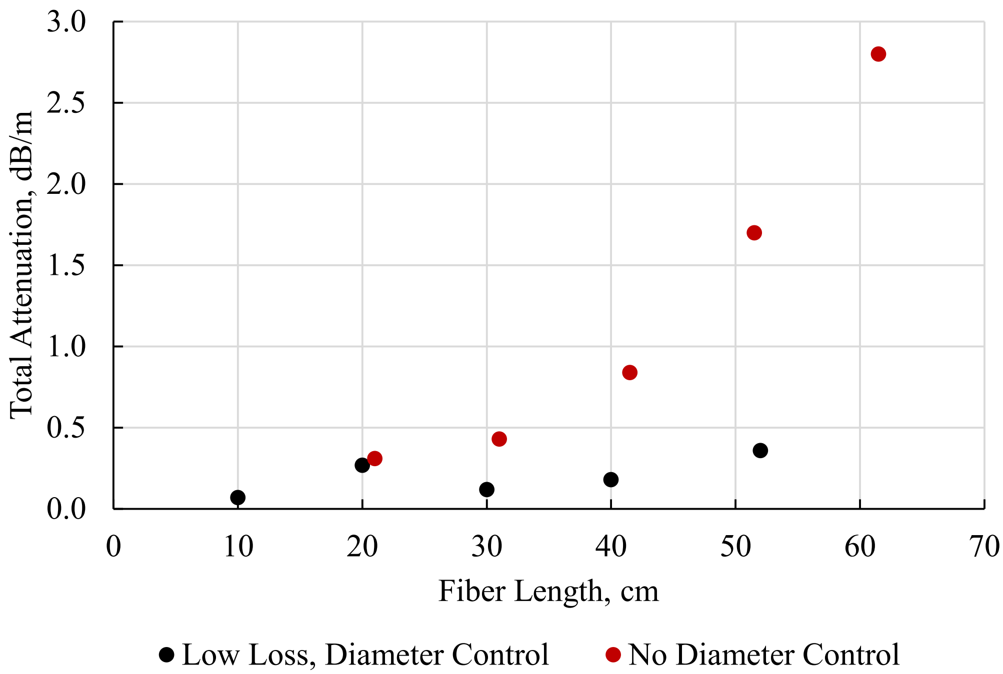

Figure 4.15 The loss for two fibers as they each have 10 cm cutoff repeatedly. One fiber is without the diameter control feedback loop, while the second had diameter control. These losses were measured at 1064 nm, but the same trend occurs at the shorter wavelengths. The diameter controlled fiber still increases in attenuation with length, but not nearly as much as the uncontrolled fiber.

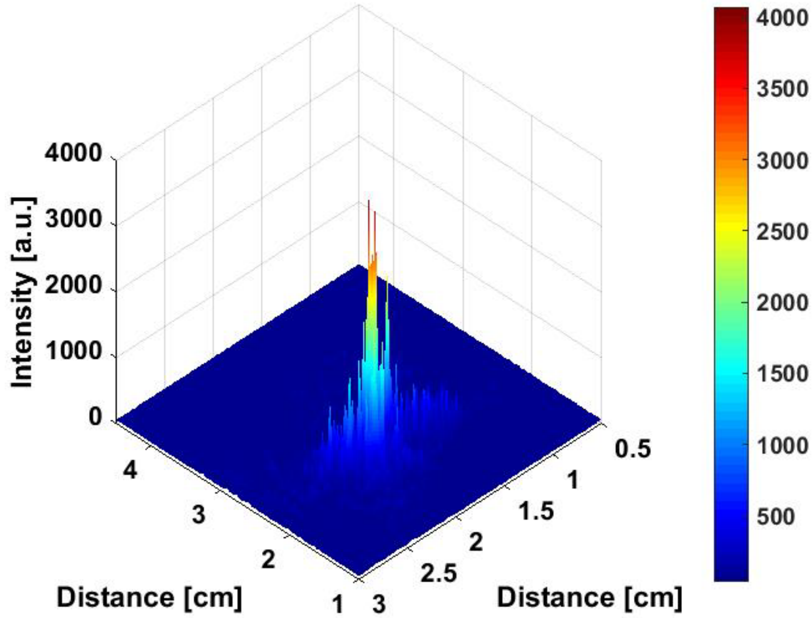

(a)

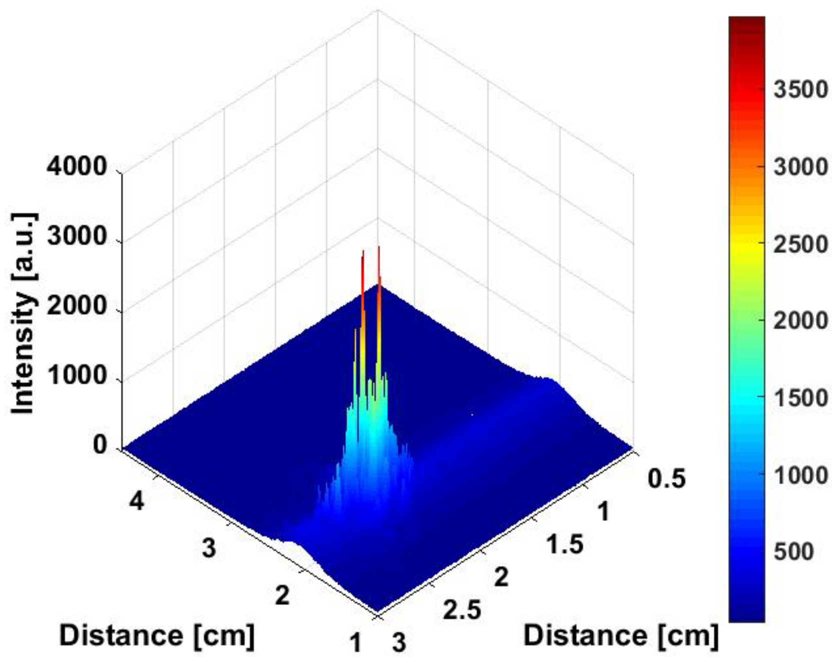

(b)

Figure 4.16 Output mode profile transmitted through a diameter controlled fiber, 10 cm long, at a wavelength of (a) 532 nm and (b) 1064 nm.

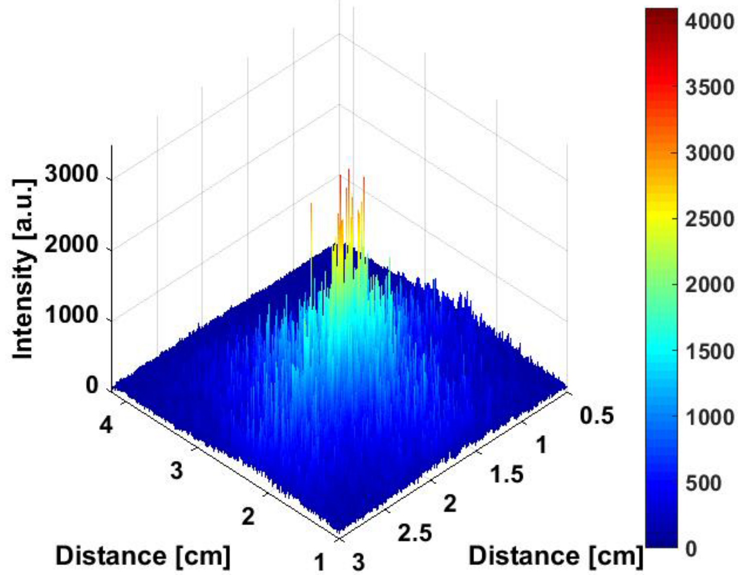

(a)

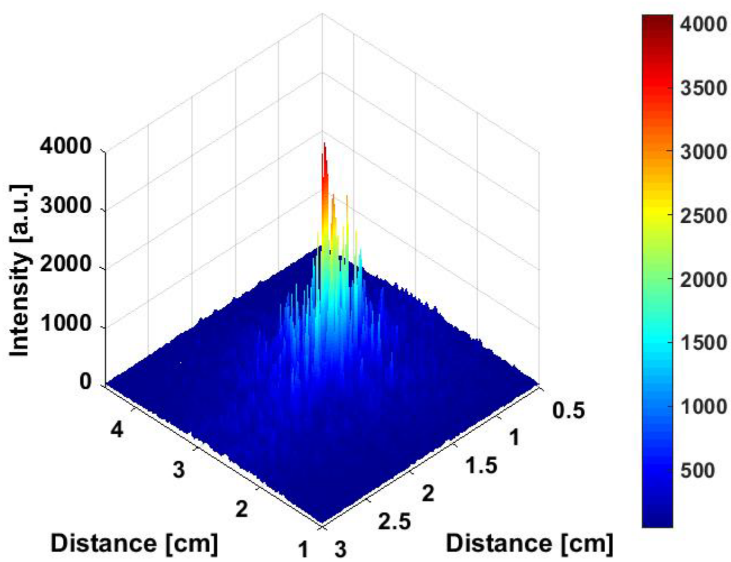

(b)

Figure 4.17 Output mode profile transmitted through a diameter controlled fiber, 52 cm long, at a wavelength of (a) 532 nm and (b) 1064 nm. At 532 nm there are more high-order modes, than the 1064 nm, but both wavelengths have more high-order modes than the 10 cm fiber length of this same fiber.

4.6 YAG Fiber ±6 μm Diameter Variation

At this point a fiber with no diameter control and a low-loss diameter controlled SC YAG fiber have been measured and compared for total attenuation, minimum scattering loss, and scattering loss at different fiber positions. The importance of diameter control and the different control parameters implemented during growth will result in different diameter responses from the programed feedback loop, controlling the change to the motor's velocity. This is demonstrated in Figure 4.18 with the motor response following nearly exact to the diameter fluctuations, with the exception of magnitude. This is because the growing velocity is limited with bounds in this case ±0.4 mm/min. In this experiment the diameter fluctuations were intentionally increased from ±2 μm to approximately ±6 μm with a standard deviation of 3.3 μm during growth. This increase in standard deviation was accomplished not by changing the feedback loop parameters, but by moving the scanning position of the laser micrometer up vertically by about 200 μm. As a known consequence of this, the feedback loop is altering the growing velocity from delayed diameter data, leading to a periodic trend seen in both the diameter and motor velocity.

Figure 4.19 represents the ideal motor response (±2 μm) for a low-loss fiber, with the laser micrometer reading at the solidus/liquidus interface rather than above it. Both Figure 4.18 and Figure 4.19 were grown at 2 mm/min. The standard deviation is three times lower when at the correct position. The total attenuation and scattering loss of this ±6 μm diameter variation does remain reasonably low loss for a fiber length of 45 cm. Figure 4.20 shows the increase in loss at shorter wavelengths for both scattering and total attenuation, then compares it to an ideal ±2 µm fiber loss. The minimum scattering is nearly the same at all wavelengths: approximately 0.1 dB/m. The scattering at all fiber positions is plotted in Figure 4.21 with a hot spot detected at 23 cm. It too begins to increase in scattering loss at the last 10 cm of the fiber, believed to be the result of back reflections at the end. The need for long fiber lengths begins to be apparent if the fiber naturally begins to increase in loss around 35 cm, but the information is lost by the back reflections of the fiber. Therefore, longer fiber lengths are needed to study this further.

Figure 4.22 directly compares the total losses of the two controlled fibers with different diameter standard deviations. The ±6 µm fiber was 45 cm so for comparison to it, the figure includes a fiber with diameter control at both 40 and 52 cm. At this point it had not been determined that the loss is length dependent. Both lengths of the diameter controlled fiber were lower loss than the ±6 µm fiber. It can be concluded that this increase in diameter fluctuation resulted in an increase in loss somewhere between 0.1 and 0.3 dB/m for this length of fiber.

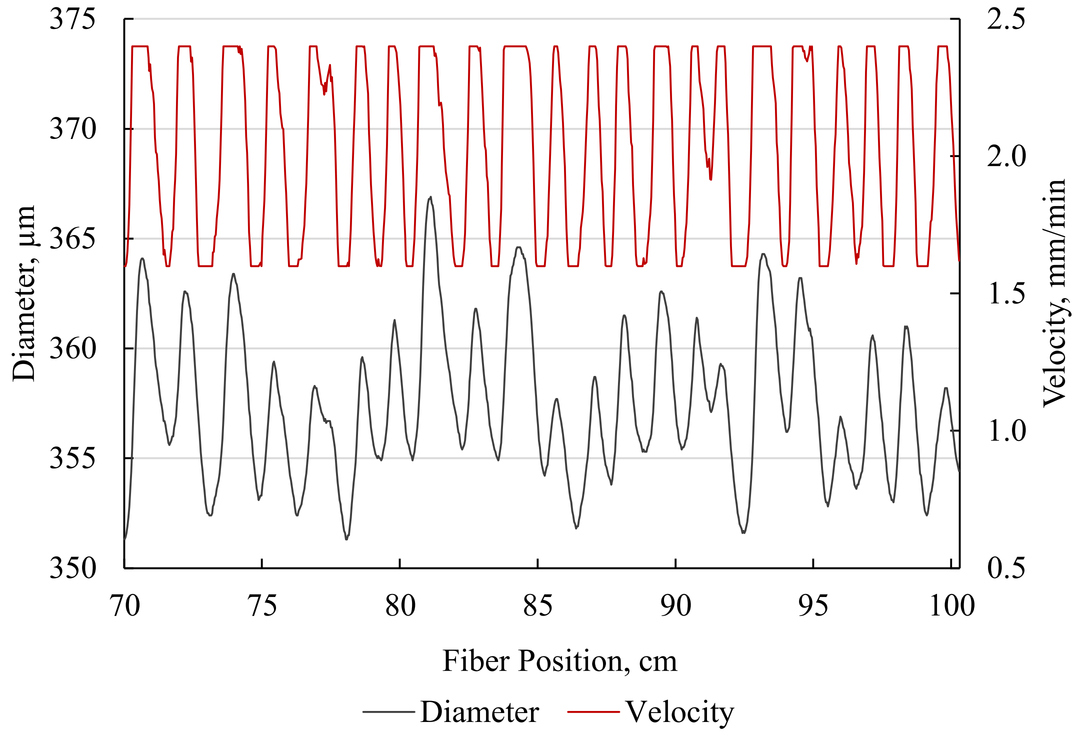

Figure 4.18 These two graphs show the motor's response from the feedback loop, to the diameter fluctuations for a fiber grown with the laser micrometer intentionally above the solidus/liquidus interface by 200 µm. There is a very strong correlation between the two, indicating that the better control over the velocity a better diameter will result. Here the standard deviation was 3.3 µm because of the delayed motor response.

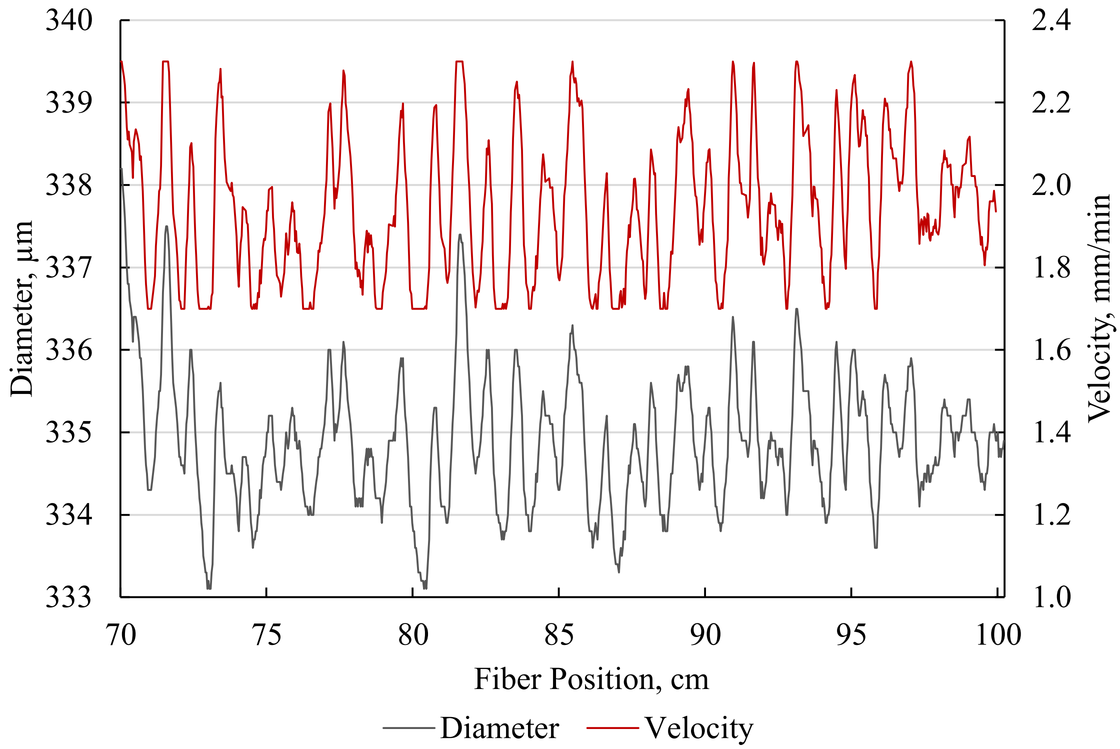

Figure 4.19 Motor response to diameter fluctuations for a fiber grown with the laser micrometer positioned at the freezing interface. The fiber diameter had a standard deviation of 0.8 µm over the full fiber length.

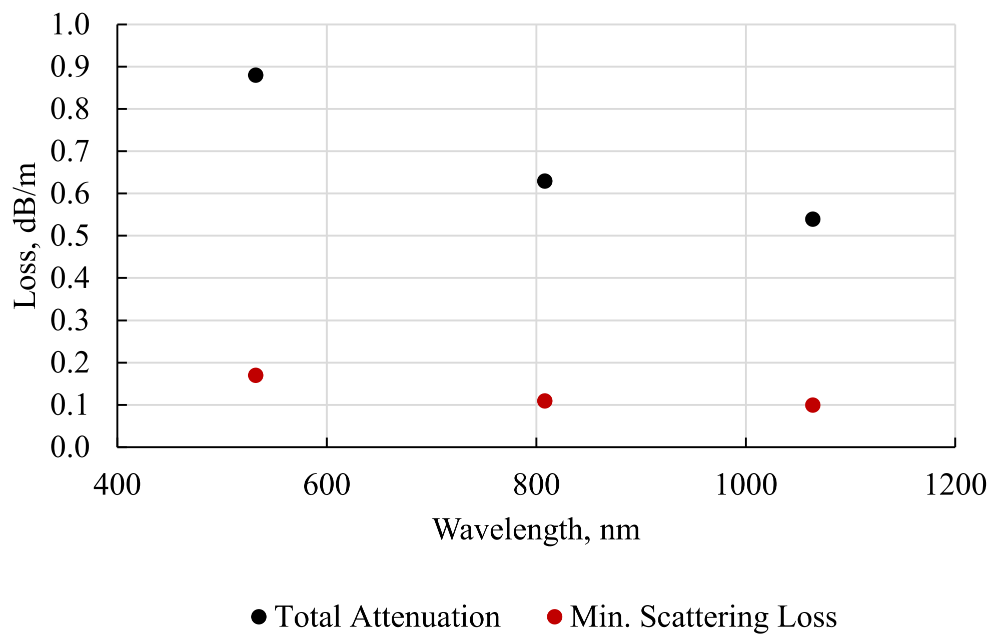

Figure 4.20 A 45 cm SC YAG fiber with an intentional diameter fluctuation of about ±6 μm. The fiber still demonstrated reasonably low-loss and minimum scattering for the first 30 cm. This fiber's total loss and minimum scattering are very comparable to the losses of fiber 2-26-16 at similar lengths.

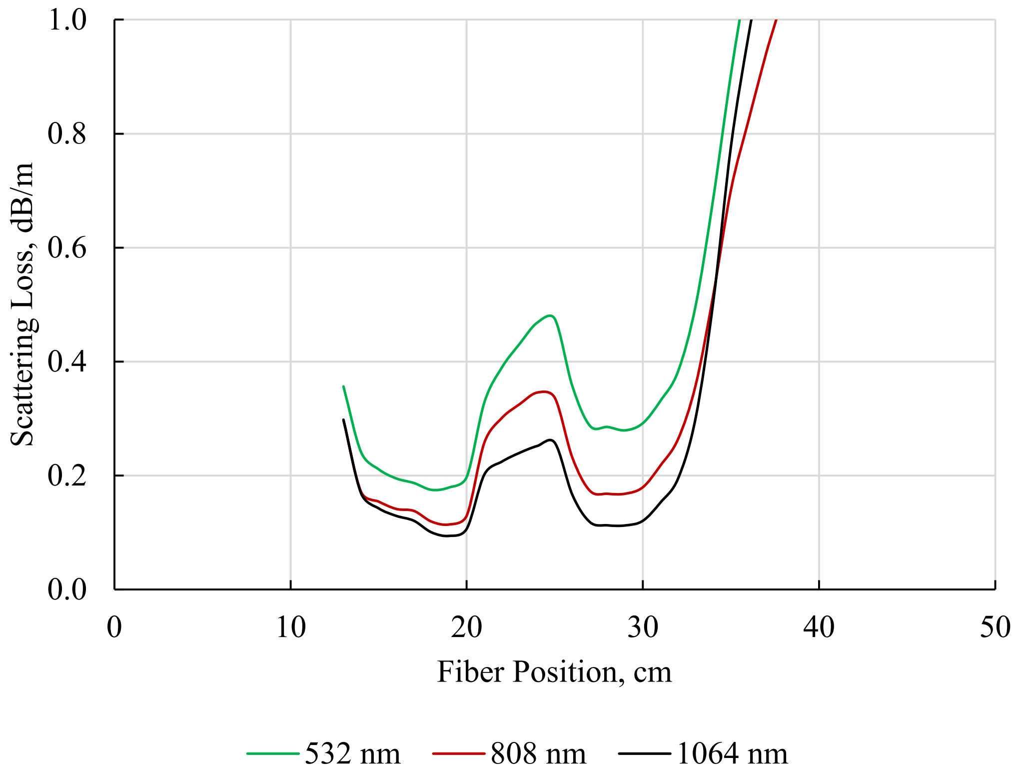

Figure 4.21 A 45 cm SC YAG fiber with an intentional diameter fluctuation of about ±6 μm. The scattering data, as a function of fiber position, demonstrates the similar effect of low scattering until the last 10-15 cm of the fiber. There is a defect at 23 cm and at the beginning of the fiber.

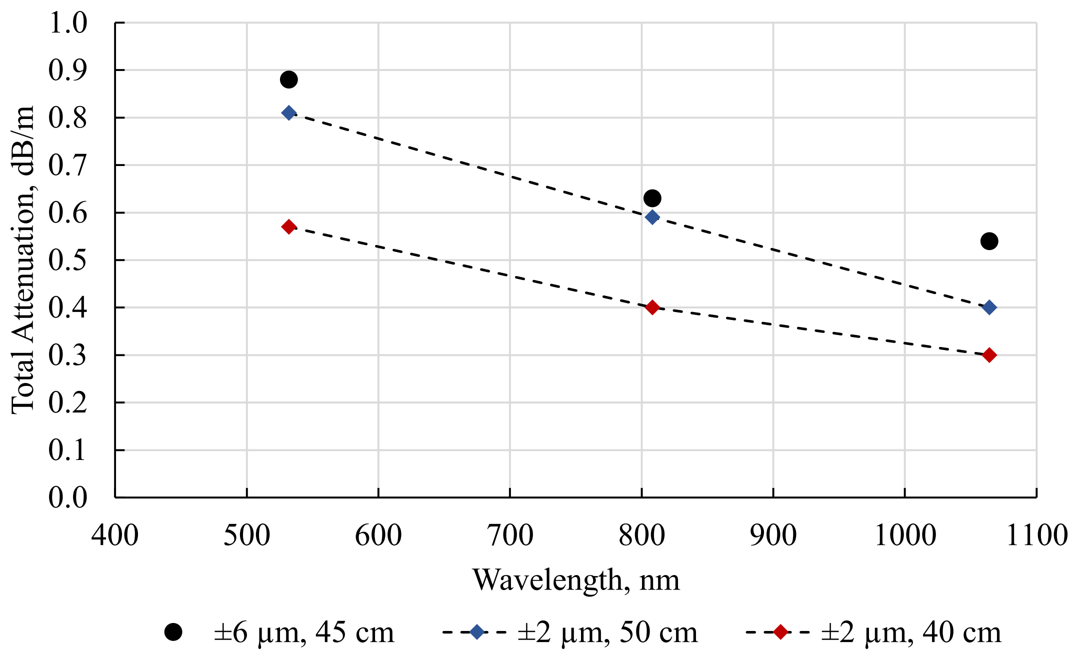

Figure 4.22 Compares the total attenuation of one diameter controlled fiber (±2 µm) at two different lengths to the ±6 µm fiber. These diameter controlled fibers are indicated with the dashed lines for both lengths. At both lengths, the total attenuation was less than the fiber with ±6 µm diameter fluctuation.

4.7 Low-Loss 1 meter YAG Fiber

The need for a longer fiber length was briefly addressed in the preceding section – in order to study the scattering increase after 35 cm. In this section, a new technique of posting the source material was used that allowed for fiber lengths up to 1.2 meter long. In theory, there is no limit on fiber length if you have a continuous source to feed into the molten zone. The old posting method had some translational issues that resulted in the growth randomly terminating in the middle, leaving a shorter fiber length than designed. Here, two SC YAG fibers were grown. The first fiber was 1.2 meters long and the second was 1 meter long. The first fiber had a few modifications to the molten zone that altered the quality. A few examples of this were moving the position of the laser micrometer during growth, momentarily stopping the source motor, and repositioning the source during growth. Performing any of these is not ideal standard procedure. The 1 meter fiber was grown using 2 W of power more than the 1.2 meter fiber and did not require any user modifications.

In this instance, the purpose for increasing the power was to prevent the corners of the source from interfering in the growth, not thinking it would affect the crystal quality. This conclusion was reached from a previous study on fiber quality as a function of CO_2 laser power. The results did not conclude a difference in attenuation at the short fiber lengths approximately 40 cm. At the time this was our standard length of fibers grown. From these two variables it cannot be concluded which was the dominant cause for the fiber improvement. In either case, both fibers are still excellent samples over a meter long with total attenuation below 1 dB/m at 1064 nm.

The 1 meter SC YAG fiber was the most recent and highest quality fiber grown to date. It was grown under very similar condition as previous fibers: velocity was 2 mm/min, 335 µm diameter, in a 350 µm guide tube, the same diameter control PID parameters, oriented SC seed, and only the increased power was varied. At a position of 90 cm during growth the diameter dipped to 310 µm, this resulted in a standard deviation of the diameter to be 1.23 µm, without this one dip the standard deviation would be approximately 0.77 µm. It is unclear what caused the dip, but the most likely cause is the source bar slipped in the translator for a moment. Resulting in a depletion of the molten zone, taking growth out of equilibrium for a moment. This fiber position is visible in the scattering data and the photo in Figure 4.23. It resulted in a surprisingly small amount of scattering for the magnitude of change in diameter. This data remains remarkably low, below 0.2 dB/m for the first 60 cm, especially when comparing it to any of the previously measured fibers or the 1.2 m fiber in Figure 4.24. The 1.2 meter long YAG fiber was grown with the same parameters mentioned above except for the power increase. It had a diameter standard deviation of 1.25 µm, slightly high due to the complications during growth. From Figure 4.24 it has higher scattering loss and increases faster than the 1 meter YAG. The two photos makes for a simple comparison of this increase. The 1.2 m fiber increases from 0.1 dB/m to 0.5 dB/m over the first 50 cm, whereas the better fiber remains fairly flat and below 0.2 dB/m over the first 60 cm.

The total attenuation measured for both fibers was excellent, but the 1 meter YAG fiber stood out. It had a total attenuation of 0.26, 0.46, and 0.79 dB/m at 1064 nm, 808 nm, and 532 nm respectively with the 9 cm focal length lens. These losses were approximately 20% higher when using a 1.5 cm focal length lens as seen in Figure 4.25. These losses are as low as fibers measured at half this length. At this time, no cut-back has been performed like in the previous sections to determine if this fiber to is length dependent. However, it would be expected to only have a slight length dependence based on both the scattering measured and visually seen. On the other hand, the 1.2 meter fiber likely has a strong length dependence with the higher total attenuation in Figure 4.26, potentially improving at shorter fiber lengths. The 1.2 meter fiber also exhibited higher losses when measured with the 1.5 cm focal length lens. Here, the difference in loss at each focal length is surprisingly similar for both fibers, approximately 0.2 dB/m at 532 nm and 0.05 dB/m at 1064 nm. This is not unexpected for the short focal length lens with a longer path length and increased number of reflections in the fiber resulting in a greater amount of loss especially over longer lengths. However, both of these fibers had the same scattering curve for each focal length indicating that this increase in loss would be absorption and not scattering losses.

A factor not yet address for these SC YAG fibers is how the losses respond to bending affects. In Figure 4.27, two separate fibers demonstrate the dependence on bending radius. First was a 60 cm SC YAG fiber that had a loss of 0.5 dB/m at 1064 nm when straight using the 9 cm lens. It had its loss increase above 1 dB/m with a bending radius of 25 cm. This same fiber had a different bending dependence when the light was focused in with the 1.5 cm lens. The loss was 1.1 dB/m when straight and only slightly increased from there for a bending radius of 25 cm. This was believed to be the result of the light converting to higher order modes that can become radiation modes as the fiber was bent to tighter radii. This idea was confirmed in the mode profiles in Figure 4.16 - Figure 4.17 as the fiber was cut-back from 52 cm to 10 cm.

The second surprising result was the 1 meter YAG fiber in Figure 4.27. The total attenuation remained constant as the fiber was bent to tighter radii. This remained true for both focal length lenses. Figure 4.28 represents the modal profile through the 1 meter fiber for both focal lengths, before and after bending at 1064 nm. There was no observable difference between these four profiles; which is not completely unexpected because the loss was virtually unchanged at 1064 nm. These exciting new results make a conclusion difficult when an affect such as bending loss varies between fibers as a result of their different loss mechanisms. However, Figure 4.29 demonstrates that the total attenuation measured in the 1 meter YAG fiber has reached the absorption of the bulk YAG material. This experimental absorption data is from Innocenzi[48] and Mann[49] seen in Chapter 1. Therefore, contamination in the raw materials is currently restricting the improvements of the SC YAG fibers further.

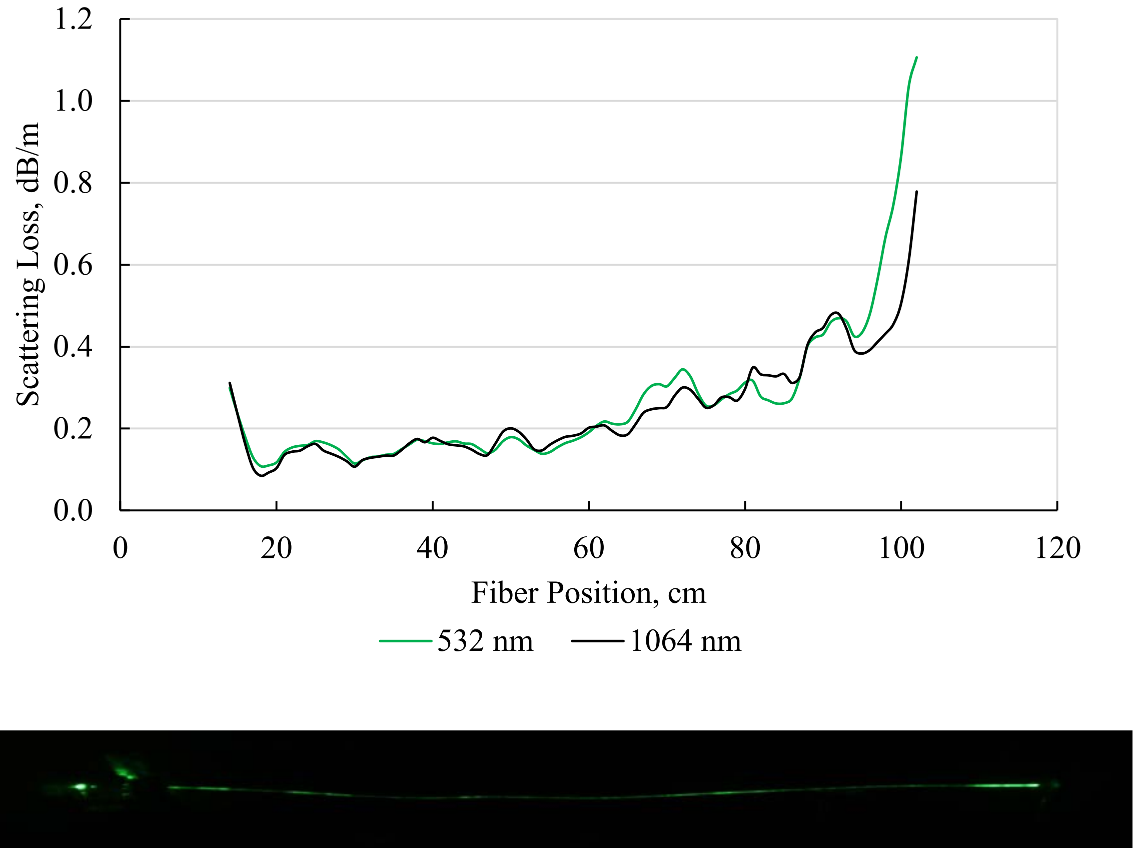

Figure 4.23 Scattering of the 1 meter SC YAG fiber, with an image of the scattering light transmitted through the fiber. Scattering loss remains unchanged with different focal length and wavelength.

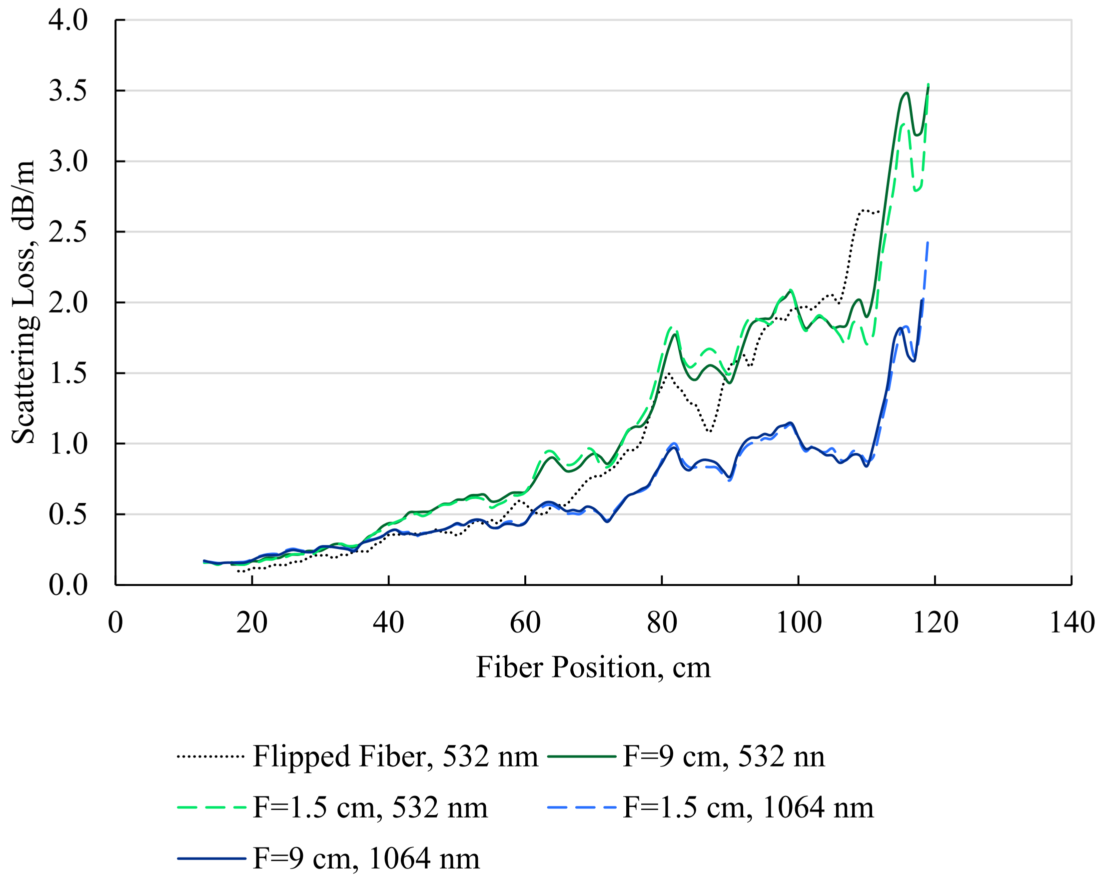

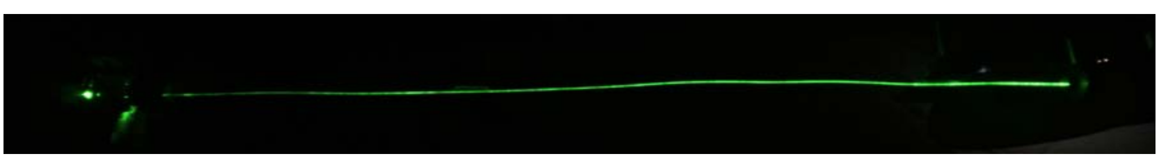

Figure 4.24 Scattering loss for the 1.2 meter SC YAG fiber, with an image demonstrating the increase visually. This increase in loss as light propagates through the fiber is believed to be modes coupling to radiation modes due to fiber irregularities. When the fiber was flipped end-for-end, the increased scattering remained.

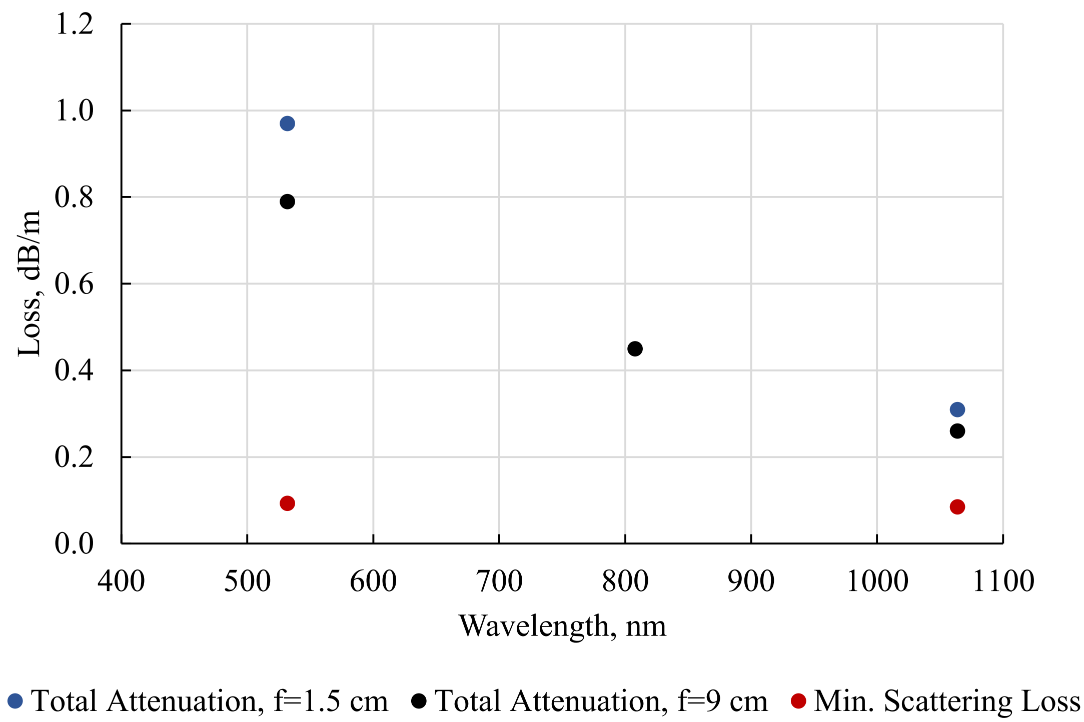

Figure 4.25 Total attenuation of the 1 meter SC YAG fiber using two different focal length lenses. The minimum scattering is included, with very little change at the two wavelengths.

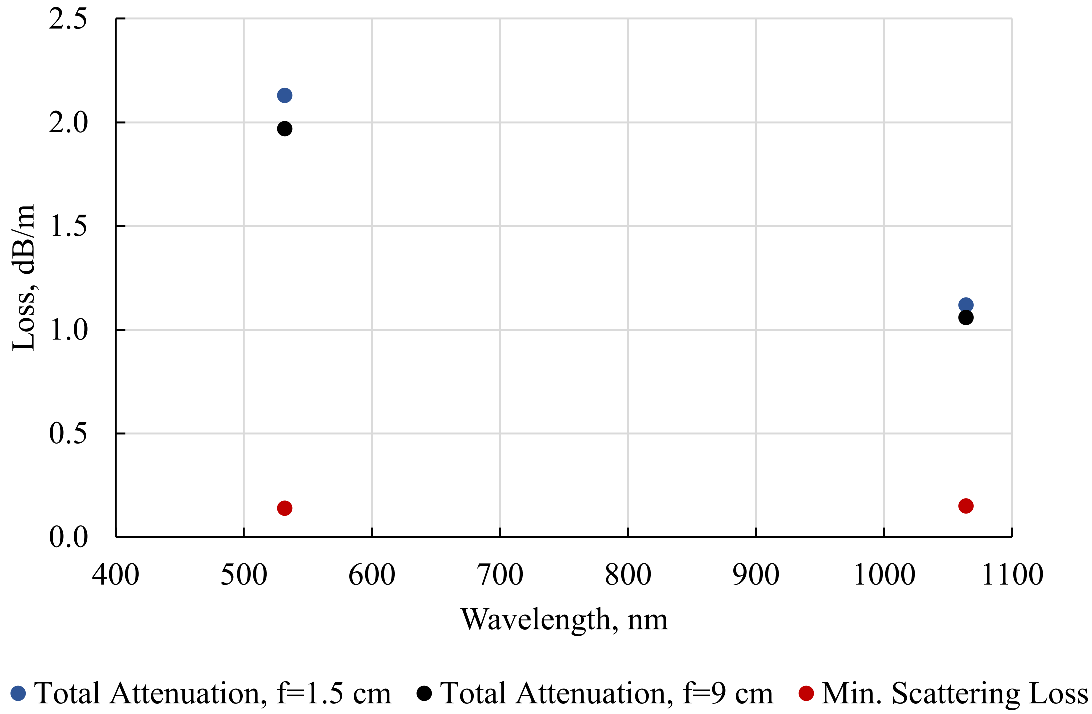

Figure 4.26 Total attenuation of the 1.2 meter SC YAG fiber using two different focal length lenses. The minimum scattering is included, with very little change at the two wavelengths.

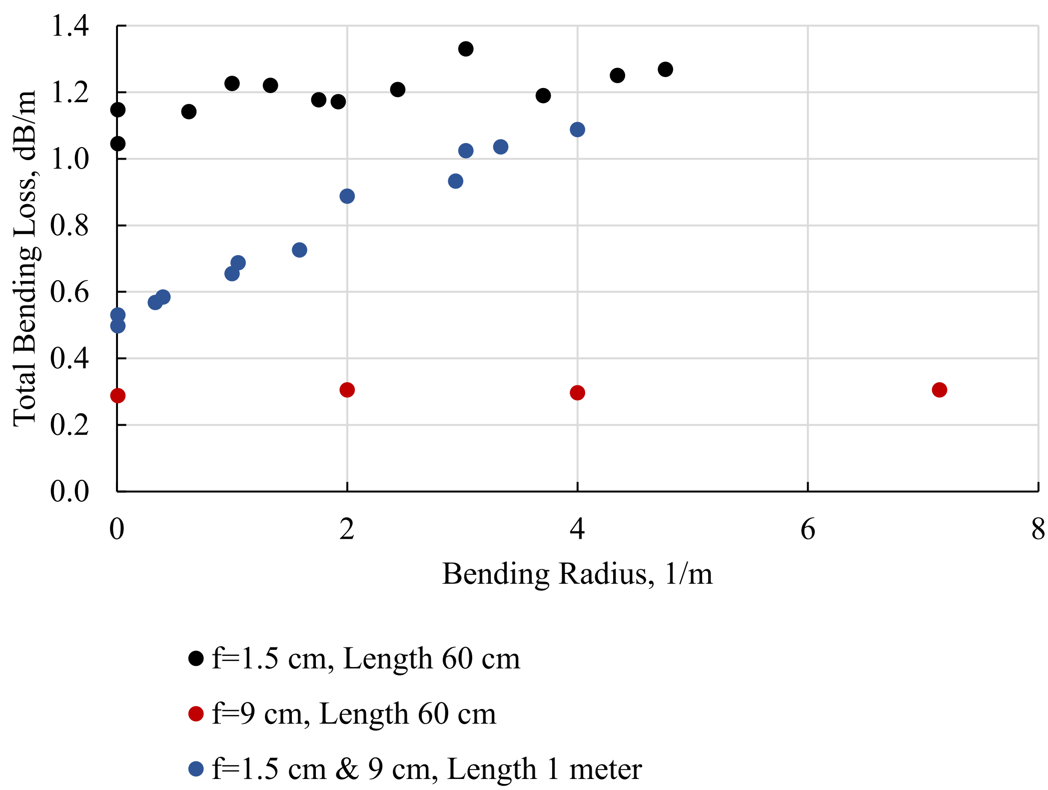

Figure 4.27 The 1 meter SC YAG fiber does not demonstrate dependence on the bending radius of the fiber. This result held true for both the 9 and 1.5 cm focal length lenses. However, a previously measured 60 cm SC YAG fiber had dependence on the bending radius at both focal lengths. There will be a critical radius that the 1 meter YAG fiber will begin to exhibit bending loss.

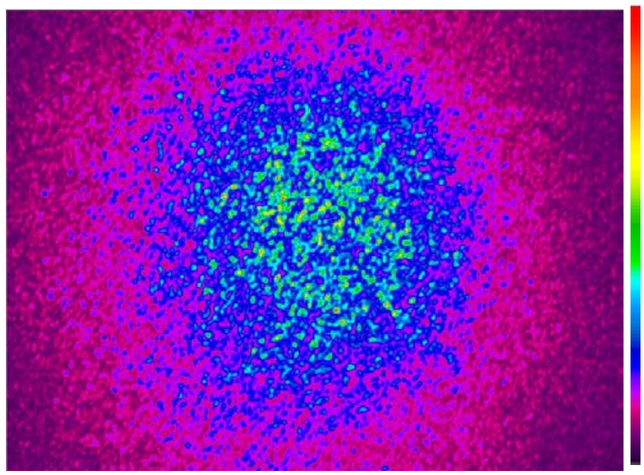

Figure 4.28 Output mode profile through the 1 meter fiber. The intensity distribution remained unchanged when bending the fiber or switching focal length of the lens. This agrees with the loss and bending loss measurements not changing at 1064 nm.

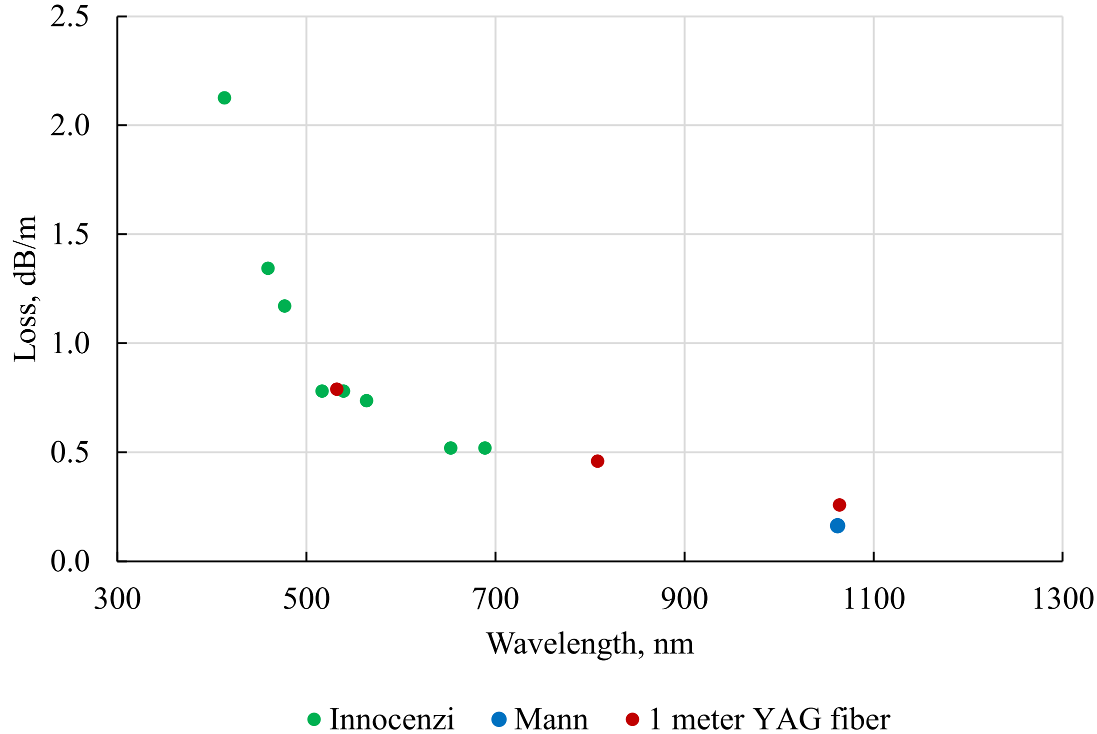

Figure 4.29 Experimental absorption loss performed separately by Innocenzi and Mann compared with the total attenuation of the 1 meter YAG fiber, measured at three wavelengths. The total loss is only slightly higher than the absorption loss.

4.8 Holmium YAG

Thus far, all loss measurements have been on undoped YAG fibers 330 µm at various lengths grown from SC source material from a Chinese vendor. It was important to be able to grow this undoped YAG material at lower-losses in order for RE YAG fibers to be fully utilized, specifically for a fiber laser. In this section, 0.5% Ho:YAG SC fibers were grown with lower losses at lengths of 50 cm. These doped SC YAG fibers remained unclad and were grown from a different source provider than the undoped source material. This source material is a key reason both the total losses and scattering losses were consistently lower. At first, it was believed to be an error in the scattering data, but the drastically low minimum scattering loss of 0.02 dB/m was consistent for multiple doped fibers of varying dopants and concentrations. Figure 4.30 demonstrates the scattering loss remained at these lower values until the last 10 cm of the fiber. Figure 4.31 demonstrates this minimum scattering loss together with the total attenuation of a 0.5% Ho:YAG SC fiber. The higher loss at 1064 nm is the result of a slight increase in absorption from holmium seen in Figure 4.28 as the curve approaches the 1117 nm peak. This increase is confirmed to be absorption loss, with the scattering loss being less at 1064 nm than at 808 nm laser. The 532 nm wavelength could not be used due to holmium's absorption.

These low scattering losses were consistently seen for both undoped and doped YAG fibers grown from SC source material purchased from Scientific Materials Corp. Once these lower scattering measurements were made for the doped SC YAG source material, undoped SC YAG source material was purchased from Scientific Materials. This supplier was about 5 times more expensive for slightly shorter SC YAG source bars, but the scattering loss from the fibers is about 0.1 dB/m lower. Indicating a higher quality SC source material when compared to the original Chinese provider. Figure 4.32 and Figure 4.33 represent an undoped SC YAG fiber 35 cm long from this provider. It has a similar minimum scattering of 0.03 dB/m at 1064 nm, but it does increase slightly faster after a short length than the doped fiber does. It too has an increase at the back end of the fiber. Even though the fiber is a little shorter at 35 cm, the loss is below 0.2 dB/m at both 808 and 1064 nm. The benefits of these low-loss SC YAG fibers will be demonstrated in Chapter 6 with fiber laser results performed at Clemson University.

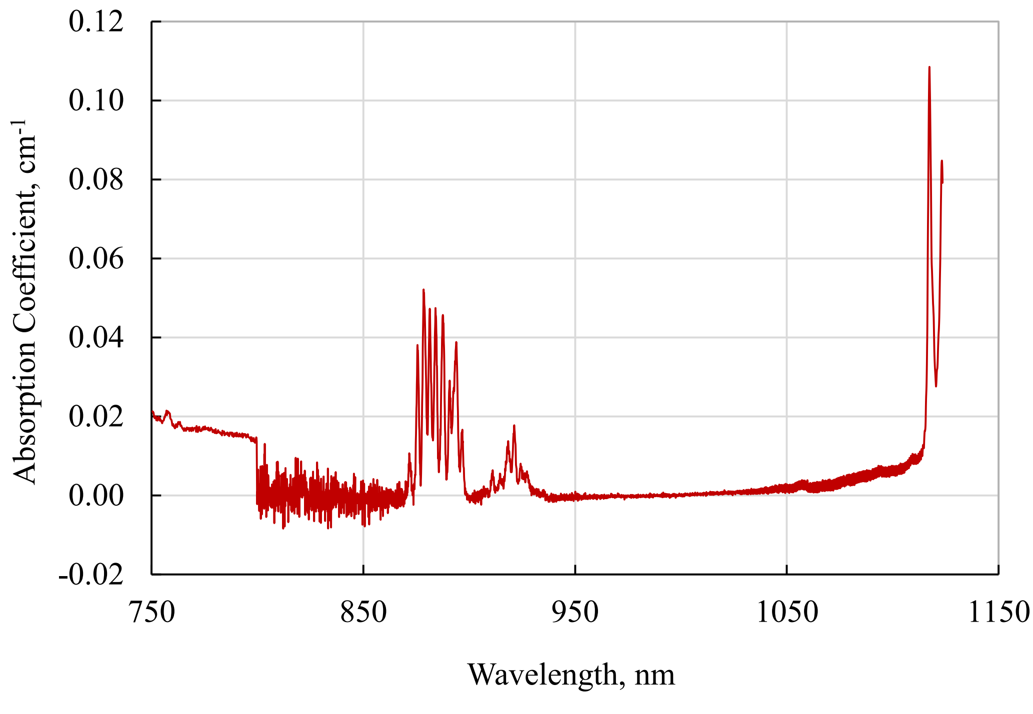

Figure 4.30 Ho:YAG spectra data from Scientific Materials showing very slight increase in absorption at 1064 nm. Raw data taken by Scientific Materials.

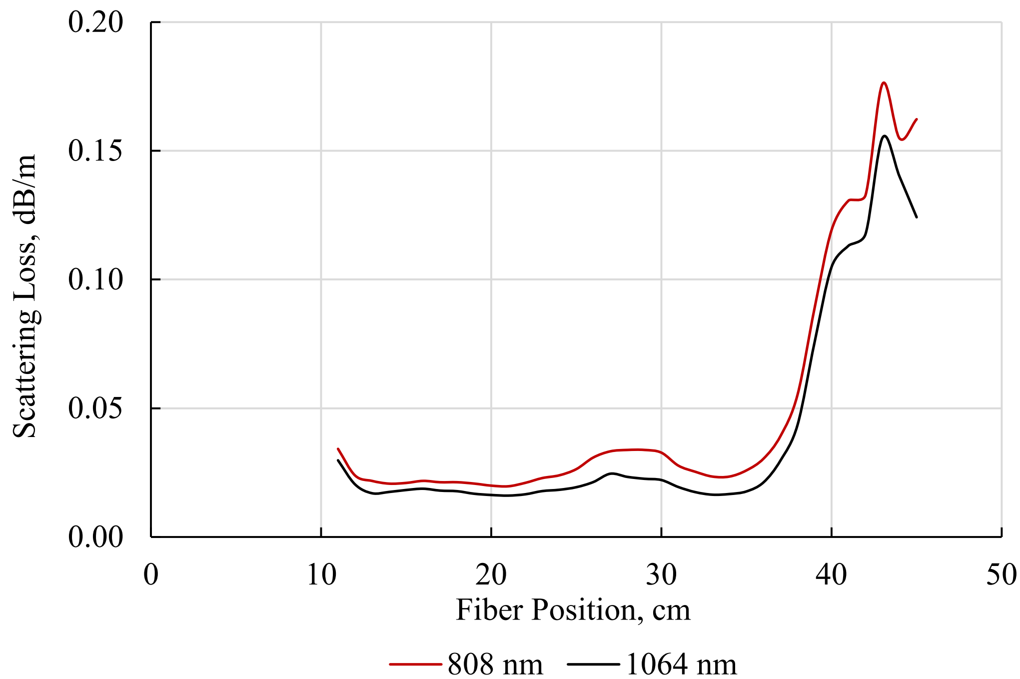

Figure 4.31 These low scattering losses were consistently measured for multiple 0.5% Ho:YAG fibers. The minimum loss of 0.02 dB/m remains nearly constant until it increases at 36 cm for the 1064 nm laser.

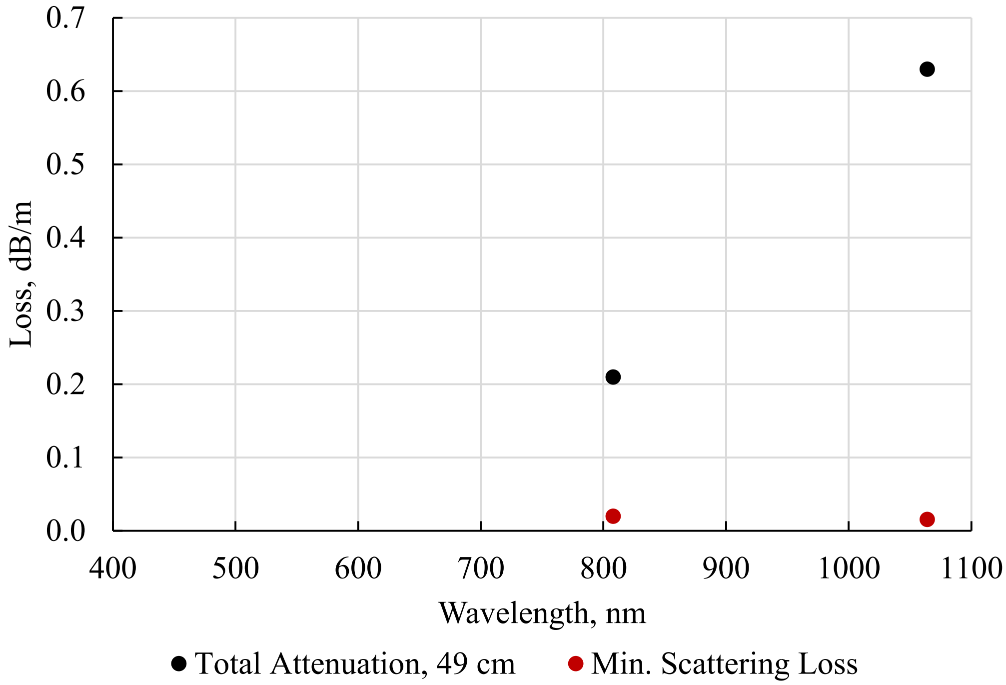

Figure 4.32 This total loss increase from 808 to 1064 nm was consistently measured for multiple 0.5% Ho:YAG fibers. With the minimum scattering loss being a very small contribution to the loss. Fiber was quite long at 49 cm.

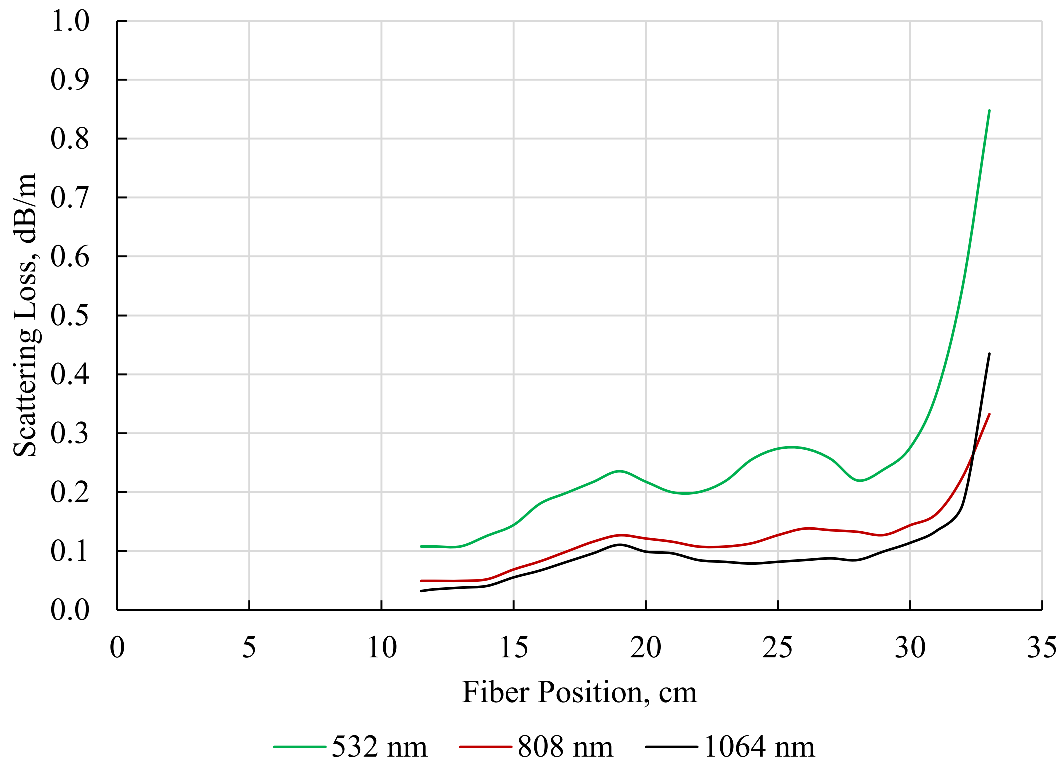

Figure 4.33 Undoped SC YAG fiber with 0.03 dB/m minimum scattering at 1064 nm. This is very similar to the scattering for the 0.5% Ho:YAG fiber from the same source provider. The undoped YAG source material was obtained from Scientific Material.

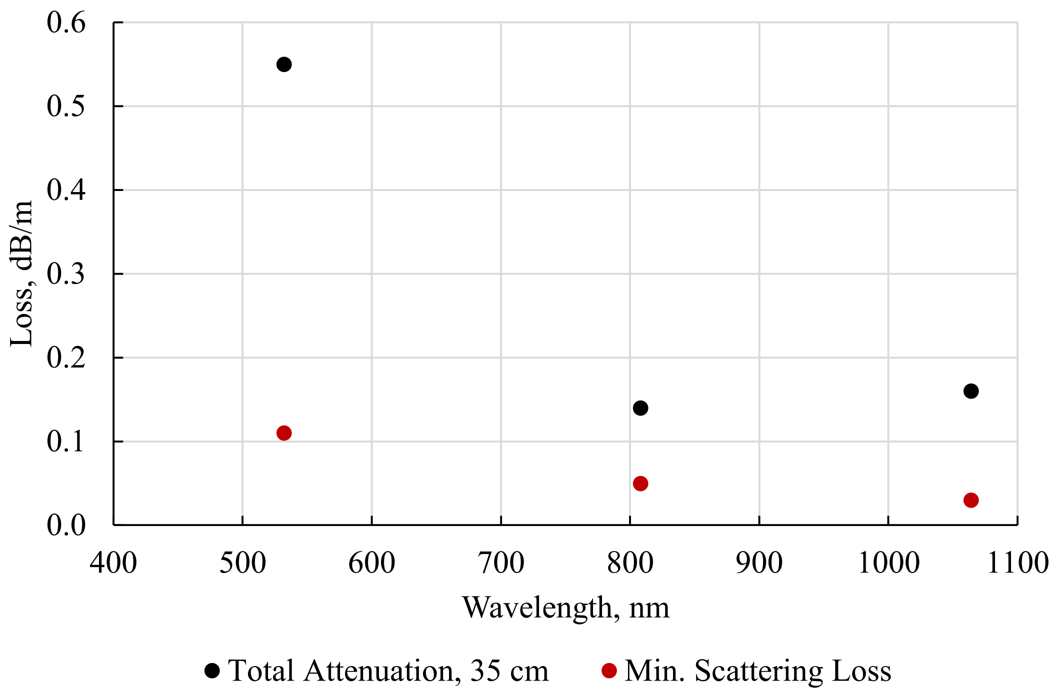

Figure 4.34 Undoped SC YAG fiber with the total loss and minimum scattering loss. The source material was obtained from Scientific Materials.

Chapter 5. Cladding Rod-in-Tube

The rod-in-tube (RiT) method has been used in pulling viscous glasses for the purpose of developing graded index fiber. RiT has been attempted for the first time to be adapted for the LHPG technique. This was attempted by inserting a 50% erbium doped YAG fiber into a pure YAG tube. This source preform was then used to grow a fiber, in expectation that more erbium would remain in the core of the fiber. To achieve this, the growing rate would need to be sufficiently fast to overcome diffusion equilibrium. It is our desire to develop a graded index of refraction by having the erbium be distributed radially, with higher concentrations in the center. Thus, the growing rate must overcome the rate of diffusion for the fiber not to diffuse to equilibrium.

A SC YAG source rod approximately 1.1 mm in diameter was initially cut into one centimeter long sections. These sections were then mechanically drilled with an inner diameter of approximately 550 µm, at which point a 50% erbium doped YAG fiber was inserted inside the tube. Multiple tubes can be stacked on top of one another but a continuous growth between them is not currently possible, because of surface tension pulling the tubes apart as it approaches the end.

During the LHPG process, the Er^{3+} ions diffuse outward into the pure YAG. Therefore, time in the molten zone has the largest impact on diffusion, with temperature held constant. These fibers were grown at approximately 370 µm and a velocity of 1, 2, and 3 mm/min and a fluorescence profile was used to determine the radial distribution. These fluorescence profiles were performed by our collaborators at the University of Michigan. Faster growing velocities were attempted: 4, 5, and 6 mm/min, but the core was slightly cracked. These were grown slightly before we fine-tuned our CO_2 laser alignment. Therefore, it remains feasible to try these growing velocities again. For the purpose of this section, the 1-3 mm/min velocities were used to calculate the diffusion coefficient.

The fluorescence profiles were used to indicate a radial distribution of erbium, which has been used to estimate the diffusion coefficient of Er in YAG. As discussed in section 2.6, Δn=0.001 is sufficient enough change to have a graded index fiber with light coupled at <3.4°. This is possible from only a 5% erbium concentration difference. A group that measured refractive index using an interferometry method between 0.25% erbium doped YAG to undoped YAG, determined $\Delta n = 5.2 \times 10^{-5}$. It is also pointed out that this low Δn will yield an ultra-low NA that should lead to a single transverse mode.[75]

Fluorescence was first performed to demonstrate that there was indeed an erbium distribution and not a homogeneous distribution from this RiT growth method. Fluorescence was measured on a thinly sliced, 1 mm thick, RiT 370 µm Er^{3+}:YAG fiber to analyze the radial distribution of erbium. The thin slices of fiber were excited at 532 nm; the relative intensity of Er^{3+} ions exhibits a curved distribution with the maximum in the center seen in Figure 5.1 and Figure 5.2 with a fitted curve at 1 and 3 mm/min respectively. This indicated that the erbium ions are diffusing outward into the YAG as expected. It is worth noting that when sampling a pure Er^{3+}:YAG fiber the fluorescence profile had a uniform intensity across the diameter, confirming that the mechanism was not segregation or a fabrication of this LHPG technique, but indeed diffusion.. Therefore, by changing the growth velocity and/or diameter, the final dopant distribution should be partially controllable. These fluorescence profiles demonstrate the distribution of erbium ions, but not the refractive index. Another technique needs to be used to demonstrate the change in index from the center to the periphery.

The fluorescence profiles were used to determine an estimated value of the diffusion coefficient of erbium in YAG. There has been no published value for the diffusion coefficient, but there has been modeling on yttrium self-diffusion in YAG. They determined that the diffusion coefficient for yttrium in YAG was 5.594×10^{-11} m^2/s.[76] This work was in reasonable agreement with our estimated erbium diffusion coefficient of 8.7×10^{-11} m^2/s in YAG. This was expected because erbium can replace all ytterbium ions in octahedral sites to form SC ErAG, due to their very similar ionic radii that allow for this exchange. From this initial work, the principle idea of creating a graded index fiber from a RiT has been demonstrated. The next step is measuring the index change or the concentration of erbium as it is radially distributed.

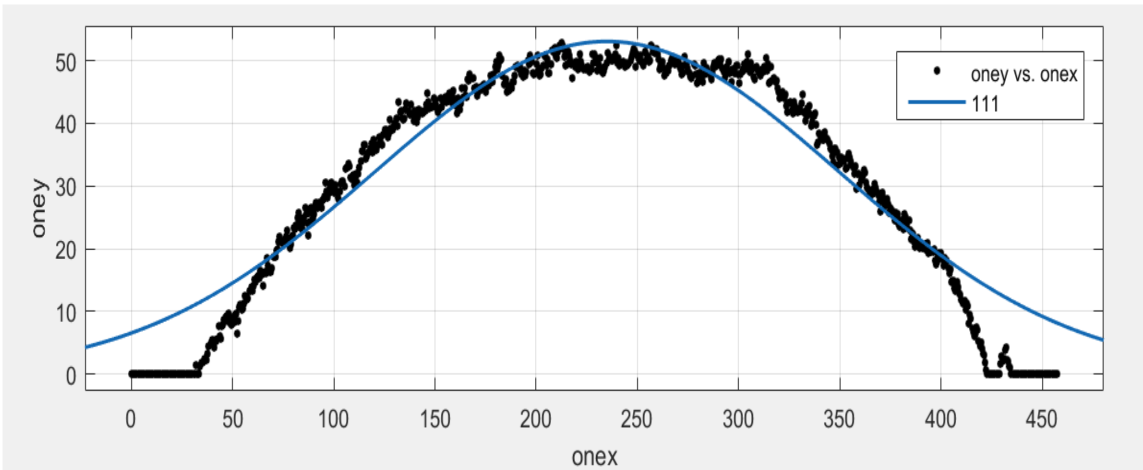

Figure 5.1 Fluorescence of erbium in a YAG fiber grown at 1 mm/min.

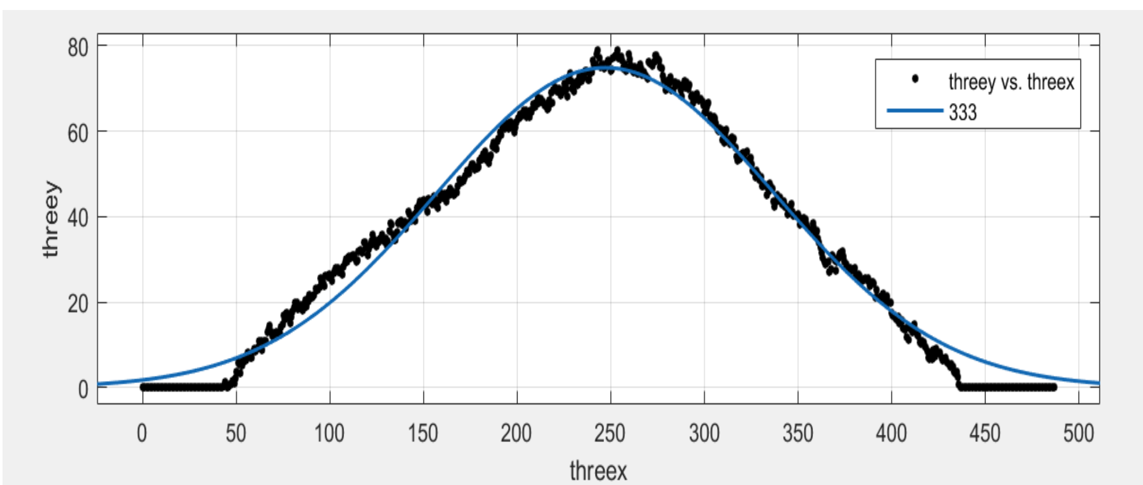

Figure 5.2 Fluorescence of erbium in a YAG fiber grown at 3 mm/min.

Chapter 6. Holmium YAG Fiber Laser

Our colleagues at Clemson University concentrated on the lasing properties of our Ho:YAG SC fibers. Clemson characterizes the absorption and emission of the holmium dopants in the fibers and their lasing performance. They prepare the SC fibers by polishing the fiber ends and checking the SC fiber quality. Figure 6.1 demonstrates the measured absorption coefficient of 0.5% Ho:YAG crystal at both the pump wavelength and the lasing wavelength. Notice the peak absorption is at 1908 nm, but in the first experiment the 1932 nm peak was used instead. This was the case because initially this tunable laser had more pump power at 1932 nm than at 1908 nm. Therefore, the increase in power was traded for less absorption. An advantage of choosing a weaker absorption line is that this allows for the pump power to be more uniformly distributed. The length can be optimized such that the absorption occurs throughout the full length, improving thermal loading. The figure also shows the absorption at the lasing wavelength, 2090 nm.[84]

Figure 6.2 demonstrated lasing at 2.09 μm in 0.5% Ho:YAG SC fiber, with a diameter of 320 μm and a length of 11.5 cm fabricated using the LHPG method. The total loss was measured for the full length of fiber, 49 cm, before sending the 11.5 cm length needed for the fiber laser. Figure 4.32represents these results with a loss of 0.2 dB/m at 808 nm and

0.6 dB/m at 1064 nm. This fiber had significantly less scattering than fibers grown from another bulk source provider. Our best results were with a slope efficiency measured to be 72.3% with respect to incident pump power, with a lasing threshold of 3.1 W. The maximum laser output power was 26.7 W with 40.9 W of absorbed pump power. The laser wavelength is centered at 2090.6 nm with a full width at half maximum (FWHM) of 1.3 nm, shown in Figure 6.4. This is, to the best of our knowledge, the highest output power achieved at 2 μm from a SC Ho:YAG fiber and similar efficiencies have been demonstrated in Yb:YAG.[12, 13] These results were achieved with the lowest total loss and lowest scattering loss of the Ho:YAG fibers. Three Ho:YAG fiber lasers will be demonstrated, showing the importance of lower loss material for laser applications.

For this lasing result, the lasing cavity consisted of a flat-flat high reflector (HR) and the uncoated distal end-facet of the SC fiber which provides 8% Fresnel reflection as the output coupler (OC). The HR was placed as close as possible to the front facet of the SC fiber to provide as much feedback as possible for the lasing wavelength. The 1908 nm Tm:fiber pump laser was operated in a pulse mode with a pulse repetition frequency of 10 Hz and a duty cycle of 50% to reduce the thermal load in the crystal rod. This exact laser cavity, set-up, and pump were also the design for a medium loss, 0.5% Ho:YAG SC fiber. The comparison of these two fibers with their lasing results are presented in Figure 6.2. This second fiber was 320 μm, 11.5 cm long with a measured loss of 0.9 dB/m at 1064 μm. The slope efficiency was 67.5% with respect to incident pump power.[13] The max output power was 23.5 W under pulsed pump mode. The continuous pump mode, however, did plateau as it approached an output power of 10 W.[13]

Finally, the poorest quality of the three SC fibers. This was our first attempt at making the holmium fiber laser and, at this stage, the poor quality was the standard of the SC fibers being grown. Figure 6.3 demonstrates the initial lasing results obtained. It was initially an exciting result to have demonstrated a SC YAG fiber laser, however the output power and optical slope efficiency were far below bulk Ho:YAG lasers and the results later obtained. These lasing results were performed on high-loss, low quality (9 dB/m) 330 μm, 10.1 cm SC 0.5% Ho:YAG fiber. This fiber remained unclad as were all lasing results. The results show an optical slope efficiency of 10.2% with respect to incident pump power; when a thulium fiber laser with a 1932 nm wavelength was used as a pump source.

Besides a lower quality crystal, this experimental laser cavity set-up was different than the more optimal one described above. Here the cavity was comprised of a highly reflective mirror and output coupler spaced apart from the fiber ends. The light from the ends was focused with two lenses, in and out of the fiber. These two lenses were un-coated calcium fluoride lenses with a focal length of 15 mm. The lenses were removed from the laser cavity already described and the fiber switched to butt-coupling to the highly reflective mirror. Also, the pump source was switched from the 1932 nm to an IPG TLR-50 1908 nm laser where it had greater pump power and the holmium has greater absorption. This laser operated in both pulsed and continuous mode.[85]

The output mode profile for the Ho:YAG SC fiber laser is shown in Figure 6.5 and Figure 6.6. Figure 6.5 demonstrates the output mode taken at highest power for the 0.9 dB/m fiber. This medium loss profile is best compared to the output mode for the lowest loss, 0.6 dB/m fiber. From these profiles, some evidence of scattering seems present in Figure 6.5 because of the improved uniformity in Figure 6.6. Therefore, these results are clearly vital to this work because they demonstrate the importance of reducing the extrinsic losses of the SC YAG fibers for the improvement of SC fiber applications. Even though the results are on relatively large air-clad fiber diameters, future efforts can continue to improve both the loss on small diameter fibers and fabricating a cladding.

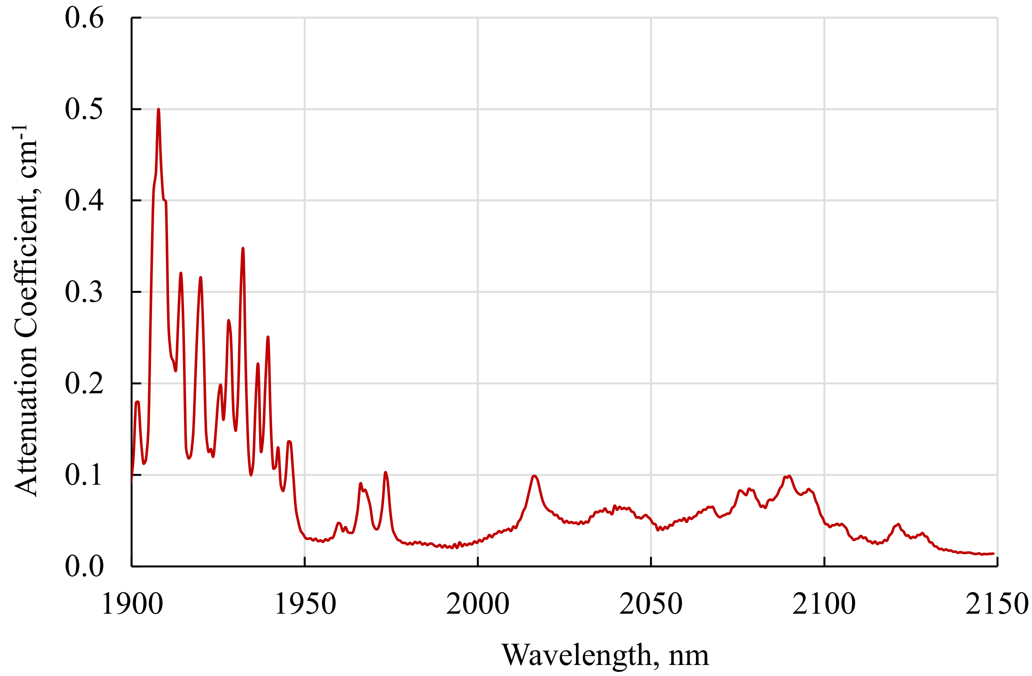

Figure 6.1 The measured absorption coefficient of 0.5% Ho:YAG crystal 10.1 cm long at both the pump and lasing wavelength. Data taken at Clemson University.

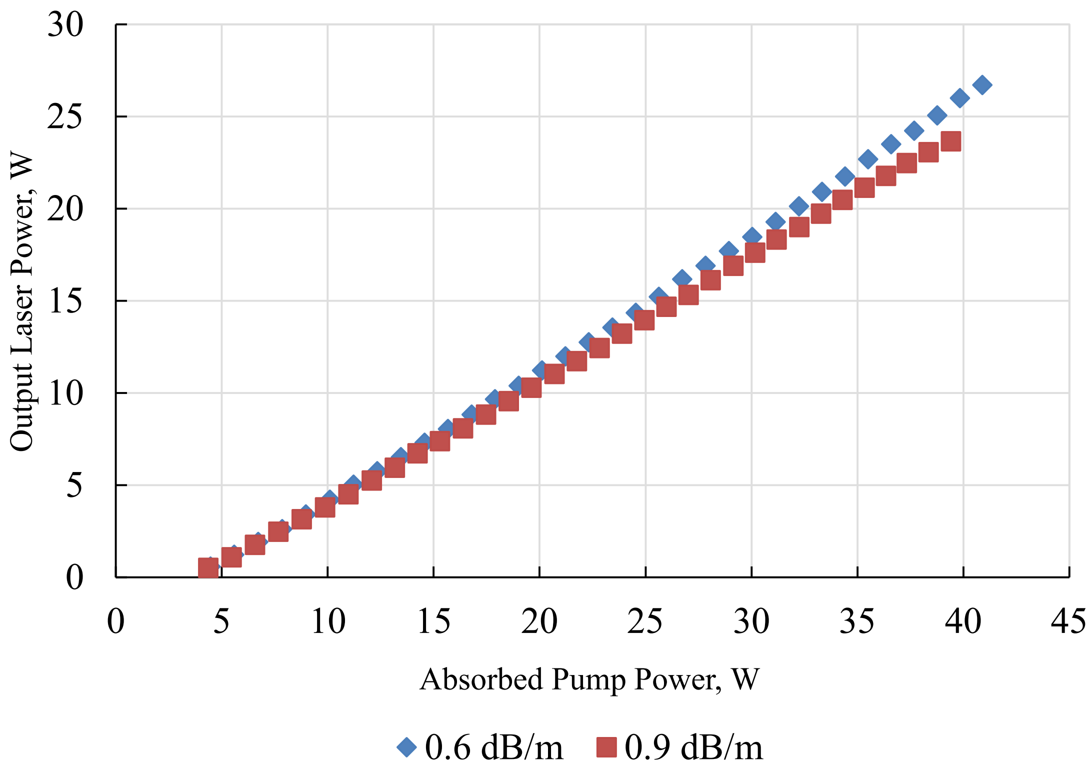

Figure 6.2 Final attempt of lasing a higher quality, 0.6 dB/m, 0.5% Ho:YAG SC fiber compared with a 0.9 dB/m 0.5% Ho:YAG SC fiber. This experiment was performed with same cavity and pump. The slope efficiency increased from 67.5% to 72.3%. Data taken at Clemson University.

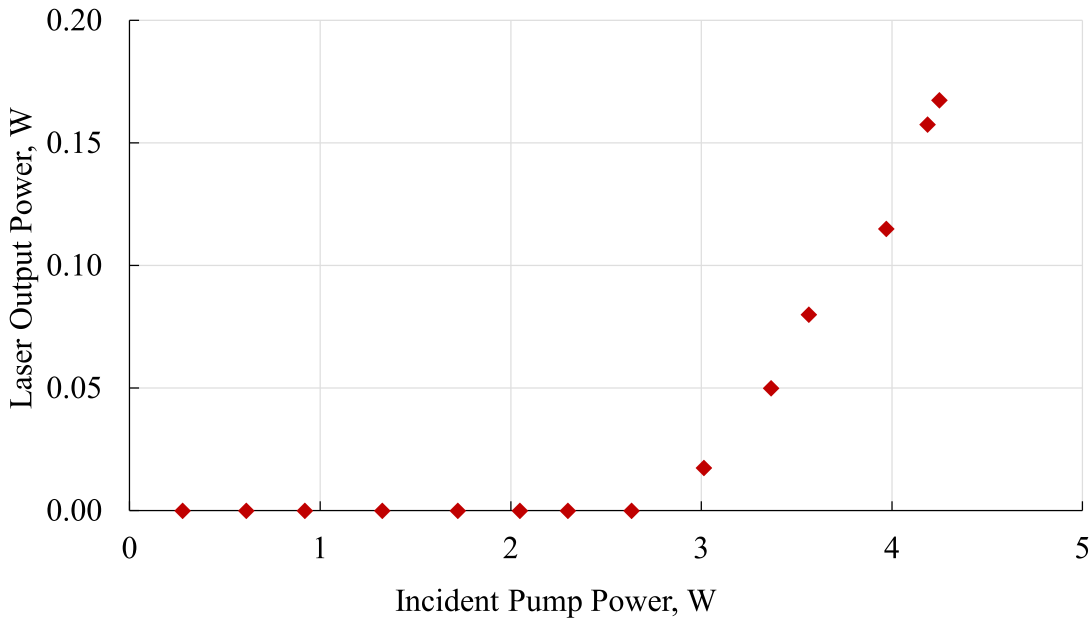

Figure 6.3 Initial lasing results of a low quality 0.5% Ho:YAG SC fiber, approximately 9 dB/m. This experiment was performed on a different laser and laser cavity. Data taken at Clemson University.

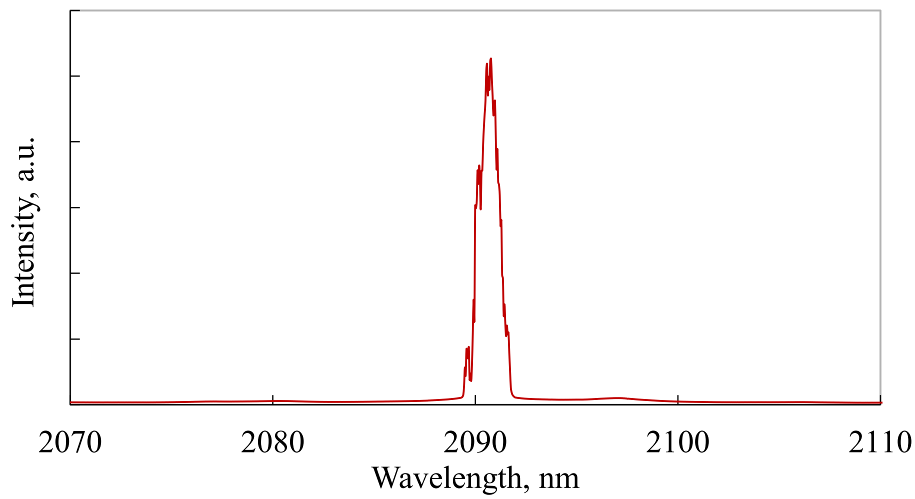

Figure 6.4The lasing peak wavelength was 2090.6 nm with a FWHM of 1.3 nm; when measured at highest output power. Same result for both high-quality SC fibers. Data taken at Clemson University.

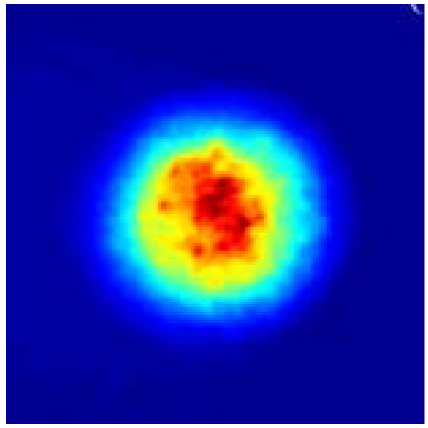

Figure 6.5 The output mode taken at highest power of the 0.9 dB/m SC Ho:YAG fiber. Data taken at Clemson University.

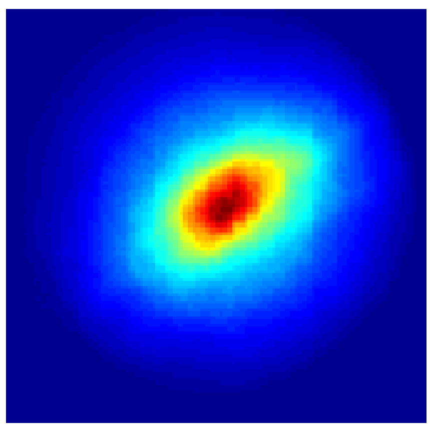

Figure 6.6 The output mode taken at highest power of the 0.6 dB/m SC Ho:YAG fiber. Data taken at Clemson University.

Chapter 7. Conclusions

High-quality SC YAG fibers have been grown with consistent losses below 0.5 dB/m at 1064 nm. Most notable was a 100 cm SC YAG fiber that maintained its orientation from end to end. It had a low loss of 0.3 dB/m at 1064 nm, with about 50% of this total loss being scattering. This fiber offered other excellent properties that was not consistent with all fibers. The total loss did not increase with decreasing bending radius, as observed in a 60 cm fiber. In all fibers measured there was a correlated increase in loss with decreasing wavelength, partially due to the increased absorption at shorter wavelengths (as demonstrated by Innocenzi). In addition to the absorption, a majority of fibers also had a wavelength dependent scattering loss. The scattering mechanism was concluded not to be Rayleigh scattering with λ^{-4} dependence. However, determining if the scattering was Rayleigh-Gans (λ^{-2}) or anomalous diffraction was inconsistent between fibers, making a further conclusion difficult.

The improvement of losses from around 10 dB/m to below 0.3 dB/m was primarily attributed to improvements made to the LHPG that allowed for adjustments during alignment of the CO_2 radiation. The first major change was replacing old optics with a new transmission based axicon. The second of these improvements was ultimately going from a single axis view point to a double axis offset by 90°. This allowed for real time changes to be observed from two different axes simultaneously. The third change was recognizing that diameter control was not enough to maintain a straight fiber with a uniform geometry. This observation was made possible with the increased magnification of the new digital cameras that showed the shifting position of the newly grown fiber over time more apparent. These effects were minimized by using a tighter inner diameter guide tube; noticeably improving the fiber waveguide geometry.

At this time, the low losses are not attributed to a few of the growing conditions that were used. First, the new seed orientation that resulted in a rounded square cross section was compared to the randomly oriented seed that resulted in an elliptical cross section. Comparing these two seeded orientations resulted in no significant difference in losses. This was also true of fibers showing ribbed facets along the fiber vs. facet-free fibers. This was an unexpected result, but for these studies the fibers were shorter (30-50 cm), and fiber diameter relatively large compared to SM optical fibers. Even with this result, significant effort was given to consistently grow facet-free fibers.

RE doped SC YAG fibers have demonstrated equally low attenuation as undoped YAG fibers. These RE doped SC YAG fibers had significantly lower scattering loss than undoped YAG, 0.02 dB/m compared with 0.1 dB/m. This has been linked to the quality of the starting RE source material, which came from Scientific Materials. Detailed analysis has yet to be performed to determine why the lower scattering, but purity of the starting powders used to grow the SC boule is most probable. Specifically a fiber laser has been made from a 0.5% Ho:YAG fibers. The lasing performance has been improved in part due to the increased quality of the SC fiber, allowing for an increased slope efficiency to 72.3%.

Low total attenuation below 0.3 dB/m has been achieved for a meter length of undoped YAG fiber. With this total attenuation, while scattering is still present, a majority of the loss can be attributed to absorption.

The three fiber diameter control experiments: ±25 µm, ±6 µm, and ±2 µm; demonstrate that for shorter lengths of fiber <30 cm the total loss was comparable. However, with >30 cm the scattering loss began to increase in all three cases and the total loss increased as a result. The major difference was the magnitude of the increase for the uncontrolled fiber vs. the controlled fiber. Assuming the bulk quality was consistent between these growths, this would be strong evidence to support surface scattering being the dominant loss mechanism from the irregular diameter variations. With greater variations there is an increase of modes coupling to higher order modes that eventually refract out. This waveguiding effect was further observed when flipping the fiber end for end.

The RiT preform with a 50% Er:YAG core and an undoped cladding have been grown to exhibit a radially graded distribution of the erbium ions. Once either the concentration difference from center to the edge or the index of refraction are measured the other can be calculated based on known changes of index as a function of concentration. At this time our collaborators at the University of Michigan are attempting to measure the radial index change. While at Rutgers we are attempting to use electron probe micro-analyzer (EPMA) to measure the concentration of erbium. Based on the calculations a 5% change in index will allow for light to propagate when coupled in at an angle of 3.4°. With this graded index waveguiding, the diameter variations, that are an inherent attribute of the LHPG growth, should have a minimal effect if the variation remains controlled.

References

1. D. J. Richardson, J. Nilsson, and W. A. Clarkson, "High power fiber lasers: current status and future perspectives [Invited]," J. Opt. Soc. Am. B **27**, B63-B92 (2010).

2. B. K. G. Dhanaraj, V. Prasad, M. Dudley, *Springer Handbook of Crystal Growth,* 1 ed. (Springer-Verlag Berlin Heidelberg, 2010).

3. N. Soleimani, B. Ponting, E. Gebremichael, A. Ribuot, and G. Maxwell, "Coilable single crystals fibers of doped-YAG for high power laser applications," Journal of Crystal Growth **393**, 18-22 (2014).

4. M. Digonnet, C. Gaeta, D. O'meara, and H. Shaw, "Clad Nd: YAG fibers for laser applications," Lightwave Technology, Journal of **5**, 642-646 (1987).

5. T. A. Parthasarathy, Hay, R. S., Fair, G., Hopkins. F. K., "Predicted preformance limits of yttrium aluminum garnet fiber lasers," Opt. Eng. **49**(2010).

6. J. W. Dawson, M. J. Messerly, J. E. Heebner, P. H. Pax, A. K. Sridharan, A. L. Bullington, R. J. Beach, C. W. Siders, C. Barty, and M. Dubinskii, "Power scaling analysis of fiber lasers and amplifiers based on non-silica materials," in *SPIE Defense, Security, and Sensing*, (International Society for Optics and Photonics, 2010), 768611-768611-768612.

7. J. W. Dawson, M. J. Messerly, R. J. Beach, M. Y. Shverdin, E. A. Stappaerts, A. K. Sridharan, P. H. Pax, J. E. Heebner, C. W. Siders, and C. P. J. Barty, "Analysis of the scalability of diffraction-limited fiber lasers and amplifiers to high average power," Opt. Express **16**, 13240-13266 (2008).

8. G. P. Agrawal, *Nonlinear Fiber Optics* (Academic Press, 2013).

9. A. Latynina, M. Watanabe, D. Inomata, K. Aoki, Y. Sugahara, E. G. Víllora, and K. Shimamura, "Properties of Czochralski grown Ce, Gd: Y 3 Al 5 O 12 single crystal for white light-emitting diode," Journal of Alloys and Compounds **553**, 89-92 (2013).

10. R. Gaumé, B. Viana, D. Vivien, J.-P. Roger, and D. Fournier, "A simple model for the prediction of thermal conductivity in pure and doped insulating crystals," Applied Physics Letters **83**, 1355-1357 (2003).

11. T. A. Parthasarathy, R. S. Hay, G. Fair, and F. K. Hopkins, "Predicted performance limits of yttrium aluminum garnet fiber lasers," OPTICE **49**, 094302-094302-094308 (2010).

12. X. Mu, S. Meissner, H. Meissner, and A. W. Yu, "High efficiency Yb:YAG crystalline fiber-waveguide lasers," Opt. Lett. **39**, 6331-6334 (2014).

13. Y. Li, K. Miller, E. G. Johnson, C. D. Nie, S. Bera, J. A. Harrington, and R. Shori, "Lasing characteristics of Ho:YAG single crystal fiber," Opt. Express **24**, 9751-9756 (2016).

14. J. Hecht, ed., *City of Light,* Revised and Expanded ed. (Oxford University Press, 2004), p. 368.

15. H. Kanamori, H. Yokota, G. Tanaka, M. Watanabe, Y. Ishiguro, I. Yoshida, T. Kakii, S. Itoh, Y. Asano, and S. Tanaka, "Transmission characteristics and reliability of pure-silica-core single-mode fibers," Journal of lightwave technology **4**, 1144-1150 (1986).

16. Y. Chigusa, Y. Yamamoto, T. Yokokawa, T. Sasaki, T. Taru, M. Hirano, M. Kakui, M. Onishi, and E. Sasaoka, "Low-loss pure-silica-core fibers and their possible impact on transmission systems," Journal of Lightwave Technology **23**, 3541 (2005).

17. H. E. LaBelle, "EFG, the invention and application to sapphire growth," Journal of Crystal Growth **50**, 8-17 (1980).

18. T. Fukuda and V. I. Chani, *Shaped Crystals: Growth by Micro-Pulling-Down Technique* (Springer Berlin Heidelberg, 2007).

19. C. A. Burrus and L. A. Coldren, "Growth of single-crystal sapphire-clad ruby fibers," Applied Physics Letters **31**, 383-384 (1977).

20. J. S. Haggerty, W. P. Menashi, and J. F. Wenckus, "Method for forming refractory fibers by laser energy," (Google Patents, 1976).

21. D. Jundt, M. Fejer, and R. Byer, "Characterization of single-crystal sapphire fibers for optical power delivery systems," Applied Physics Letters **55**, 2170-2172 (1989).

22. M. Saifi, B. Dubois, E. Vogel, and F. Thiel, "Growth of tetragonal BaTiO 3 single crystal fibers," Journal of Materials Research **1**, 452-456 (1986).

23. R. K. Nubling and J. A. Harrington, "Optical properties of single-crystal sapphire fibers," Applied Optics **36**, 5934-5940 (1997).

24. C. D. Nie, S. Bera, and J. A. Harrington, "Growth of single-crystal YAG fiber optics," Opt. Express **24**, 15522-15527 (2016).

25. R. S. F. Chang, S. Sengupta, L. B. Shaw, and N. Djeu, "Fabrication of laser materials by laser-heated pedestal growth," *Proc. SPIE 1410*, 125-132 (1991).

26. R. S. Feigelson, "Pulling optical fibers," Journal of Crystal Growth **79**, 669-680 (1986).

27. A. GOLUBOVIC, S. NIKOLIC, R. GAJIC, and S. DJURIC, "The growth of Nd: YAG single crystals," Journal of the Serbian Chemical Society (2002).

28. D. Yuan, Z. Jia, Y. Li, B. Wu, and X. Tao, "Micro-pulling-down furnace modification and single crystal fibers growth," in 2016), 97260E-97260E-97268.

29. A. Yoshikawa and V. Chani, "Growth of Optical Crystals by the Micro-Pulling-Down Method," MRS Bulletin **34**, 266-270 (2009).

30. K. Lebbou, D. Perrodin, V. I. Chani, A. Brenier, O. Tillement, O. Aloui, J. M. Fourmigue, J. Didierjean, F. Balembois, and P. Gorges, "Fiber Single-Crystal Growth from the Melt for Optical Applications," Journal of the American Ceramic Society **89**, 75-80 (2006).

31. Y. Zaouter, I. Martial, X. Délen, N. Aubry, J. Didierjean, C. Hönninger, E. Mottay, P. Georges, F. Druon, and F. Balembois, "12 W, 350 fs ultrashort pulses from a micro-pulling down Yb:YAG single crystal fiber amplifier," in *CLEO/Europe and EQEC 2011 Conference Digest*, OSA Technical Digest (CD) (Optical Society of America, 2011), CA6_3.

32. J. Didierjean, N. Aubry, D. Perrodin, J. M. Fourmigue, I. Martial, A. Aubourg, F. Balembois, X. Delen, D. Sangla, and P. Georges, "Oxide crystal-fibers grown by micro-pulling-down technique and applications for lasers and scintillators," in 2012), 82630Q-82630Q-82613.

33. J. Didierjean, M. Castaing, F. Balembois, P. Georges, D. Perrodin, J. M. Fourmigué, K. Lebbou, A. Brenier, and O. Tillement, "High-power laser with Nd: YAG single-crystal fiber grown by the micro-pulling-down technique," Opt. Lett. **31**, 3468-3470 (2006).

34. C. A. Burrus and J. Stone, "Single−crystal fiber optical devices: A Nd:YAG fiber laser," Applied Physics Letters **26**, 318-320 (1975).

35. B. Shaw, C. Askins, W. Kim, S. Bayya, J. Peele, R. Thapa, S. R. Bowman, R. R. Gattass, and J. S. Sanghera, "Cladding Pumped Single Crystal Yb: YAG Fiber Amplifier," in *Advanced Solid State Lasers*, (Optical Society of America, 2015), AM4A. 4.

36. G. Maxwell, N. Soleimani, B. Ponting, and E. Gebremichael, "Coilable single crystal fibers of doped-YAG for high power laser applications," in 2013), 87330T-87330T-87338.

37. X. Mu, S. Meissner, H. Meissner, and W. Y. Anthony, "High efficiency Yb: YAG crystalline fiber-waveguide lasers," Opt. Lett. **39**, 6331-6334 (2014).

38. M. Digonnet, C. Gaeta, and H. Shaw, "1.064- and 1.32 um Nd:YAG single crystal fiber lasers," Journal of Lightwave Technology **4**, 454-460 (1986).

39. P. C. W. Shi, I. A. Watson, and J. H. Sharp, "High-concentration Er:YAG single-crystal fibers grown by laser-heated pedestal growth technique," Opt. Lett. **36**, 2182-2184 (2011).

40. K. Y. Huang, K. Y. Hsu, D. Y. Jheng, W. J. Zhuo, P. Y. Chen, P. S. Yeh, and S. L. Huang, "Low-loss propagation in Cr4+:YAG double-clad crystal fiber fabricated by sapphire tube assisted CDLHPG technique," Opt. Express **16**, 12264-12271 (2008).

41. F. Urbach, "The Long-Wavelength Edge of Photographic Sensitivity and of the Electronic Absorption of Solids," Physical Review **92**, 1324-1324 (1953).

42. E. D. Palik, *Handbook of optical constants of solids* (Academic press, 1998), Vol. 3.

43. J. A. Harrington, *Infrared fibers and their applications* (SPIE Optical Engineering Press, Bellingham, Wash., 2004), pp. xi, 298 p.

44. D. A. Pinnow, T. C. Rich, F. W. Ostermayer, and M. DiDomenico, "Fundamental optical attenuation limits in the liquid and glassy state with application to fiber optical waveguide materials," Applied Physics Letters **22**, 527-529 (1973).

45. R. W. Dixon, "Photoelastic Properties of Selected Materials and Their Relevance for Applications to Acoustic Light Modulators and Scanners," Journal of Applied Physics **38**, 5149-5153 (1967).

46. A. Yariv, *Optical Electronics,* 3rd Edition ed. (Harcourt College Publishers, 1985).

47. Z. Huang, J. Feng, and W. Pan, "Elastic properties of YAG: First-principles calculation and experimental investigation," Solid State Sciences **14**, 1327-1332 (2012).

48. M. E. Innocenzi, R. T. Swimm, M. Bass, R. H. French, and M. R. Kokta, "Optical absorption in undoped yttrium aluminum garnet," Journal of Applied Physics **68**, 1200-1204 (1990).

49. G. Mann and G. Phillipps, "Rough surface absorption of Nd:YAG laser rods," Optical Materials **4**, 811-814 (1995).

50. M. Fejer, R. Byer, R. Feigelson, and W. Kway, "Growth and characterization of single crystal refractory oxide fibers," in *1982 Los Angeles Technical Symposium*, (International Society for Optics and Photonics, 1982), 50-55.

51. J. S. Haggerty, "Production of fibers by a floating zone fiber drawing technique," (Final Report NASA-CR-120948, 1972).

52. M. M. Fejer, G. A. Magel, and R. L. Byer, "High-speed high-resolution fiber diameter variation measurement system," Applied Optics **24**, 2362-2368 (1985).

53. M. R. B. Andreeta, L. C. Caraschi, and A. C. Hernandes, "Automatic diameter control system applied to the laser heated pedestal growth technique," Materials Research **6**, 107-110 (2003).

54. M. Toshiaki and K. Yasuhiko, "Effects of Oxygen Pressure on Optical Absorption of YAG," Japanese Journal of Applied Physics **24**, 546 (1985).

55. S. U. William A. Tiller, "The influence of an interface electric field on the distribution coefficient of chromium in LiNbO3," Journal of Crystal Growth **121**, 93-110 (1992).

56. V. Phomsakha, R. S. F. Chang, and N. Djeu, "Novel implementation of laser heated pedestal growth for the rapid drawing of sapphire fibers," Review of Scientific Instruments **65**, 3860-3861 (1994).

57. V. Phomsakha, Chang, R., Djeu, N., "Novel implementation of laser heated pedestal growth for the rapid drawing of sapphre fibers," Rev. Sci. Instrum., 3860-3861 (1994).

58. M. Fejer, *Single crystal fibers: Growth dynamics and nonlinear optical interactions* (Stanford Univ. Ph.D. Thesis, 1986).

59. K. Kim, Dreeben, A., Schujko, A., "Maximum stable zone length in float-zone growth of small-diameter sapphire and silicon crystals," Journal of Applied Physics, 4472-4474 (1979).

60. M. M. Fejer, J. L. Nightingale, G. A. Magel, and R. L. Byer, "Laser-heated miniature pedestal growth apparatus for single-crystal optical fibers," Review of Scientific Instruments **55**, 1791-1796 (1984).

61. T. Surek, "Theory of shape stability in crystal growth from the melt," Journal of Applied Physics **47**, 4384-4393 (1976).

62. R. Nubling, "Sapphire fibers for erbium:YAG and hollow waveguides for industrial carbon dioxide laser power delivery," (Rutgers University, 1996).

63. P. C. Nordine, J. Weber, and J. G. Abadie, "Properties of high-temperature melts using levitation," Pure and applied chemistry **72**, 2127-2136 (2000).

64. I. Manabu, U. Takemi, W. Masaki, and Y. Norikuni, "Gate Oxide Defects in MOSLSIs and Octahedral Void Defects in Czochralski Silicon," Japanese Journal of Applied Physics **37**, 1228 (1998).

65. T. Inoue and H. Komatsu, "Effects of the Crystal Diameter on the Dislocation Density in KCl Crystals Grown by the Czochralski Method," Kristall und Technik **14**, 1511-1519 (1979).

66. W. C. Dash, "Growth of Silicon Crystals Free from Dislocations," Journal of Applied Physics **30**, 459-474 (1959).

67. P. R. D. T. Hurle, "A brief history of defect formation, segregation, faceting, and twinning in melt-grown semiconductors," Journal of Crystal Growth **264**, 550-564 (2004).

68. S. Kostić, Z. Ž. Lazarević, V. Radojević, A. Milutinović, M. Romčević, N. Ž. Romčević, and A. Valčić, "Study of structural and optical properties of YAG and Nd:YAG single crystals," Materials Research Bulletin **63**, 80-87 (2015).

69. M. ŒWIRKOWICZ, M. Skórczakowski, J. Jabczynski, A. Bajor, and E. Tymicki, "Investigation of structural, optical and lasing properties of YAG: Yb single crystals," Opto-Electronics Review **13**, 213-220 (2005).

70. K. C. Kao and G. A. Hockham, "Dielectric-fibre surface waveguides for optical frequencies," Electrical Engineers, Proceedings of the Institution of **113**, 1151-1158 (1966).

71. G. Tao, H. Ebendorff-Heidepriem, A. M. Stolyarov, S. Danto, J. V. Badding, Y. Fink, J. Ballato, and A. F. Abouraddy, "Infrared fibers," Adv. Opt. Photon. **7**, 379-458 (2015).

72. H.-C. Lee, X. Mu, and H. Meissner, "Interferometric measurement of refractive index difference applied to composite waveguide lasers," in *CLEO:2011 - Laser Applications to Photonic Applications*, OSA Technical Digest (CD) (Optical Society of America, 2011), AMB4.

73. G. L. A. S. F. Akhmetov, G. A. Gazizova, V. S. Kovalenko, and T. F. Mirenkova, "Rare earth metal aluminum garnets," Russ. J. Inorg. Chem. **22**, 1613-1615 (1977).

74. M. J. F. Digonnet, C. J. Gaeta, D. Omeara, and H. J. Shaw, "Clad Nd-Yag Fibers for Laser Applications," Journal of Lightwave Technology **5**, 642-646 (1987).

75. N. Ter-Gabrielyan, V. Fromzel, X. Mu, H. Meissner, and M. Dubinskii, "Resonantly pumped single-mode channel waveguide Er:YAG laser with nearly quantum defect limited efficiency," Opt. Lett. **38**, 2431-2433 (2013).

76. C. Jun, C. Dong-Quan, and Z. Jing-Lin, "Molecular dynamics simulation of thermodynamic properties of YAG," Chinese Physics **16**, 2779 (2007).

77. "Opto Engine LLC", retrieved November, 1, 2016, http://www.optoengine.com/Pages/default.aspx.

78. A. Al-Azzawi, *Fiber Optics: Principles and Practices* (Taylor & Francis, 2006).

79. A. Sa'ar and A. Katzir, "Scattering effects in crystalline infrared fibers," J. Opt. Soc. Am. A **5**, 823-833 (1988).

80. D. E. Zelmon, D. L. Small, and R. Page, "Refractive-index measurements of undoped yttrium aluminum garnet from 0.4 to 5.0 μm," Applied Optics **37**, 4933-4935 (1998).

81. J. A. Harrington and M. Sparks, "Inverse-square wavelength dependence of attenuation in infrared polycrystalline fibers," Opt. Lett. **8**, 223-225 (1983).

82. S. Ishibashi, K. Naganuma, and I. Yokohama, "Cr, Ca : Y3Al5O12 laser crystal grown by the laser-heated pedestal growth method," Journal of Crystal Growth **183**, 614-621 (1998).

83. L. T. Banner, A. Richter, and E. Pinkhassik, "Pinhole-free large-grained atomically smooth Au(111) substrates prepared by flame-annealed template stripping," Surface and Interface Analysis **41**, 49-55 (2009).

84. Y. Li, E. G. Johnson, C. D. Nie, J. A. Harrington, and R. Shori, "Ho:YAG single crystal fiber: fabrication and optical characterization," Opt. Express **22**, 14896-14903 (2014).

85. Y. Li, Z. Zhang, I. Buckley, J. K. Miller, E. G. Johnson, C. D. Nie, J. A. Harrington, and R. K. Shori, "Investigation of the amplification properties of Ho: YAG single crystal fiber," in *SPIE LASE*, (International Society for Optics and Photonics, 2015), 934205-934205-934206.